Oncogenic and inflammatory signaling in the pathogenesis of myeloproliferative neoplasms

Ph.D. Thesis

Ján Štetka

Department of Biology, Faculty of Medicine and Dentistry, Palacky University Olomouc

Olomouc 2020

〉Declaration / Prohlášení

Hereby I declare that I have written this work on my own under the supervision of Assoc. Prof. Vladimír Divoký, Ph.D., and that all used literature is cited and mentioned in references.

Tímto prohlašuji, že předloženou práci jsem napsal samostatně, pod vedením školitele doc. RNDr. Vladimíra Divokého, Ph.D. a s použitím citované literatury.

_____

〉Abstract

Myeloproliferative neoplasms (MPNs) are disorders of hematopoietic stem cells (HSCs), characterized by abnormal proliferation of one or more myeloid lineages and driven by underling oncogenic signaling with high prevalence of *JAK2* V617F mutation. Chronic inflammation, changes in metabolism and DNA damage response are major hallmarks of MPN. MPN patients with *JAK2* V617F mutation have variable phenotype manifestation, resulting in different clinical entities. The two most represented are polycythemia vera (PV) with expansion of red cell lineage and essential thrombocythemia (ET) with increased megakaryopoiesis. Unique disease properties of MPN, including relatively low incidence of leukemia transformation, provide a model for investigating mechanisms of oncogene interaction with inflammation-induced DNA damage and changes in metabolism which are then reflected in disease initiation, phenotype manifestation and eventually disease progression. In general, inflammation and gradual increase in DNA damage creates a tissue microenvironment permissive for neoplastic transformation, as discussed here in the case of preleukemia disease states. However, in the case of *JAK2* V617F oncogene, the disease evolution is characterized by long and stable latent phase. Here, I present a dataset uncovering *JAK2* V617F-dependent protective mechanisms, which in PV cells ameliorate inflammation-mediated oxidative stress and stress-activated protein kinase signaling. The fail-safe mechanisms against inflammatory stress and DNA damage are mediated by up-regulation of reactive oxygen species buffering system and through dual-specificity phosphatase 1 (DUSP1) actions. These protection mechanisms then create a barrier preventing progression to myelofibrosis. Furthermore, we show, that PV progenitors are strongly dependent on DUSP1 activity, providing a potential therapeutic target. Currently the most effective treatment of MPN is a therapy with pegylated interferon alpha (pegIFNα). This suggests that excess of inflammatory signaling might eventually overrun protection mechanisms in a pool of hematopoietic stem cells (HSCs). We have thus studied effects of treatment with pegIFNα on HSCs in mouse models of MPN. We found an increased expression of surface marker CD41 in a subset of MPN HSCs ($CD41^{hi}$ HSC) which show impaired self-renewal and repopulation capacity. Treatment with pegIFNα further induced shift towards $CD41^{hi}$ HSCs and provides a possible mechanistic link and a marker of pegIFNα therapy effectiveness. Finally, we also examined the influence of iron metabolism on the phenotype manifestation in MPN. Iron deficiency was shown to promote megakaryocytic commitment of megakaryocyte-erythroid progenitors (MEPs). We studied mice expressing *JAK2* V617F and displaying pure ET or full PV phenotypes and a *JAK2* exon

12 (*E12*) mouse model with erythrocytosis and exposed them to iron deficiency or iron supplementation. Iron deficiency in PV models led to microcytic anemia and increased platelet counts. Conversely, iron injections lowered the platelet counts and promoted erythrocytosis. However, the *JAK2* V617F ET model was unresponsive to changes of iron availability. Analyses of the stem cell and progenitor compartment show that ET mice are feeding the megakaryopoiesis through the megakaryocyte-biased common myeloid progenitor (CMP) path. Furthermore, PV models tend to use both iron responsive MEP and nonresponsive megakaryocytic-biased LT-HSC/CMP path. In contrast, the mutant JAK2 exon12 protein appears to selectively stimulate iron dependent stage of MEPs resulting in erythrocytosis at the expense of platelet production. Exploring means of limiting erythropoiesis through iron restriction may benefit PV patients requiring repeat therapeutic phlebotomy. Overall, these studies contribute to better understanding of unique pathophysiology of MPN and create a platform for new therapeutic interventions.

〉Abstrakt

Myeloproliferativní onemocnění (MPN) jsou poruchy hematopoetických kmenových buněk (HSC) s nadprodukcí myeloidních krevních řad, které jsou způsobeny onkogenní signalizací a vyznačují se vysokou prevalencí mutace *JAK2* V617F. Chronický zánět, změny v metabolismu a odpovědi na poškození DNA jsou důležitými znaky MPN. Pacienti s MPN a mutací *JAK2* V617F tvoří několik navzájem neostře ohraničených jednotek s variabilní fenotypovou manifestací, což vede ke klasifikaci různých klinických entit. Nejvíce zastoupené jsou polycythemia vera (PV) s expanzí červené krevní řady a esenciální trombocytémie (ET) se zvýšenou mírou megakaryopoézy. Díky jedinečným vlastnostem, mezi které patří relativně nízká míra leukemické transformace s dlouhou latencí, slouží MPN jako model pro zkoumání mechanismů interakce onkogenu a odpovědi na poškození DNA způsobené zánětem a změnami v metabolismu, které se pak projeví v iniciaci nemoci, fenotypovém projevu a případně i v progresi nemoci. Obecně, zánět a postupná akumulace poškození DNA vytváří mikroprostředí krvetvorné tkáně, které zvyšuje riziko neoplastické transformace, jak je zde diskutováno u preleukemických stavů. V případě onkogenu *JAK2* V617F u MPN je však vývoj choroby charakterizován dlouhou a stabilní latentní fází. V této práci představuji soubor dat, který odhaluje mechanismy závislé na signalizaci *JAK2* V617F, které v progenitorech PV snižují jak oxidativní stres zprostředkovaný zánětem, tak stresem aktivovanou signalizaci proteinkináz. Těmito mechanizmy jsou upregulace systému antioxidační ochrany proti reaktivním formám kyslíku a fosfatáza s dvojí specificitou DUSP1. Tyto ochranné mechanismy pak vytvářejí bariéru zabraňující progresi do myelofibrózy. Dále ukazujeme, že PV progenitory jsou silně závislé na aktivitě DUSP1, což poskytuje potenciální cíl pro budoucí terapeutické přístupy. V současné době je léčba pegylovaným interferonem alfa (pegIFNα) nejúčinnější terapií u MPN. To naznačuje, že nadbytek zánětové signalizace může nakonec překonat ochranné mechanismy u hematopoetických kmenových buněk (HSCs). Rozhodli jsme se proto studovat účinky pegIFNα na HSCs v myších modelech MPN. Naše analýza ukázala zvýšenou expresi povrchového markeru CD41 u MPN HSCs ($CD41^{hi}$ HSCs), které vykazují sníženou schopnost samoobnovy a repopulace. Léčba pegIFNα následně indukuje konverzi HSCs s nízkou expresí CD41 na $CD41^{hi}$ HSCs a poskytuje představu o možném mechanizmu účinku pegIFNα a marker účinnosti terapie. Nakonec jsme také zkoumali vliv metabolismu železa na projev fenotypu u MPN. Ukázalo se, že nedostatek železa podporuje sklon společných progenitorů megakaryocytů a červené krevní rady (MEP) k diferenciaci do progenitorů megakaryocytů. V této části studie jsme použili myši

exprimující *JAK2* V617F s fenotypovým projevem ET nebo PV a myší model *JAK2* exon 12 (E12) s erytrocytózou a vystavili jsme je nedostatku železa nebo jeho dodatečnou suplementací. Nedostatek železa v modelech PV vedl k mikrocytární anémii a zvýšenému počtu krevních destiček. Naopak parenterální doplnění železa snížilo počet krevních destiček a indukovalo erytrocytózu. Avšak model ET s *JAK2* V617F nereagoval na změny dostupnosti železa. Následující analýza kompartmentu kmenových buněk a progenitorů ukazuje, že u ET myšího modelu dochází k zvýšené megakaryopoéze prostřednictvím společného myeloidního progenitoru (CMP), který nereaguje na dostupnost železa. PV modely mají tendenci používat jak MEP reagující na železo, tak nereagující cestu prostřednictvím LT-HSC / CMP se sklonem k diferenciaci do progenitorů megakaryocytů. Naproti tomu se zdá, že mutantní protein JAK2 exon12 selektivně stimuluje MEP, které jsou závislé na železe, což vede k erytrocytóze na úkor produkce destiček. Zkoumání způsobů omezení erytropoézy omezením dostupnosti železa může prospět pacientům s PV vyžadujících opakovanou terapeutickou flebotomii. Celkově tyto studie přispívají k lepšímu pochopení jedinečné patofyziologie MPN a vytvářejí platformu pro nové terapeutické intervence.

〉Acknowledgement

Firstly, I would like to express my sincere gratitude to my supervisor Assoc. Prof. RNDr. Vladimír Divoký, Ph.D., for the continuous support of my Ph.D. study and related research, for the excellent ideas he brought to my scientific projects and for time he spent by critically reviewing my results.

I would like to thank my all fellow labmates, especially Dr. Pavla Kořalková, Dr. Lucie Láníková and Dr. Ján Gurský for the stimulating discussions, for the sleepless nights we were working together, and for all the fun we have had in the last years.

My special thanks belong also to prof. Radek C. Skoda at Department of Biomedicine, Experimental Hematology, University Hospital Basel and University of Basel and his lab members and institute core facilities members. During my stay in Basel, I gained incredible amount of new knowledge and scientific experience.

I would also like to thank all the collaborators joining our projects, mainly Prof. Jiří Bártek, Dr. Zdeněk Hodný, all the clinicians for collecting, evaluating and processing patients' samples and vice-dean Prof. Mgr. Martin Modrianský, Ph.D. for support in my studies and help with mobility in Basel.

Last but not the least, I would like to thank my family: my wife Ivanka (+1), daughter Laura and my parents, who supported me throughout my studies and my life in general.

My work at Palacký University was supported, in whole or in part, by the Czech Science Foundation grants numbers 14-10687P and 17-05988S, by the LTAUSA17142 project from the Ministry of Education, Youth and Sports, Czech Republic, and by the Internal Grant Agency of Palacký University, projects numbers IGA_LF_2017_015, IGA_LF_2018_010 and IGA_LF_2019_006. In addition, my stay in Basel was partially supported by the Mobility Support on Palacký University project no. CZ.02.2.69/0.0/0.0/16_027/0008482 and by the aforementioned 17-05988S project.

〉Content

1. Introduction 1
1.1 Role of DDR in acute leukemia development 1
1.1.1 DNA damage and genomic instability in the pathogenesis of leukemia 2
1.1.2 Involvement of inflammation induced-oxidative stress in leukemogenesis 3
1.1.3 DNA damage repair genes polymorphisms in the pathogenesis of leukemia 4
1.1.4 DDR as a potential barrier against leukemia development 6
1.2 Role of DDR in PV disease initiation and progression 8
1.2.1 *JAK2* V617F and DNA damage 8
1.2.2 Inflammation signaling and oxidative stress in PV 9
1.2.3 Stress-associated protein kinases and DDR in PV 11
2. Aims of the thesis 13
3. Results and discussion 14
Aim 1 Critically review the literature concerning contribution of oncogene-induced DNA-damage response and inflammatory signaling cooperation in suppressing and promoting malignant transformation of chronic myeloid leukemia and polycythemia vera. 14
Publications related to this aim: 14
Aim 2 Describe JAK2 V617F-driven cell autonomous and non-cell autonomous inflammatory signature of hematopoietic progenitors in PV 15
JAK2 V617F^{+} hematopoietic progenitors activate intrinsic IFNγ transcription program and its IFNγ-dependent STAT1 signaling 15
Description of robust inflammatory signature in PV patient's BM sections from different PV disease stages 22
Publications related to this aim: 25
Aim 3 Characterize inflammation-induced oxidative stress and how it fosters DDR activation in progression of PV. 27
The *JAK2* V617F^{+} CD34^{+} P-ECs limit production of ROS and hyperactivate ROS buffering system 27
PV cells are protected against accumulation of inflammation-evoked DNA damage 31
Overexpression of DUSP1 facilitates survival and proliferation of *JAK2* V617F^{+} cells in inflammatory conditions 39
Publications related to this aim: 48

Aim 4 Investigate the role of interferon signaling in hematopoietic stem cells heterogeneity in MPN mouse model 50
Publications related to this aim: 59
Aim 5 Explore role of iron availability on MPN phenotype manifestation. 60
Publications related to this aim: 70
4. Materials and methods 71
4.1 Laboratory equipment and software 71
4.2 Biological material 71
4.3 Other chemicals, cytokines and reagents 72
4.4 Comercial Kits 73
4.5 Culture of undifferentiated iPSCs 73
4.6 iPSC hematopoietic differentiation 74
4.7 Generation of *JAK2*-corrected (*JAK2* wt) HEL cell line 74
4.8 Mice 75
4.9 pIpC, pegIFNα, and TPO *in vivo* treatment 75
4.10 Bone marrow transplantations 75
4.11 Microarray and data analysis 76
4.12 Quantitative Real-Time Polymerase Chain Reaction 76
4.13 Flow cytometry analysis 77
4.14 Enzyme assays 78
4.15 Immunocytochemistry on EBs in agarose gel matrix saturated with paraffin 78
4.16 Immunocytochemistry of $CD34^+$ P-ECs 79
4.17 Inhibition of dual-specificity phosphatases (DUSPs) 79
4.18 Western blotting 80
4.19 Immunohistochemistry of patient samples 80
4.20 Iron deficient diet and iron injections 81
4.21 Liver iron content 81
4.22 Iron parameters and regulatory cytokines 82
4.23 Statistical analysis 82
5. Summary 83
6. References 85
7. Supplements 102
8. Acronyms and abbreviations 105
9. List of publications 110

1. Introduction

This part of the thesis elaborates on DNA damage response (DDR) alterations within inflammatory bone marrow (BM) milieu and how these alterations attenuate or promote disease progression in myeloproliferative neoplasms (MPNs) and pre-leukemia (relates to the Aims 1-3). Theoretical background for Aims 4-5 is briefly introduced at the beginning of each aim.

1.1 Role of DDR in acute leukemia development

Acute leukemias, with the most prevalent acute myeloid leukemia (AML), are multistep transforming diseases, which evolve from former preleukemic phase characterized by genetic and epigenetic changes in hematopoietic stem cells (HSCs), establishing pre-leukemia stem cells (pre-LSCs), which drive clonal hematopoiesis and myeloid linage expansion (Pandolfi et al., 2013). Eventually, through the process of clonal evolution, pre-LSCs transform to leukemia stem cells (LSCs), defined by their capacity to induce aggressive, short-onset leukemias with clonal expansion of immature hematopoietic cells (Pandolfi et al., 2013). AML-associated mutations in preleukemia phase create substantial mutational landscape, with several mutations frequent also in aging hematopoiesis, which modulate epigenome activities, self-renewal, proliferation and activation of DDR (Busque et al., 2018; Jaiswal and Ebert, 2019). Besides important predisposing mutations in epigenome modifiers like *DNMT3A*, *TET2* or *EZH2*, some mutations present in preleukemic phase of AML are high risk mutations, significantly associated with AML transformation. These includes classical oncogenes like *FLT3*, *RAS* or *KIT*, but also important DDR components like *TP53*, *CHEK2* and *IDH1/2* (Corces-Zimmerman et al., 2014; Desai et al., 2018; Haferlach et al., 2014; Zhou et al., 2015) (for more DDR genes see Figure 1). Besides generally appreciated functions of IDH1 and 2 in modulation of global DNA methylation, it was recently shown to play a critical role in downregulating ATM expression, significantly impairing DNA damage response and homeostasis of HSCs (Inoue et al., 2016). Importantly, a long follow-up study on peripheral blood samples collected years before AML diagnosis showed that patients with *TP53* and *IDH* mutations at the baseline eventually all developed AML (Desai et al., 2018). In addition, syndromes with mutations in genes encoding important DNA repair genes, such as Fanconi Anemia, Werner, Bloom and Down Syndrome have inherited tendency for developing AML (Auerbach, 1992; Poppe et al., 2001; Tao et al., 1971; Xavier and Taub, 2010). Significance of functional DNA repair and ability to actively

resolve accumulation of DNA damage in hematopoietic compartment is further highlighted by development of therapy-related AML in patients with prior cytotoxic and/or radiation therapy for a primary malignancy or autoimmune disease (Borthakur and Estey, 2007; Godley and Larson, 2008). Thus, this growing body of literature supports the notion that impaired DNA damage response at least in subset of early pre-leukemic HSC clones drives biological changes leading inevitably later in life to onset of acute leukemias.

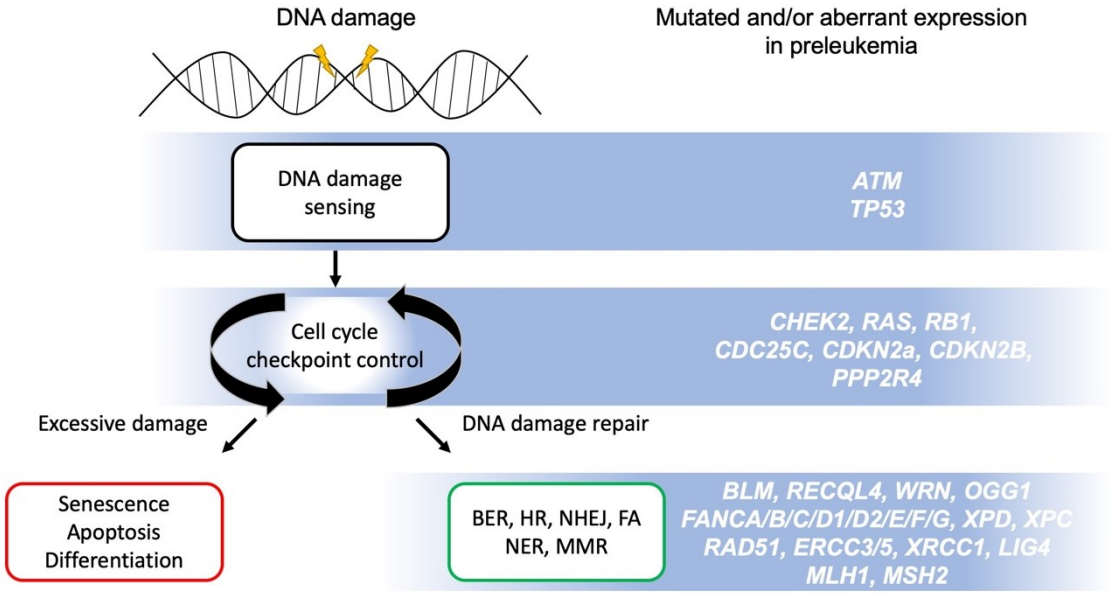

Figure 1: Important components of DNA damage response (*left*) are depicted with genes (*right*) playing important roles in individual signaling nodes of DDR, which were found to be mutated or aberrantly expressed in preleukemia (Allan et al., 2004; Bănescu et al., 2014; Jankowska et al., 2008; Jawad et al., 2006; Kuramoto et al., 2002; Mao et al., 2008; Sheikhha et al., 2002; Strom et al., 2010; Zhou et al., 2015; Zhu et al., 1999).

1.1.1 DNA damage and genomic instability in the pathogenesis of leukemia

The prevalence of myeloid leukemias is increasing with age of individuals and was previously attributed to accumulation of age-selected mutations (Genovese et al., 2014; Jaiswal et al., 2014; Steensma et al., 2015; Xie et al., 2014; Young et al., 2016) and development of chronic inflammation (Busque et al., 2018; Steensma, 2018), associated increase of reactive oxygen species (ROS) (Yahata et al., 2011) and DNA damage (Flach et al., 2014). Previous work has also shown that aged HSCs are more prone to proliferate and expand (Pang et al., 2011), however they have decreased engraftment potential (Kuranda et al., 2011). Additionally, if HSCs are pushed towards exit of the dormancy they are much more prone to accumulate excessive DNA damage,

especially under the prolonged stress hematopoiesis and inflammation (Walter et al., 2015). These cell-intrinsic changes thus create a functional landscape influencing fitness of HSCs such that the best ones retain their self-renewal and differentiation capacity and are most likely to expand over prolonged time/aging (Bowman et al., 2018). However, contribution of gradual DNA damage accumulation has so far not been very well characterized in preleukemia and clonal hematopoiesis. On the other side of the spectrum with increased DNA damage and cytogenetic instability, we have myelodysplastic syndromes (MDS), which were established by Block et al. in 1953 as a heterogeneous group of hematopoietic disorders with high rate of transformation to acute leukemias. Thus, originally preleukemia phase was mainly covered by classification of MDS (Cazzola et al., 2011; Haferlach et al., 2014). Jeopardized genomic stability is a major hallmark of preleukemic MDS, with around half of the patients having clonal cytogenetic abnormalities in *de novo* MDS and in up to 80% patients with therapy induced MDS (Haase et al., 2007; Solé et al., 2005; Toyama et al., 1993). Unbalanced chromosomal abnormalities reflecting a gain or loss of chromosomal material (Haase et al., 2007), microsatellite instability (Ben-Yehuda et al., 1996; Casorelli et al., 2003; Olipitz et al., 2002) and increased number of micronuclei (Kuramoto et al., 2002) further support development of strong mutator phenotype of MDS hematopoietic progenitors. These data also points to aberrant regulation of DNA repair, with microsatellites being a major hallmark of ineffective mismatch repair (MMR), which helps to recognize and correct errors that occur during DNA replication and recombination (Li, 2008). Low expression of *XPC*, *ERCC3* and *ERCC5*, important genes in nucleotide excision repair, that removes a range of bulky DNA lesions, were also shown to be decreased in 40% of patients in high-risk group for AML transformation (Kuramoto et al., 2002). Furthermore, aberrant processing of double strand breaks and gradual accumulation of DNA damage over progression of preleukemia to leukemia has been observed in various preleukemic mouse models (Lin et al., 2005; Lutzmann et al., 2019; Omidvar et al., 2007; Puthiyaveetil et al., 2013) and patient samples (Popp et al., 2017; Valka et al., 2017). Taken together, increased DNA damage and alteration of the DDR are closely linked to cytogenetic instability and progression of preleukemia, creating essential driving force of clonal evolution towards full-blown leukemia across the pre-leukemia disease entities.

1.1.2 Involvement of inflammation induced-oxidative stress in leukemogenesis

Inflammation has been long recognized as an essential part of preleukemia niche in clonal hematopoiesis harboring recurrent preleukemic mutations and also in MDS

(Jaiswal and Ebert, 2019; Sallman and List, 2019). Patients with mutated versions of *DNMT3A*, *ASXL1* and especially *TET2* have higher prevalence of cardiovascular and autoimmune diseases as well as increased risk of atherosclerosis, which was connected to increased activity of inflammasome and development of systemic inflammatory responses (Fuster et al., 2017; Jaiswal et al., 2017). Also, the presence of associated increased levels of proinflammatory cytokines and chemokines in periphery and BM of MDS patients has been well documented. Profound dysregulation of IL-1/TNFα/NF-κB axis, elevated production of interferons, TGFβ, IL-6 and IL-8 among other proinflammatory cytokines are all important components of inflammatory response of MDS with prognostic value through affecting clinical outcomes of patients. (Gañán-Gómez et al., 2015; Sallman and List, 2019). Such perturbation of inflammatory signaling was shown to induce mitochondrial dysfunction (Dela Cruz and Kang, 2018) and accumulation of ROS, with potentially mutagenic effects through increase in oxidative DNA damage, mainly oxidative byproduct 8-oxoguanine (Kay et al., 2019), phenomena observed also in MDS (Gonçalves et al., 2015; Jankowska et al., 2008; Novotna et al., 2009; Peddie et al., 1997; Saigo et al., 2011). Consequentially, DNA damage response exacerbate inflammation and senescence associated secretory profiles, creating viscous self-regulatory loop, driving genotoxic effects in preleukemia (Kay et al., 2019). Moreover, oxoguanine glycosylase (OGG1), which is the primary enzyme that tackles oxidative stress by excision of 8-oxoguanine, was shown to be significantly downregulated in MDS (Jankowska et al., 2008). Certain cases showed also opposite trend towards upregulation of OGG1, but they proved to be a compensatory up-regulation, due to dysfunctional *OGG1* polymorphism previously associated with a functional change in enzyme activity (Jankowska et al., 2008; Kohno et al., 1998). Its therefore likely that increased inflammation-induced oxidative stress and impaired resolution of oxidative byproducts significantly contributes to propensity of preleukemia for genomic instability.

1.1.3 DNA damage repair genes polymorphisms in the pathogenesis of leukemia

Mutations in genes responsible for key components of DNA repair has been linked to development of many human cancer types, with most frequent targets in homology-dependent recombination (HR) and direct repair (Knijnenburg et al., 2018). Such modifications of DDR has been also linked to development of AML, mainly to therapy-related acute myeloid leukemia (t-AML, Coombs et al., 2017). Homologous recombination has a central role in repairing double-stranded DNA breaks (DSBs) with

high fidelity using homologous region of another chromatid as a replicative template (O'Kane et al., 2017). Comprehensive protein machinery orchestrates this process with RAD51 paralogs having crucial role in searching for homology and facilitating recruitment of essential proteins like BRCA2 to DSBs (O'Kane et al., 2017). Several studies showed direct correlation between polymorphic variants of *RAD51* paralogs *RAD51-135C* (Jawad et al., 2006) and *XRCC3-241Met (Seedhouse et al., 2004)* and incidence of t-AML and *de novo* AML (Hamdy et al., 2011). Besides HR, as outlined in 1.1.2, polymorphisms of base excision repair enzymes like *OGG1* have been proven to have functions in preleukemia etiology. Another protein involved in efficient repair of single-stranded DNA (ssDNA) breaks is XRCC1, which acts as scaffolding protein for multiple repair enzymes (London, 2015). Two polymorphisms *Arg194Trp* and *Arg399Gln* affecting functions of this protein has been linked to genetic predisposition for AML (Bănescu et al., 2014, p. 1) and higher accumulation of DNA damage (Wang et al., 2003). Additionally polymorphisms *XPD Lys751Gln* and *XPC Ala499Val* involved in ssDNA damage repair through nucleotide excision repair were likewise increasing risk of t-AML and could be also used as a prognostic markers as they were significantly associated with decreased overall survival (Allan et al., 2004; Strom et al., 2010). As mentioned in 1.1.1. microsatellite instability is a major hallmark of preleukemic MDS, with aberrant mismatch repair. Polymorphisms and changed methylation status of *MLH1* and *MSH2* involved in MMR has been extensively studied in leukemogenesis, showing importance of decreased MMR activity in AML development (Mao et al., 2008; Sheikhha et al., 2002; Zhu et al., 1999). Overall, these data highlight importance of DDR dysfunction as an important event in the preleukemic stem cells, making them primed towards malignant transformation when recurrent driving mutations occur (Figure 2).

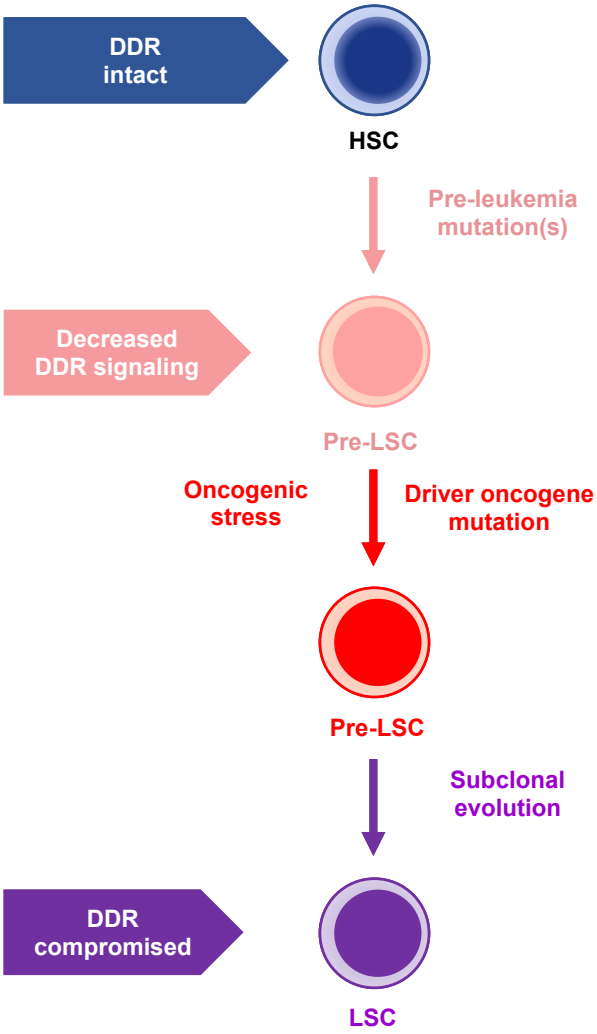

Figure 2: Outline of events at the HSC level leading to transformation of benign pre-leukemia to full-blown leukemia. Altered DDR of hematopoietic stem cells is an important priming step in pre-leukemia development, altering the faith of pre-LSCs when recurrent preleukemic mutations occur and clonal hematopoiesis begins. Due to DDR evasion pre-LSCs suffer from increased genomic instability, which creates a lethal driving force of increased subclonal evolution propensity, establishing LSCs from which eventually clonogenic leukemic progenitors originate.

1.1.4 DDR as a potential barrier against leukemia development

As delineated in previous sections, pre-leukemic mutations and diminished DDR are important steps which pave way towards leukemia prior oncogenic, driver mutation insult. However, exceptions do exist with report showing primary oncogenic hit through *MLL* gene rearrangement delineating onset of covert, protracted preleukemic phase with intact myeloid differentiation (Zuna et al., 2009). Colleagues in my laboratory have

previously described Mll-ENL knockin mouse model, in which the oncogenic fusion is induced by tamoxifen through truncated form of mutant estrogen receptor (ERtm) and expressed in the physiological context of the *Mll* gene (Takacova et al., 2012). Induction of oncogene eventually led to sustained myeloproliferation both in BM and spleen, however upon prolonged chronic phase, *Mll-ENL-ERtm*-expressing myeloid cells suffered from oncogene-induced replication stress, marked by the ATR/Chk1-mediated DDR activation and gradually progressed to senescence, resulting in inhibition of leukemia progression. Activation of such fail-safe mechanisms was much stronger in BM, where it was reinforced by ATM/p53/p21 checkpoint switched on by inflammatory microenvironment. Thus DDR in this model induces a barrier against leukemogenesis, consistent with the hypothesis of oncogene-induced replication stress limiting the pre-neoplastic disease potential and progression (Bartkova et al., 2005; Di Micco et al., 2006). Strikingly, inhibition of ATM and ATR signaling was able to bypass the DDR barrier and accelerated the onset of leukemia (Figure 3).

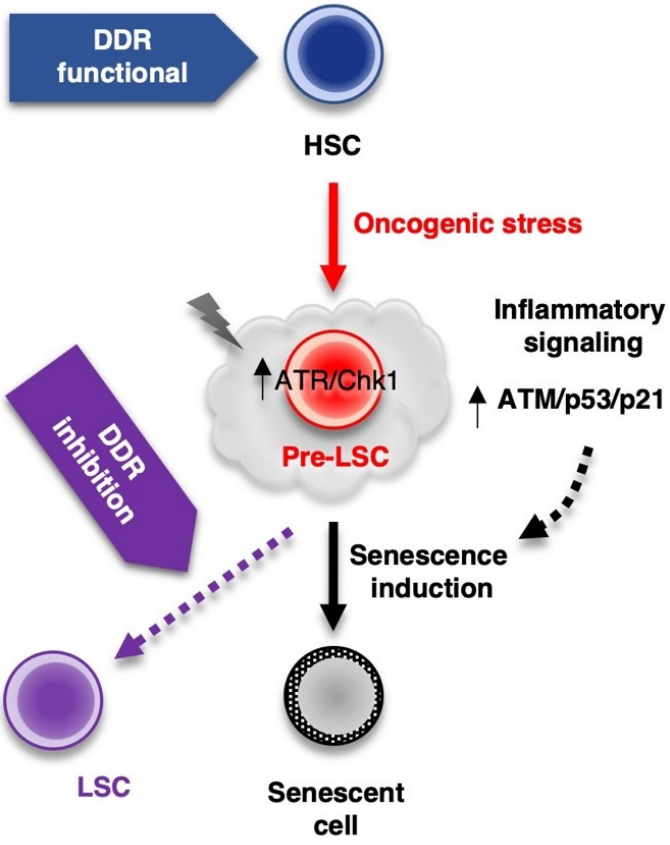

Figure 3: Model summarizing the molecular mechanisms of the barrier that delays acute leukemia onset. Oncogenic lesion initiates aberrant propagation of the preleukemic clone, which upon prolonged myeloproliferation and replication stress activates cell-intrinsic ATR/Chk1 signaling pathway. This effect is further reinforced by development of inflammation, which potentiates activation of ATM/p53/p21 axis and drives cells

towards senescence, limiting the disease development. Inhibition of DDR thus prevents such terminal fate and accelerates progression to AML.

1.2 Role of DDR in PV disease initiation and progression

Myeloproliferative neoplasms (MPNs) encompass a spectrum of clonal hematological disorders of the BM, with most common Philadelphia chromosome negative clinical entities: polycythemia vera (PV), essential thrombocythemia (ET) and primary myelofibrosis (PMF) (Arber et al., 2016). Similar to the phase of preleukemia, MPNs are characterized by chronic proliferation of functional myeloid elements and systemic inflammation driven by oncogenic JAK-STAT-mediated signaling (Hasselbalch et al., 2015). However, MPNs differ from preleukemia (in terms of disease states described above, such as MDS or germline mutant hematopoietic clone) in long clinical course of chronic phase and near-normal life expectancy, with exception of PMF with early onset of progressive BM fibrosis (Campbell and Green, 2006). About 95–98% of PV patients and 50–60% of ET and PMF patients carry an oncogenic driver mutation in the *JAK2* gene (*JAK2* V617F) (Baxter et al., 2005; James et al., 2005; Kralovics et al., 2005; Levine et al., 2005), which constitutively activates type-1 myeloid cytokine receptors signaling (Tefferi, 2016; Vainchenker and Kralovics, 2017). Although the exact role played by *JAK2* V617F in initiation of BM microenvironment remodeling is not fully elucidated, recent studies show the dysregulation of cytokine receptors signaling driving vicious circle of inflammatory cytokines production, leading to systemic response reflected by elevated inflammatory markers in circulation (Hasselbalch et al., 2015; Vaidya et al., 2012). Thus, oncogenic and inflammatory signaling, both known to fuel genotoxic stress and tumorigenesis in the hematopoietic system in cell autonomous (Bartek et al., 2008; Chen et al., 2014) and non-autonomous (Zambetti et al., 2016) manner respectively, converge in disease evolution of PV. This provides an excellent model of inflammation-associated neoplasia for investigating mechanisms of DNA damage accumulation and DDR activation throughout early pre-cancerous ontogeny.

1.2.1 *JAK2* V617F and DNA damage

Cytogenetic stability as a readout of frequency of cytogenetic abnormalities, which are always connected inevitably to DNA damage accumulation, has been shown previously to be significantly increased in primary myelofibrosis, but low percentage (less than 5%) has been documented for proliferative PV (Reilly, 2008). This was further supported with much bigger cohort of MPN patients at high resolution, using Affymetrix

SNP array, where *JAK2* V617F–positive patients, including PMF, didn't have a higher frequency of chromosomal aberrations (Klampfl et al., 2011). On the top of that, longitudinal studies indicate that MPN patients remain clinically and cytogenetically stable over decades of chronic proliferation (Tefferi et al., 2014). However, these clinical observations are in contrast to some studies based on mouse models and *in vitro* cultures of cell lines and *ex vivo* expanded progenitors from patients. These studies described V617F-dependent accumulation of DSBs (Li et al., 2010), improper regulation of HR (Plo et al., 2008) and processing of stalled replication forks representing a potential source of DSBs (Chen et al., 2014). This in turn may lead to mutagenic phenotype similar to phenotypes observed in pathogenesis of leukemia. But, again, the V617F-induced mutagenicity was not confirmed upon exome sequencing of MPN patients reveling modest amount of mutations per exome (Nangalia et al., 2013). We have recently published data from PV induced pluripotent stem cells (iPSCs) disease modeling as a competitive approach to tackle this unresolved conundrum, which stems from the usage of either immortalized cell lines or progenitors pushed too much over the thresholds of non-physiological expansion (Stetka et al., 2019). In agreement with clinical phenotypes we have detected lower DNA damage accumulation and normal usage of HR in V617F-positive hematopoietic progeny, which is further presented in the results section (Stetka et al., 2019). In addition, recent publication shows that *JAK2* V617F-positive cells upregulate expression and functions of RECQL5 helicase. Helicases from *RECQ* family are also called as a 'caretakers of the genome' (Bohr, 2008; Chu and Hickson, 2009), having important roles in stabilizing replication forks and safeguarding the intersection between DNA replication and transcription (Popuri et al., 2013). Therefore, studies (including our own) of phenomena that have been of high importance for decades, chronic proliferation under oncogenic pressure, have led to the identification of possible mechanisms that act as a suppressor of genomic instability in PV. Thus, compared to early leukemogenesis, the disease evolutionary trade-off between bypassing DNA damage-checkpoint blockade and loss of genome stability maintenance is largely avoided in PV.

1.2.2 Inflammation signaling and oxidative stress in PV

Mouse model-based studies proved to be important tool for functional analysis of progressively remodeled BM microenvironment in PV, which suggested development of systemic inflammation and inflammation-mediated neuropathy of hematopoietic stem cell niche (Arranz et al., 2014), with leukemic-like microenvironment transformation that impairs normal hematopoiesis and contributes to development of BM fibrosis (Schepers

et al., 2013). Retrospective cohorts of MPN patients clearly confirmed observation from mouse models having plethora of pro-inflammatory cytokines and chemokines gradually increased over disease development in plasma profiles and BM niche, including among others IL-1, IL-6, IL-8, Interferons type I and II, TNFα and TGFβ1 and on the other hand deregulated levels of anti-inflammatory cytokines, like IL-4 and IL-10 (Hasselbalch et al., 2015; Pourcelot et al., 2014; Tefferi et al., 2011; Vaidya et al., 2012). As discussed in section 1.1.2, inflammatory milieu is a strong inducer of ROS accumulation in hematopoietic compartment, however, output to total amount of oxidative stress depends also on counteracting ROS buffering system. With the right balance, it keeps excessive and genotoxic oxidative stress in check (Kumari et al., 2018). In the context of MPN, increased levels of ROS were observed in mouse models and *in vitro* (Marty et al., 2013), but also in patients samples *in vivo* (Hurtado-Nedelec et al., 2013; Vener et al., 2010). In our recent paper, we confirm increased accumulation of ROS in PV progenitors, however, we also show upregulated enzyme activities of key ROS buffering enzymes counteracting oxidative stress, with the absence of 8-oxoguanine both *in vivo* and *in vitro* (Stetka et al., 2019). Apart from effects of inflammation induced-ROS on genotoxicity, increased ROS were shown to modulate activities of signaling pathways involved in malignant proliferation and apoptosis. Proliferative stimuli from phosphoinositide 3-kinase/protein kinase B (PI3K/PKB) and mitogen activated protein kinase (MAPK) signaling were shown to be hyper-activated by protein oxidation of negative feedback loop regulators and transcription factors (Kwon et al., 2004; Salmeen et al., 2003; Seth and Rudolph, 2006). Nevertheless, for such tumor-promoting functions, ROS need to be tightly regulated by ROS-buffering system at slightly increased, but still not toxic levels, especially for highly sensitive hematopoietic progenitors (Galadari et al., 2017), reminiscent of ROS accumulation in MPN progenitors (Stetka et al., 2019). Furthermore, excessive ROS production in MPNs was shown to increase proliferative advantage of *JAK2* V617F-postitive clones (Hasselbalch, 2014; Xu et al., 2013; Yalcin et al., 2010). As discussed in subsections of 1.1, with advent of ultra-sensitive DNA-sequencing, various publications showed presence of persisting pre-leukemia-associated mutations, including *JAK2* V617F at very low frequencies in most of aged, healthy individuals together with clonal hematopoiesis (Genovese et al., 2014; Jaiswal et al., 2014; Steensma et al., 2015; Xie et al., 2014; Young et al., 2016). As aging in general is also associated with increased DNA damage, inflammation and senescence-associated secretory phenotype, with myeloid skewing in hematopoietic compartment (Rossi et al., 2005; Sun et al., 2014), this likely provides potent selective pressure for the expansion of genetic variants providing advantage in such conditions, which would be great fit for integral phenotypes of *JAK2* mutants. Consequentially, age-related clonal

hematopoiesis with mutations like *JAK2* V617F would be extremely common, if not inevitable.

1.2.3 Stress-associated protein kinases and DDR in PV

Important axis of DNA damage and inflammatory response involves stress-activated protein kinases (SAPKs) from MAPK superfamily, which include Jun kinases (JNKs) and p38MAPK (Lee et al., 2018). Activity of this important signaling node, plays pivotal role in decision making over survival of cells in DNA-damaging inflammatory conditions (Arthur and Ley, 2013; Karigane et al., 2016; Wood et al., 2009). Stimulation of p38MAPK-mediated signaling in chronic inflammatory conditions, such as in PV, would impair proliferation and push cells towards apoptosis or senescence (Iwasa et al., 2003; Lu et al., 2010), cellular conditions resembling status of fibrotic BM. Indeed, excessive activation of the p38–MAPK cascade was shown to be associated with PMF (Desterke et al., 2011). However, faith of such cells in indolent, proliferative PV is at odds with increased SAPK activity. In fact, we have shown up-regulation of dual-specificity MAPK phosphatases (DUSPs), negative inhibitors of SAPKs, in hematopoietic progenitors derived from PV-patient specific iPSCs, with enrichment of those with substrate specificity for p38 and JNK (Stetka et al., 2019). The combination of these 'in-built' features of *JAK2* V617F oncogene, which protects against the overall impact of the inflammatory-mediated DNA damage in PV progenitors, may contribute to the understanding of increased fitness and clonal expansion of *JAK2* V617F-positive cells in patients with such a unique pathobiological behavior (Figure 4).

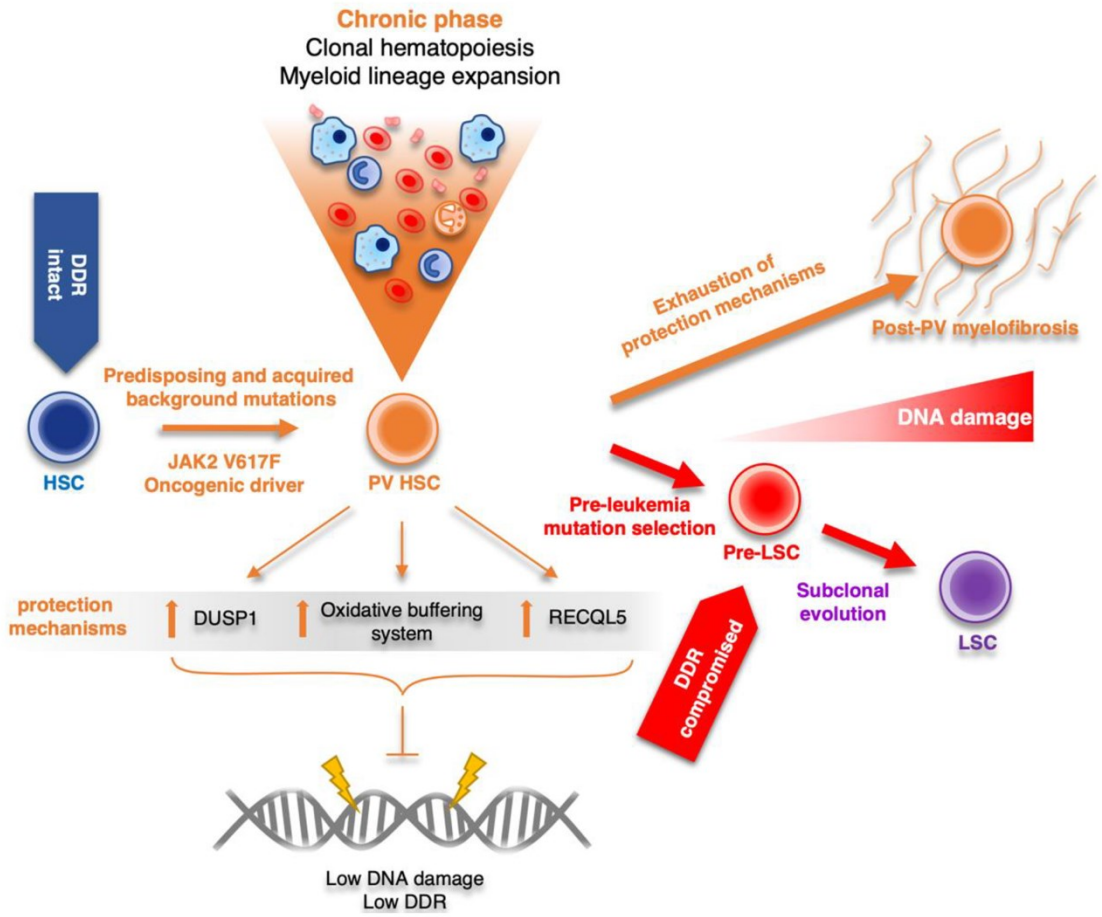

Figure 4: Schematic model of PV disease evolution, showing central role of JAK2 V617F-dependent protection mechanisms, which decrease DNA damage and sustain genomic stability over decades of chronic proliferation phase. Disease has tendency to progress towards post-PV myelofibrosis after exhaustion of protection mechanisms by gradually increased inflammation. In a minor subset of cases, selection of pre-leukemia mutations inhibiting DDR and subclonal evolution towards leukemia stem cell (LSC) marks the onset of secondary acute myeloid leukemias.

2. Aims of the thesis

1 Critically review the literature concerning contribution of oncogene-induced DNA-damage response and inflammatory signaling cooperation in suppressing and promoting malignant transformation of chronic myeloid leukemia and polycythemia vera.

2 Describe *JAK2* V617F-driven cell autonomous and non-cell autonomous inflammatory signature of hematopoietic progenitors in PV.

3 Characterize inflammation-induced oxidative stress and how it fosters DNA damage response activation in progression of PV.

4 Investigate the role of interferon signaling on hematopoietic stem cells heterogeneity in MPN mouse model.

5 Explore role of iron availability on MPN phenotype manifestation.

3. Results and discussion

Aim 1 Critically review the literature concerning contribution of oncogene-induced DNA-damage response and inflammatory signaling cooperation in suppressing and promoting malignant transformation of chronic myeloid leukemia and polycythemia vera.

The presented article provides a comprehensive overview of the current knowledge regarding involvement of DDR alterations in chronic myeloid leukemia within inflammatory BM milieu and how these alterations promote rapid clonal evolution and transformation to blast crisis. This paper also elaborates on a concept of *JAK2* V617F oncogene-dependent protection mechanisms driving the bulk of myeloproliferative neoplasms, exemplified by PV, fueling not only proliferation-promoting events, but also mitigating the potential genotoxic impact of the overall oncogenic and inflammatory program. Apart from reviewing interplay of DDR and inflammatory signaling in different preleukemia states, paper also summarizes implications for therapy as understanding of DDR roles in the leukemogenesis of discussed models constitutes a platform for designing effective therapeutic interventions.

Publications related to this aim:

Article:

Stetka, J., Gursky, J., Liñan Velasquez, J., Mojzikova, R., Vyhlidalova, P., Vrablova, L., Bartek, J., Divoky, V., 2020. Role of DNA Damage Response in Suppressing Malignant Progression of Chronic Myeloid Leukemia and Polycythemia Vera: Impact of Different Oncogenes. Cancers (Basel) 12. https://doi.org/10.3390/cancers12040903

Aim 2 Describe JAK2 V617F-driven cell autonomous and non-cell autonomous inflammatory signature of hematopoietic progenitors in PV.

Elevated pro-inflammatory cytokines and chemokines levels in peripheral blood of PV patients correlate with disease phenotype and prognosis, suggesting their involvement in disease development and clinical manifestation (Pourcelot et al., 2014; Tefferi et al., 2011; Vaidya et al., 2012) but also in the development of premature atherosclerosis and cardiovascular events (Landolfi et al., 2007; Lussana and Rambaldi, 2017). Furthermore, the concept of these cytokines contributing to BM milieu re-modelling and neuropathy has been well established in pre-clinical mouse models (Arranz et al., 2014; Schepers et al., 2013).

Thus, in order to decipher hierarchy and consequences of cell-autonomous and non-cell autonomous inflammatory signaling in PV progenitors, we have implemented iPSCs PV disease modeling using PV patient-specific *JAK2* V617F^{+} (PVB1.4: kindly provided by prof. Josef T. Prchal, University of Utah) and control *JAK2* wt (BXS0116) iPSC lines, reprogrammed from BM CD34^{+} cells. Undifferentiated iPSCs cultures were then differentiated with specific morphogens in serum- and stromal-free cultures through embryonic bodies into CD34^{+} hematopoietic progenitor-enriched cultures (CD34^{+} P-ECs) as described in Materials and methods (section 4.6.), and used for downstream experiments. Immunohistochemistry (IHC) staining of patients' bone marrow sections were also used to test expression of key inflammatory mediators in BM microenvironment along the progression of PV to post-PV myelofibrosis.

JAK2 V617F^{+} hematopoietic progenitors activate intrinsic IFNγ transcription program and its IFNγ-dependent STAT1 signaling

Recent advances in research of hematopoietic stem cells (HSCs) revealed significant intra-pool heterogeneity in biological properties (Haas et al., 2018) and inflammatory responses, with subpopulations of HSCs with different levels of IFN responsiveness and intrinsic expression of a subset of IFN-stimulated genes (Haas et al., 2017; Wu et al., 2018). In the context of MPN and its clinical disease entities, IFNγ/STAT1 signaling axis also proved to be important for disease phenotype manifestation (Chen et al., 2010; Duek et al., 2014) and very high expression levels of downstream IFNγ signaling-dependent chemokine CXCL10 were recorded both in MPN patients and V617F^{+} cell lines (Manshouri et al., 2011; Schnöder et al., 2017). Thus, we hypothesized that *JAK2* V617F mutation skews HSCs heterogeneity towards IFN-primed

state and affects IFNγ-dependent transcription profile and signaling already at the level of HSCs and immediate progeny.

In agreement with our hypothesis we have observed significant up-regulation of *IFNG* mRNA expression in *JAK2* V617F$^+$ cells of CD34$^+$ P-ECs during the course of differentiation, compared to wildtype progenitors, which was further enhanced by treatment with key inflammatory mediators (IFNγ, TNFα, TGFβ1 for 24 hours) present in PV BMs (Chagraoui et al., 2002; Chen et al., 2010; Fleischman et al., 2011) (Figure 5).

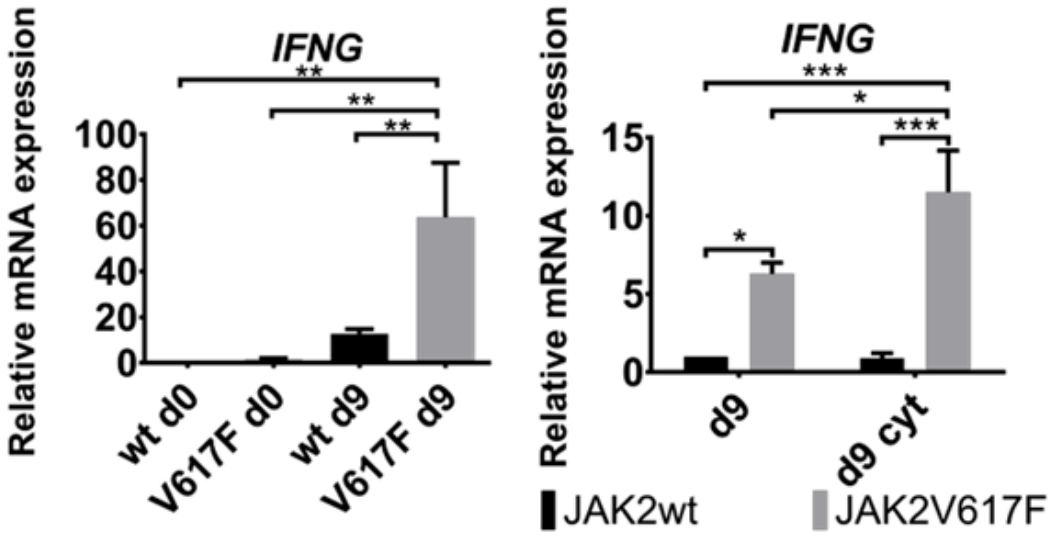

Figure 5: *Left graph*: mean ± SD of intrinsic *IFNG* mRNA expression (n=3) along the course of differentiation in undifferentiated *JAK2* wt and V617F$^+$ iPSC lines (day 0; d0) and day 9 (d9) *JAK2* V617F$^+$ CD34$^+$ P-ECs. *Right graph*: mean ± SD of *IFNG* mRNA expression (n=3) in either untreated (d9) or treated CD34$^+$ P-ECs with inflammatory cytokines (d9 cyt). *P ≤ 0.05, **P ≤ 0.01, ***P ≤ 0.001, one-way and two-way ANOVA, respectively.

To prove that IFNγ was upregulated also at the protein level and expressed mainly by major CD34$^+$ HSC fraction of CD34$^+$ P-ECs and not by CD34$^-$ contaminating cell types from other than hematopoietic lineages, we stained sections of paraffin-embedded EBs by immunofluorescence for CD34 and IFNγ. We have observed significant expression of IFNγ mainly in V617F$^+$ EBs, which colocalized with CD34 antigen (Figure 6).

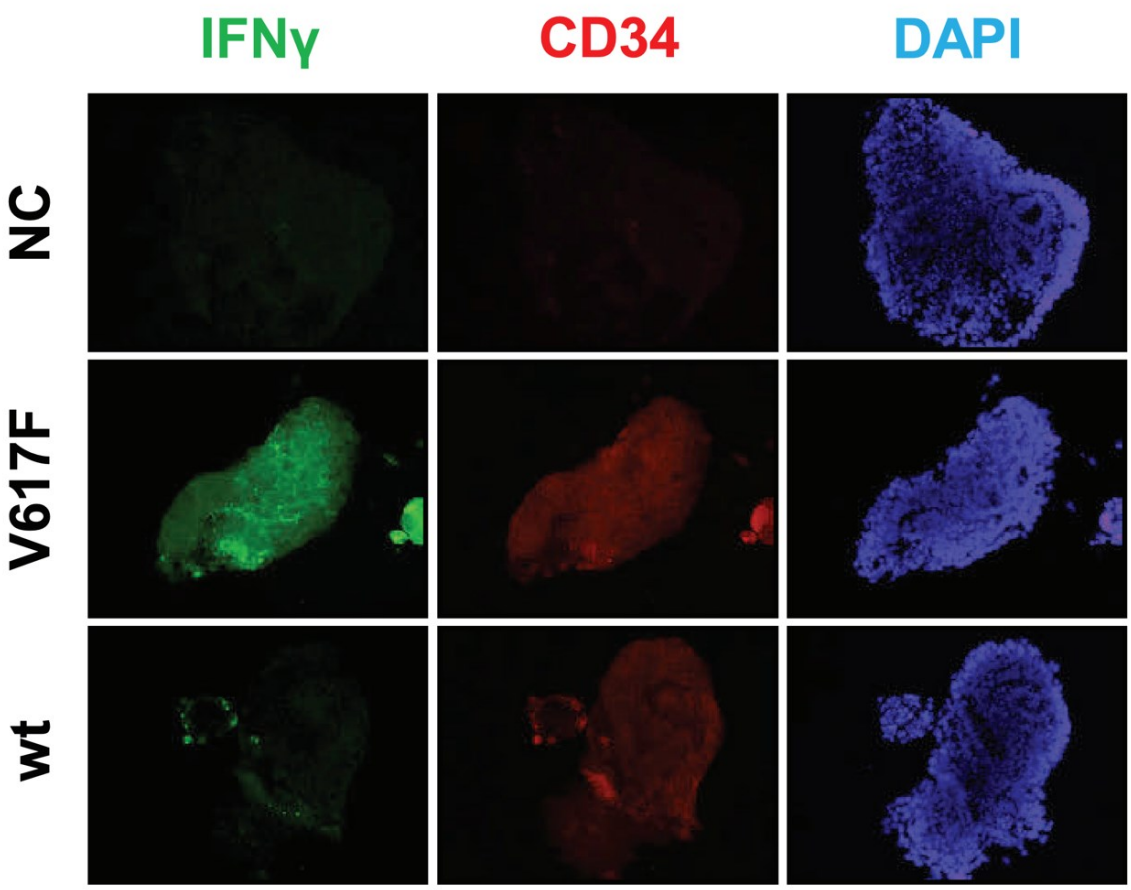

Figure 6: Immunocytochemical dual staining against IFNγ and CD34 in paraffin-embedded *JAK2* wt (wt) and V617F^{+} (V617F) EBs counterstained by DAPI. Negative control (NC) describes sample without primary antibodies incubation used for setup of exposure time to eliminate background fluorescence

Moreover, we have observed intrinsic STAT1 phosphorylation at residue tyrosine 701, that mediates IFNγ responses, which was further potentiated by inflammatory cytokines treatment, in V617F^{+} cells, compared to wt progenitors. (Figure 3A). To further investigate if IFNγ/STAT1 axis in V617F^{+} cells activates downstream targets genes expression, we have measured relative mRNA expression of potent profibrogenic chemokines CXCL9 and CXCL10 in untreated and inflammatory cytokines treated CD34^{+} P-ECs. We have seen more than 100x and 1000x fold increase in CXCL9 and CXCL10 chemokine production, respectively, only in *JAK2* V617F^{+} P-ECs (Figure 3B), suggesting that PV progenitors in the presence of inflammatory microenvironment are prone to drive vicious circle of profibrogenic chemokines production.

A

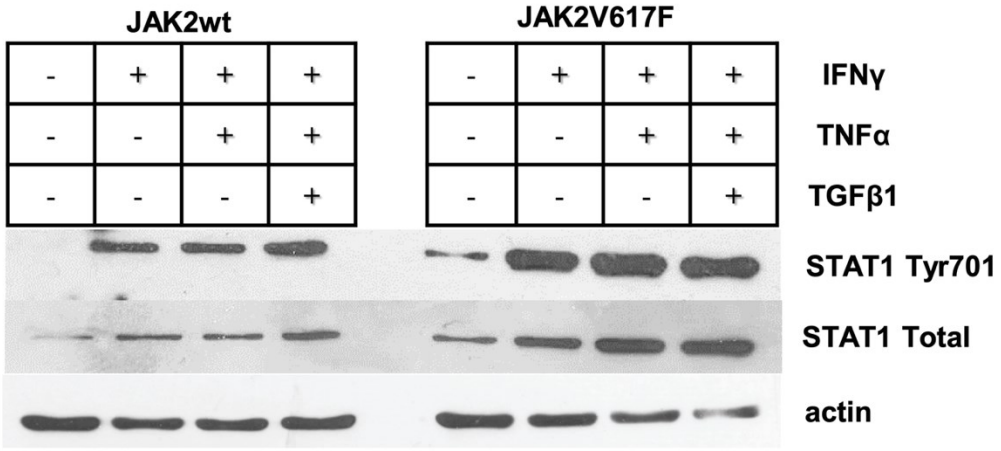

B

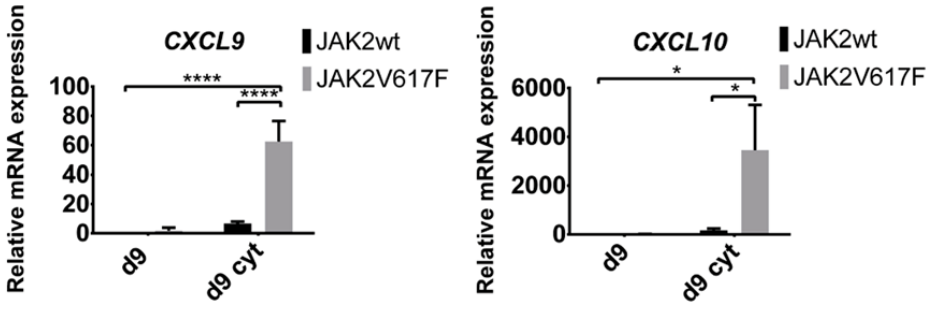

Figure 7: **A** Western blotting analysis of both total and phosphorylated form of STAT1 at Tyr701 in *JAK2* wt and V617F$^+$ CD34$^+$ P-ECs, untreated or treated with various combinations of inflammatory cytokines. **B** mRNA expression (mean ± SD, n = 3) of CXCL9 and CXCL10 in day 9 (d9) *JAK2* wt and V617F$^+$ CD34$^+$ P-ECs, either untreated (d9) or treated (d9 cyt) with inflammatory cytokines. *P ≤ 0.05, ****P ≤ 0.0001.

To further investigate deregulation of IFN-signaling and inflammatory pathways in HSCs of CD34$^+$ P-ECs at a whole transcriptome level, we have isolated total RNA of day 9 *JAK2* wt and *JAK2* V617F$^+$ CD34$^+$ P-ECs, either untreated or treated with inflammatory cytokines (IFNγ, TNFα, TGFβ1 for 24 hours) and performed microarray analysis. Comprehensive data analysis and normalization with general cut-off logFC > |1|, q < 0.1 between untreated and treated CD34$^+$ P-ECs yielded top 20 differentially expressed genes (DEGs) enriched mainly with IFNγ-dependent genes (*TAP1, IRF1, UBD, CXCL10, B2M, VCAM1, STAT1, GBP1, GBP2*) and genes involved in inflammatory responses (Figure 8A, *left*). On top of that, all inflammatory mediators present in DEGs of both genotypes, were significantly more expressed in *JAK2* V617F$^+$ P-ECs, further highlighting robust inflammatory program in PV HSCs and early progenitors (Figure 8A, *right*). Overrepresentation, network module and gene set enrichment analysis (GSEA)

analysis of DEGs, showed type II interferon, NF-κB and antigen presentation as significantly affected pathways, supporting IFNγ priming of PV HSCs and suggesting its impact on immunogenicity and eventually immune surveillance in BM niche (Figure 8B).

A

DEGs: JAK2wt d9 vs. d9 cyt			
Rank	Symbol	logFC	Adjusted p-Value
1	TAP1	2.46	1.90E-05
2	CCL2	2.18	3.02E-04
3	IRF1	1.59	4.72E-03
4	OPTN	1.52	4.72E-03
5	UBD	3.37	4.72E-03
6	IL32	1.7	4.72E-03
7	CXCL10	2.43	4.72E-03
8	B2M	1.32	4.72E-03
9	IL32	2.26	4.72E-03
10	VCAM1	1.49	4.72E-03
11	LTB	2.53	9.90E-03
12	NODAL	1.39	9.90E-03
13	PLA2G4C	1.14	9.90E-03
14	FGA	-1.54	9.90E-03
15	SPACA6	1.09	1.08E-02
16	STAT1	1.23	1.21E-02
17	STAT1	1.01	2.02E-02
18	PARP9	1.16	2.24E-02
19	RARRES3	1.52	2.86E-02
20	CD70	1.13	4.02E-02

DEGs: JAK2V617F d9 vs. d9 cyt			
Rank	Symbol	logFC	Adjusted p-Value
1	GBP1	4.01	7.52E-07
2	CXCL10	6.73	1.18E-06
3	TAP1	2.94	1.18E-06
4	VCAM1	2.38	3.70E-06
5	VCAM1	3.26	5.20E-06
6	CSAG3	2.4	5.20E-06
7	IL32	4.41	9.61E-06
8	CCL2	2.67	9.61E-06
9	IRF1	2.79	9.61E-06
10	GBP1	3.49	9.61E-06
11	RARRES3	3.74	1.36E-05
12	GBP2	2.85	2.67E-05
13	UBD	5.35	2.76E-05
14	IL32	2.63	3.57E-05
15	STAT1	2.04	3.84E-05
16	PSMB9	3.28	4.05E-05
17	B2M	2.05	4.08E-05
18	STAT1	2.2	5.64E-05
19	SERPINA3	3.25	9.43E-05
20	HCP5	1.37	1.04E-04

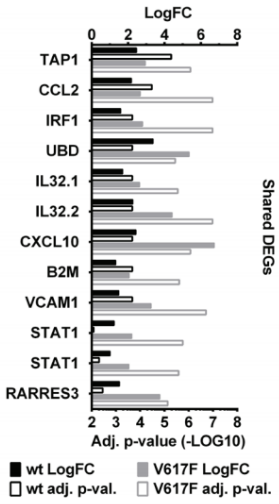

B

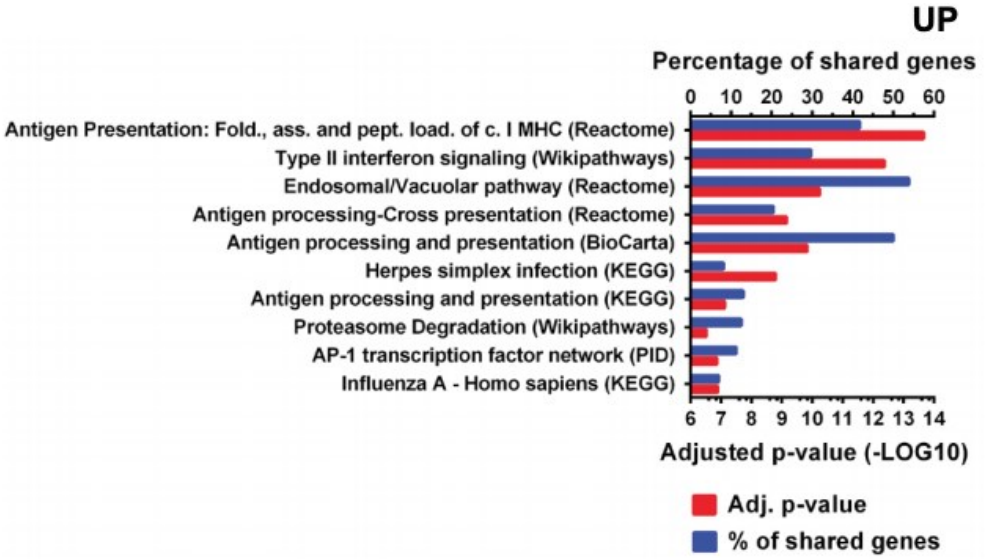

Figure 8: **A** *Left* - tables list top 20 DEGs, ranked according to adjusted p-value, between d9 and d9 cyt *JAK2* wt (table in black) or *JAK2* V617F$^+$ (table in gray) CD34$^+$ P-ECs. List of genes was created using logFC > 1, q < 0.1 cut-off. Expression and adjusted p-values of shared DEGs from both tables are depicted by *right* bar chart showing higher expression of all shared DEGs in *JAK2* V617F$^+$ CD34$^+$ P-ECs. B Overrepresentation analysis of differentially upregulated genes between d9 and d9 cyt *JAK2* wt and V617F$^+$ CD34$^+$ P-ECs compared to listed biological pathways using ConsensusPathDB with minimum overlap of 4 genes in pathway and p-value cut-off of 0.001.

A

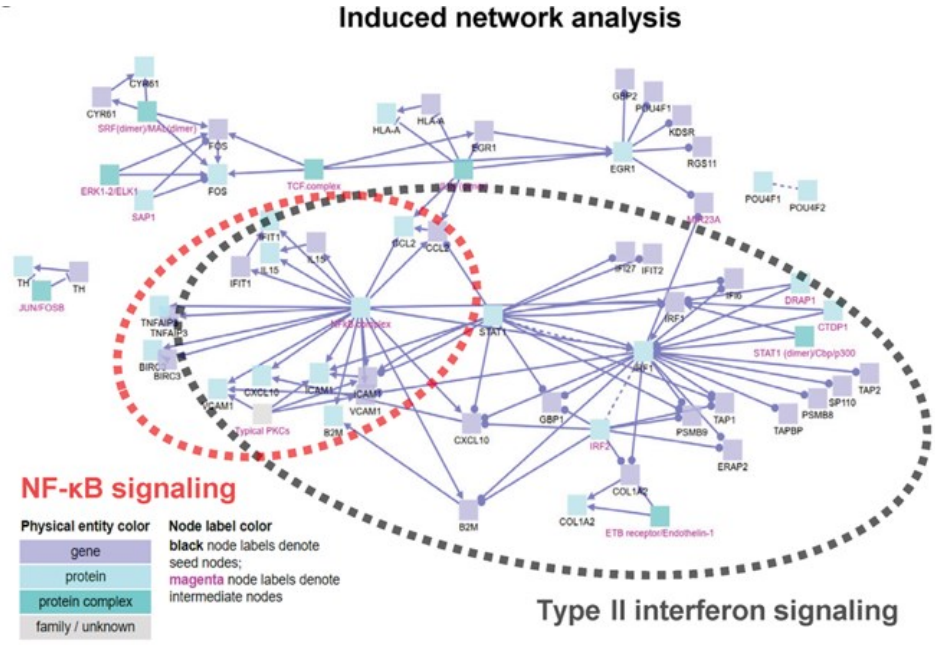

B

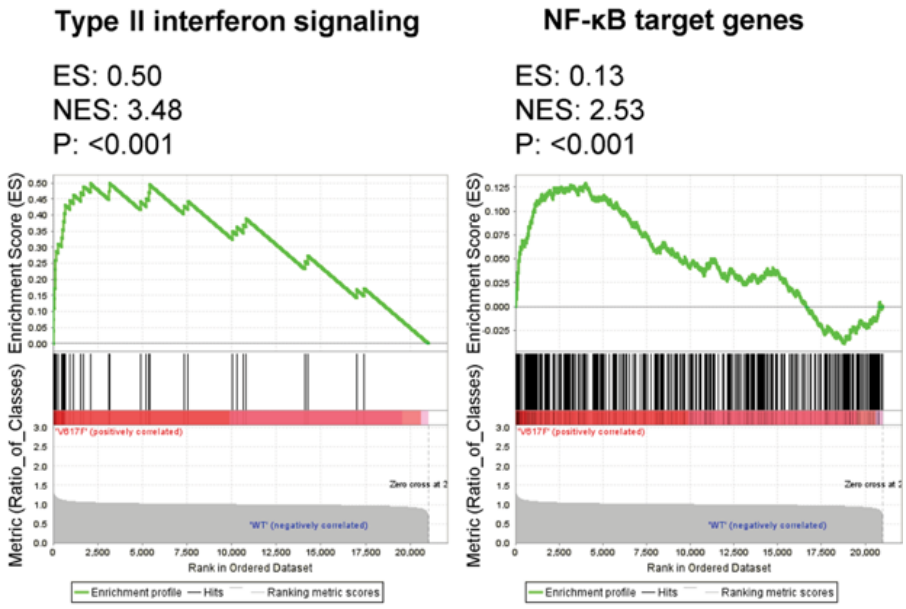

Figure 9: **A** Induced network module analysis depicting seed genes with seed nodes (font in black color) and intermediate nodes (font in magenta color) connected through functional and physical links (ConsensusPathDB) of DEGs between *JAK2* wt and V617F^{+} CD34^{+} P-ECs treated with inflammatory cytokines **B** GSEA enrichment plot with graphical view of the enrichment score on *left* side for type II interferon signaling gene set members (WikiPathway, n = 37) and on *right* side for NF-κB target gene set members (http://www.bu.edu/nf-kb/gene-resources/target-genes/ n = 424) in day 9 *JAK2* V617F^{+} and *JAK2* wt CD34^{+} P-ECs, treated with inflammatory cytokines.

Clustering analysis of type II interferon signaling gene set members (WikiPathway, n = 37), based on expression patterns of individual gene set members, identified cluster of intrinsically up-regulated genes (cluster #B) unique to IFN-primed *JAK2* V617F^{+} P-ECs (Figure 10). Additional treatment with inflammatory cytokines led to up-regulation of genes across the gene set in the *JAK2* V617F^{+} cells, creating cluster #A, showing powerful IFNγ response solely in *JAK2* V617F^{+} P-ECs.

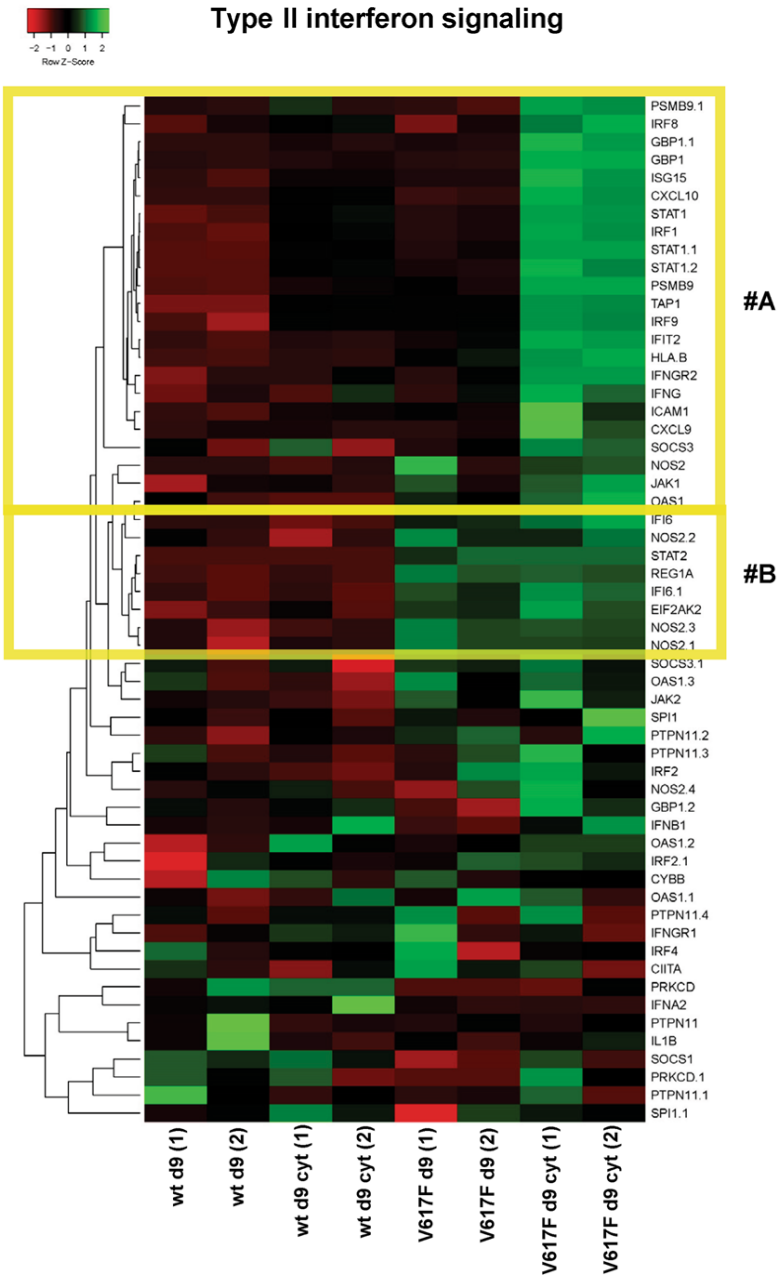

Figure 10: Heatmap representation of differential expression of type II interferon signaling gene set members in d9 *JAK2* wt and *JAK2* V617F^{+} CD34^{+} P-ECs, untreated (d9) or treated with inflammatory cytokines (d9 cyt). Columns in the heatmap represent individual samples in experimental duplicates (1, 2).

Description of robust inflammatory signature in PV patient BM sections from different PV disease stages

As PV HSCs thrives in BM niches in a 'bad seed' (HSCs) and a 'soil' (stromal cells) interaction, we were also interested in describing expression profile of other proinflammatory cytokines in PV patient BM sections during disease progression from proliferative PV state to senescence-associated post-PV myelofibrosis (myelofibrosis grade 1-2 (MF1/2), grade 3 (MF-3), according to revised 2016 WHO classification (Arber et al., 2016)).

In agreement with the detection of IFNγ-dependent signaling in *JAK2* V617F^{+} CD34^{+} P-ECs, we have detected significant expression of pro-fibrogenic chemokines CXCL10 and CXCL9 in the microenvironment of PV patient BMs along the progression of the disease (Figure 11). CXCL10 was expressed constitutively across disease stages while CXCL9 expression was highest in progressed post-PV MF-3. Thus, these data suggest that activation of IFNγ program early in the hematopoietic system has profound and system-wide consequences on pro-inflammatory components of BM milieu. Tumor necrosis factor alpha (TNFα) was shown to mediate proliferative advantage of MPN cells over normal cells (Fleischman et al., 2011), but its anti-proliferative effects and negative impact on self-renewal and long-term repopulating capacity of HSCs was shown before (Bryder et al., 2001; Dybedal et al., 2001). As PV cells are known to be equipped with various protective pathways enabling them to surpass their wt counterparts in inflamed BM niche (Ahn et al., 2016; Chen et al., 2015; Stetka et al., 2019), certain sub-threshold TNFα expression levels might select for PV clones, while exhaustion of protection mechanisms by supra-threshold of TNFα-mediated signaling might lead to senescence, apoptosis and burn-out state of post-PV myelofibrosis. In line with this hypothesis we have detected progressively increased expression of TNFα in BM niche of PV patients spiking in MF-3 stage (Figure 11). Furthermore, in later disease stages TNFα was produced mainly by fibrotic tissue. TGFβ signaling is a strong inducer of fibrosis in multiple organs (Pohlers et al., 2009) and has been previously suggested to have predominant role in development of BM fibrosis in MPN (Chagraoui et al., 2002; Kreipe et al., 2012), however consistently with earlier study (Bock et al., 2005), we have detected high and constitutive expression of TGFβ1 throughout disease development (Figure 11). This suggests modulation of TGFβ signaling downstream of TGFβ1 ligand together with signaling input from other niche components that underline TGFβ signaling-dependent fibrogenesis in PV.

As IL-6 and CCL3 were also shown to be significantly upregulated in PV patient plasma profiles (Vaidya et al., 2012), we have analyzed their presence in PV patient BM sections.

Constitutive expression of both IL-6 and CCL3 was present across the disease stages with modest IL-6 expression and high expression of CCL3 derived mainly from basophil-like progenitor cells, as previously described in CML (Baba et al., 2016).

Taken together, these results confirm presence of persistent IFNγ-dependent inflammatory response also *in vivo* and show participation of other inflammatory mediators in disease development and evolution, complementing CXCL10 and CXCL9 roles in disease development.

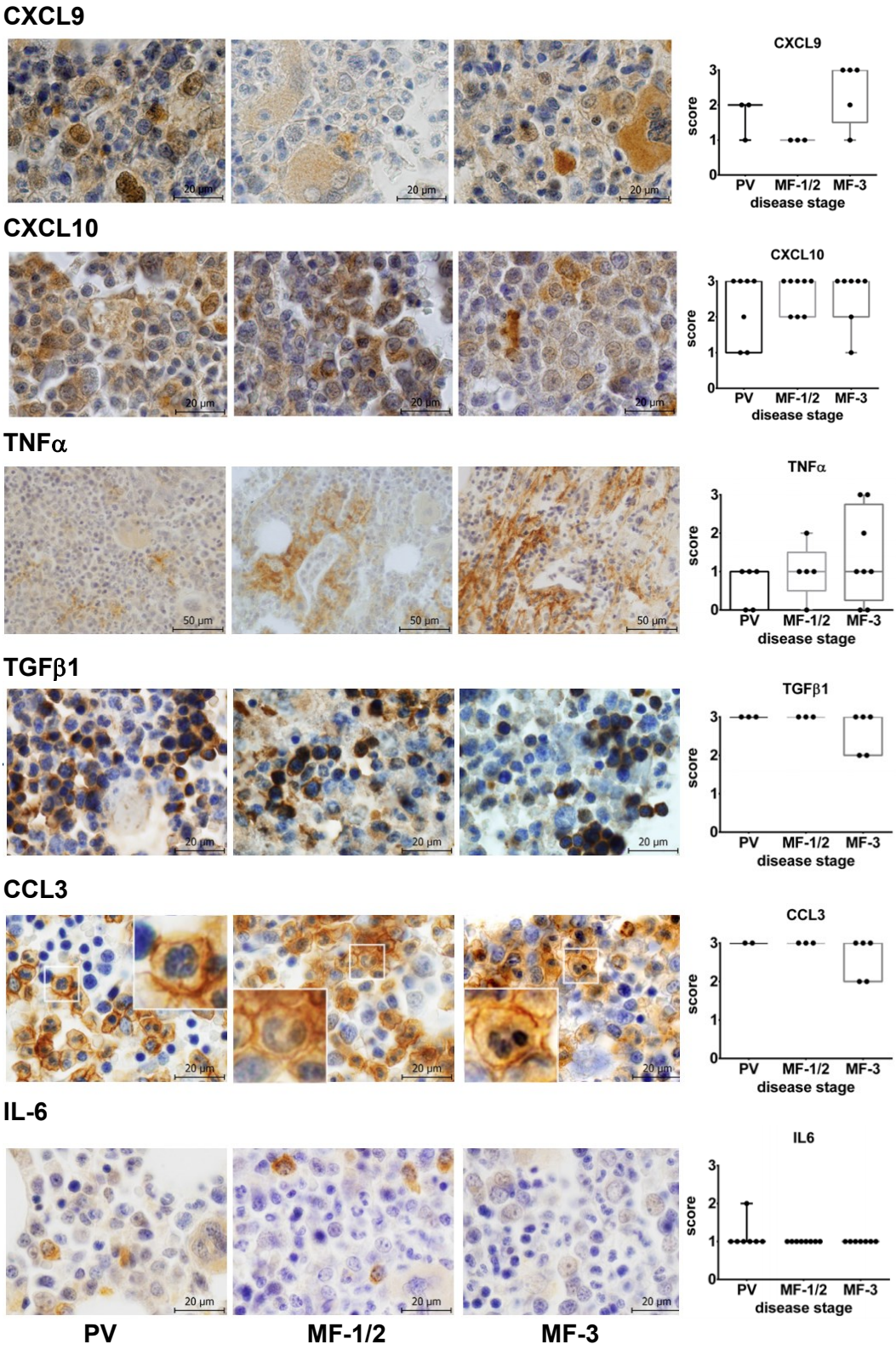

Figure 11: IHC staining of key inflammatory mediators in representative BM sections from patients along the progression of PV. Scale bar, 50 µm and 20 µm. Boxplots show quantification of the number of cells expressing individual cytokines in sections of patients from grouped disease stages. Insets in CCL3 staining show magnification of main CCL3 producers, individual basophile-like cells with segmented nuclei.

Publications related to this aim:

Articles:

Stetka, J., Vyhlidalova, P., Lanikova, L., Koralkova, P., Gursky, J., Hlusi, A., Flodr, P., Hubackova, S., Bartek, J., Hodny, Z., Divoky, V., 2019. Addiction to DUSP1 protects JAK2V617F-driven polycythemia vera progenitors against inflammatory stress and DNA damage, allowing chronic proliferation. Oncogene 38, 5627–5642. https://doi.org/10.1038/s41388-019-0813-7

Abstracts:

Stetka, J., Luzna, P., Lanikova, L., Bartek, J., Divoky, V., 2015. Inflammatory response of hematopoietic progenitors differentiated from polycythemia vera patient-specific induced pluripotent stem cells. International Conference on the tumour microenvironment in the haematological malignancies and its therapeutic targeting, 2015, Lisbon, Portugal, abstracts, poster 24

Stetka, J., Luzna, P., Lanikova, L., Bartek, J., Divoky, V., 2015 Inflammatory response of polycythemia vera hematopoietic progenitors differentiated from patient-specific induced pluripotent stem cells. Olomouc Hematological Days, 2015, Olomouc, abstracts, ISBN 978-80-244-4697-4, page 6

Stetka, J., Luzna, P., Lanikova, L., Koralkova, P., Hodny, Z., Prchal, J., Bartek, J., Divoky, V., 2016. JAK2 V617F progenitors exhibit intrinsic inflammatory signaling and protection against inflammation induced DNA damage. ESH 7th International Conference on MYELOPROLIFERATIVE NEOPLASMS, 2016, Estoril, Portugal, abstracts, poster 21

Stetka, J., Luzna, P., Lanikova, L., Koralkova, P., Hodny, Z., Bartek, J., Divoky, V., 2016. JAK2 V617F progenitors exhibit intrinsic inflammatory signaling and protection against inflammation induced DNA damage. Olomouc Hematological Days, 2016, Olomouc, abstracts, ISSN 1213-5763, page 28-29

Stetka, J., Luzna, P., Lanikova, L., Koralkova, P., Hodny, Z., Bartek, J., Divoky, V., 2016. JAK2 V617F progenitors exhibit intrinsic inflammatory signaling and protection against inflammation induced DNA damage. 12th International Congress of Cell Biology in Prague, 2016, Praha, abstracts, page 110

Stetka, J., Luzna, P., Lanikova, L., Koralkova, P., Gursky, J., Hodny, Z., S., Bartek, J., Divoky, V., 2017. JAK2 V617F Progenitors Utilize Adaptations to Cell-Autonomous and Microenvironment-Dependent Inflammatory Stress in Polycythemia Vera, Likely Exhibiting Barrier Against Rapid Transformation to Myelofibrosis. Blood 130, (Supplement 1): 1667

Aim 3 Characterize inflammation-induced oxidative stress and how it fosters DNA damage response activation in progression of PV.

As evidenced in previous aims (2.1 and 2.2) and presented publication record, essential factors in MPN initiation and long-term disease evolution are inflammation and aging (Hasselbalch et al., 2015; Lussana and Rambaldi, 2017). Increasing evidence suggests that *JAK2* V617F is relatively frequent in the aging healthy population (Genovese et al., 2014; Jaiswal et al., 2014; Xie et al., 2014), and it is possible, that chronic inflammation precedes acquisition of the somatic *JAK2* V617F leading to clonal hematopoiesis (Perner et al., 2019). Given the long and stable clinical course of chronic indolent phase of *JAK2* V617F$^+$ PV (Klampfl et al., 2011; Tefferi et al., 2014), where, despite inflammatory microenvironment and oncogene-driven myeloproliferation the frequency of transformation is relatively low (Tefferi, 2016), we hypothesized that presence of fail-safe mechanisms, related to DDR serve as a barrier that either delays or prevents progression to myelofibrosis or leukemia.

We have therefore decided to better characterize inflammation-evoked oxidative stress and DDR along the progression of PV using patient-specific iPSCs, alongside with genetically modified *JAK2* V617F-positive or *JAK2* wildtype HEL cells as well as immunohistochemistry staining of PV patients' bone marrow.

The *JAK2* V617F$^+$ CD34$^+$ P-ECs limit production of ROS and hyperactivate ROS buffering system

Overproduction of ROS upon inflammation insults is an important source of oxidative stress, DNA damage, increased genomic flux and related cellular senescence or death (Blaser et al., 2016; Hubackova et al., 2016, 2012). It was previously shown that acquisition of *JAK2* V617F mutation induces inflammation and accumulation of ROS in HSC compartment of knock-in mouse model and *ex vivo* cultured CD34$^+$ patient stem cells isolated from periphery (Marty et al., 2013). Recently measurement of ROS levels later in hematopoietic differentiation program did not show elevated levels of ROS at baseline or following stimulation with inflammatory mediators in leukocytes *of Jak2* V617F knock-in mouse model and/or MPN patients (Craver et al., 2020). To reconcile the apparent paradox of inflammation-driven oxidative stress in V617F$^+$ HSCs and early progenitors with the latent clinical course and cytogenetic stability characteristic (Klampfl et al., 2011; Tefferi et al., 2014) we hypothesized that the *JAK2* V617F$^+$ progenitors must utilize antioxidant buffering systems to avoid genotoxic effects of oxidative stress.

In order to study ROS levels and kinetics of ROS production/accumulation, we have used CellROX fluorogenic probe in various time points after treatment with inflammatory cytokines. We have detected differences in the amplitudes and kinetics of ROS between *JAK2* wt and V617F^{+} CD34^{+} P-ECs, with wildtype cells gradually increasing ROS levels after treatments with IFNγ alone or in combination with other cytokines, unable to detoxify cells of ROS after 24-hour time point (Figure12A). V617F^{+} CD34^{+} P-ECs however, exhibited less steep rise in ROS levels over time, with significant drop between 12 and 24-hour time point, restoring ROS levels even under initial values (Figure12A). Despite highly constrained levels of ROS in *JAK2* V617F^{+} progenitors, the total rates of ROS were maintained at relatively high levels, compared to wildtype progenitors (Figure 12B), resembling many types of malignancies, where elevated ROS levels promote many aspects of cancer development and progression (Aggarwal et al., 2019; Kwon et al., 2004; Salmeen et al., 2003; Seth and Rudolph, 2006).

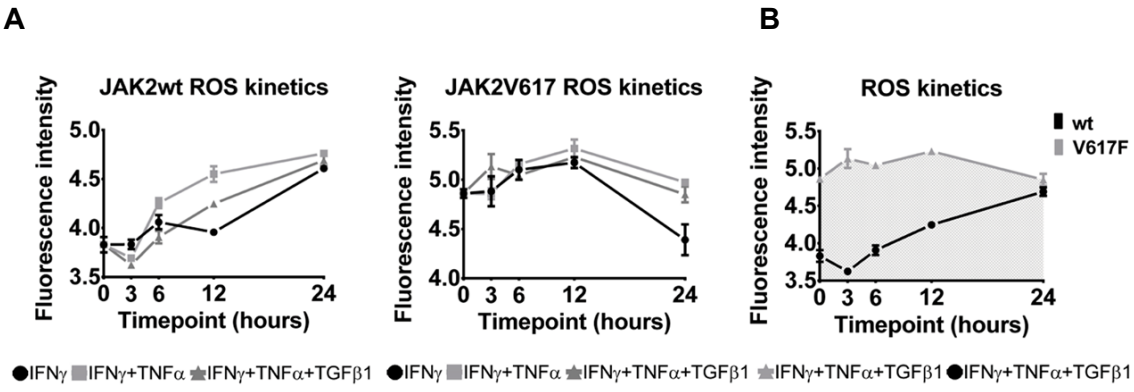

Figure 12: Effect of defined combinations of inflammatory cytokines on kinetics of ROS production in *JAK2* wt and V617F^{+} CD34^{+} P-ECs. **A** Charts present different amplitudes of ROS production between *JAK2* wt and V617F^{+} cells respectively as a mean ± SD (n= 3) of samples' fluorescence intensities upon treatment with inflammatory cytokines for 3, 6, 12, and 24 h. **B** Chart is depicting higher but stable levels of ROS in V617F^{+} CD34^{+} P-ECs treated with inflammatory cytokines.

To analyze if the tightly regulated levels of ROS accumulation in *JAK2* V617F^{+} CD34^{+} P-ECs are associated with increased activity of antioxidant buffering system we have measured, activity of antioxidant enzymes, glutathione reductase (GR), glucose-6-phosphate dehydrogenase (G6PD), hexokinase (HK) and glutathione peroxidase (GPx), and gluconolactone dehydrogenase (GLD) in cellular lysates. We have detected significantly increased intrinsic activity of GR, G6PD and HK in *JAK2* V617F^{+} CD34^{+} P-ECs, compared to *JAK2* wt cells (Figure 13A). Activity of these enzymes was further increased upon treatment with inflammatory cytokines in both genotypes, however much higher in V617F^{+} cells (Figure 13A). This was reflected in a significantly increased total

antioxidant capacity of the *JAK2* V617F^{+} CD34^{+} P-ECs when compared with the *JAK2* wt controls (Figure 13B).

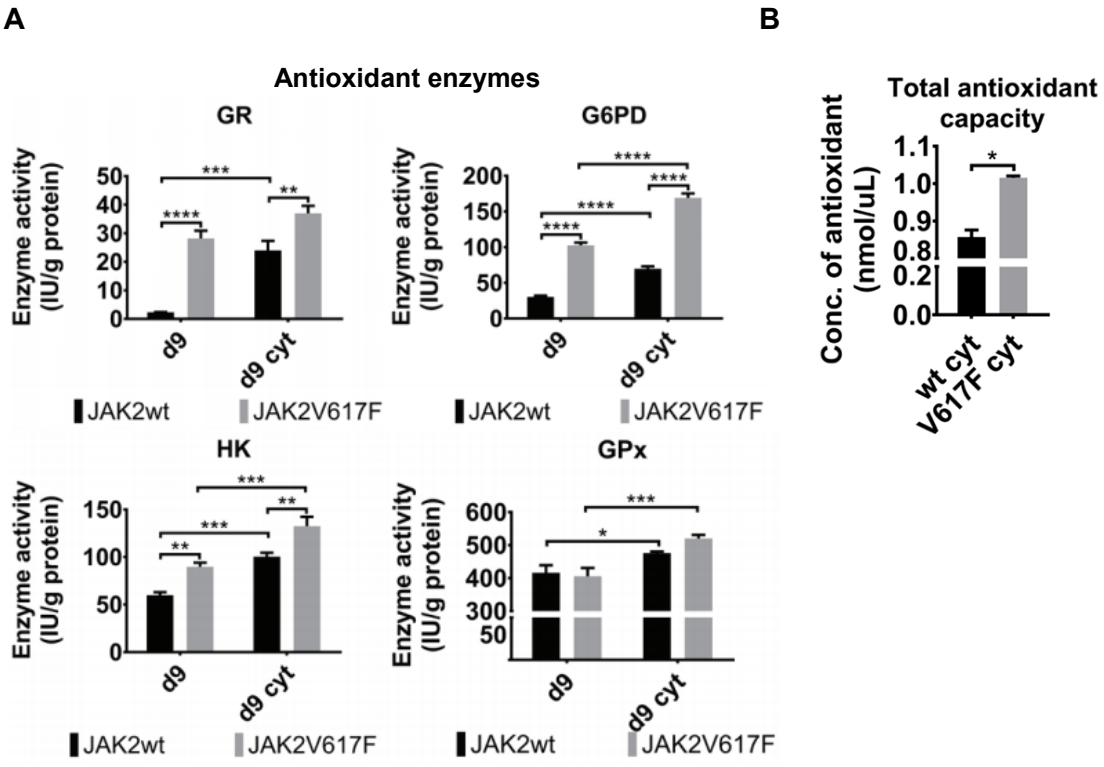

Figure 13: A Bar graphs show mean ± SD (n=3) of antioxidant buffering system enzymes activity (glutathione reductase (GR), glucose-6-phosphate dehydrogenase (G6PD), hexokinase (HK) and glutathione peroxidase (GPx)) either in untreated (d9, in day 9 of differentiation) or inflammatory cytokine treated (d9 cyt) JAK2 wt and V617F^{+} CD34^{+} P-ECs. **P ≤ 0.05, **P ≤ 0.01, ***P ≤ 0.001, ****P ≤ 0.0001,* two-way ANOVA. **B** Bar graph depicts total antioxidant capacity presented as a concentration of antioxidant ± SD (n = 2) in *JAK2* wt and *JAK2* V617F^{+} CD34^{+} P-ECs treated with inflammatory cytokines for 24 h. *P ≤ 0.05, unpaired Student's t-test (two-tailed).

Moreover, analysis of whole-transcriptome revealed differentially upregulated expression of key components of antioxidant defense system in *JAK2* V617F^{+} CD34^{+} P-ECs. Expression of peroxiredoxins, cyclooxygenases, thioredoxins, and catalase were intrinsically upregulated in the *JAK2* V617F^{+} CD34^{+} P-ECs (Figure 14).

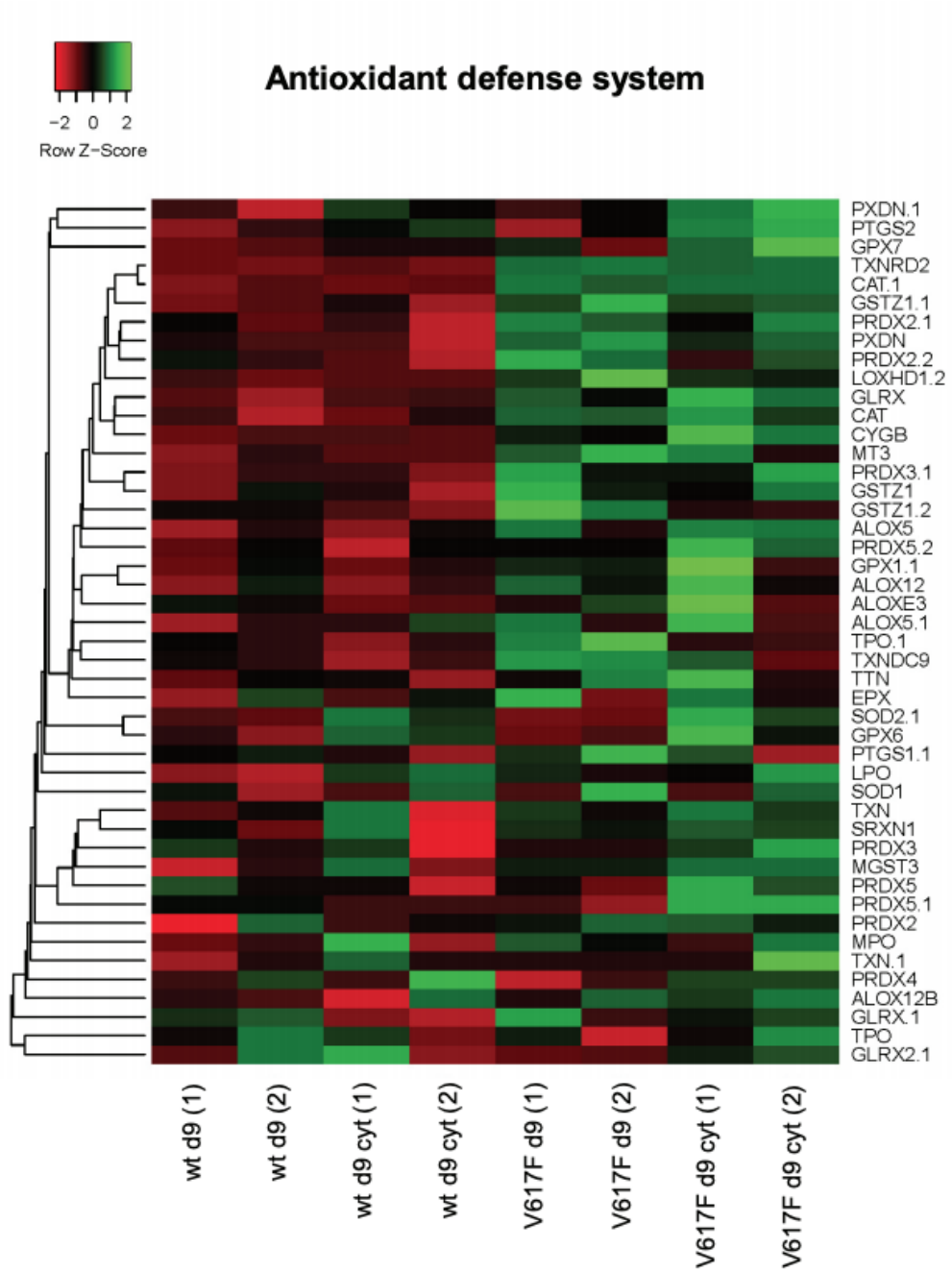

Figure 14: Heatmap of antioxidant defense system gene set (n = 33; https://www.qiagen.com/ca/shop/pcr/primer-sets/rt2-profiler-pcr-arrays/?catno=PAHS-065Z#geneglobe) expression in untreated (d9) and inflammatory cytokine treated (d9 cyt) *JAK2* wt and *JAK2* V617F^{+} CD34^{+} P-ECs. Columns represent individual samples in experimental duplicates (1, 2).

Collectively these results suggest increased intrinsic and induced ROS buffering capacity of *JAK2* V617F^{+} progenitors by overexpressing and hyper-activating cellular anti-oxidative enzymes, which are helping to keep delicate balance of elevated

intracellular ROS levels, required for propagation of malignant clone in inflammatory conditions.

PV cells are protected against accumulation of inflammation-evoked DNA damage

As discussed previously some studies suggested increased inflammation-evoked oxidative-DNA damage in the *JAK2* V617F hematopoietic compartment (Lundberg et al., 2014; Marty et al., 2013; Plo et al., 2008), a result at odds with increased buffering capacity of *V617F*$^{+}$ cells presented in previous section and known disease course (Klampfl et al., 2011; Tefferi et al., 2014).

Therefore, to better understand how *JAK2* V617F-mutation causes oncogenic stress and modulate responses to inflammation-evoked DNA damage in BM progenitors, we first analyzed the overall degree of DDR activation in BM sections from patients at different PV disease stages. We have observed very low levels of DNA damage in proliferative stage of PV, marked by barely detectable global DNA damage marker Ser 139-phosphorylated histone H2AX (γH2AX), with positivity increase in MF-1/2 and highest levels in MF-3 (Figure 15). The same applied for oxidative DNA damage marker 8-oxoguanine (8-oxoG), which was detectable only in megakaryocytes of MF-3 (Figure 15). Our staining also revealed constitutive presence of auto-phosphorylated form of ataxia-telangiectasia, mutated (ATM) protein (pATMS1981) and ataxia telangiectasia and Rad3-related protein (pATRT1989) (Figure 15). While pATRT1989 was localized mainly in nucleus, pATMS1981 was detectable predominantly in cytoplasm, suggesting activation by ROS a mechanism not necessarily involving DNA double strand breaks as published before (Alexander and Walker, 2010; Guo et al., 2010; Kozlov et al., 2016). That being the case, staining of BM sections suggested a minor level of oxidative and replication-induced stress, not crossing genotoxic levels, which would be converted into double-strand DNA breaks and concomitant increase in γH2AX positivity throughout proliferative stage of PV.

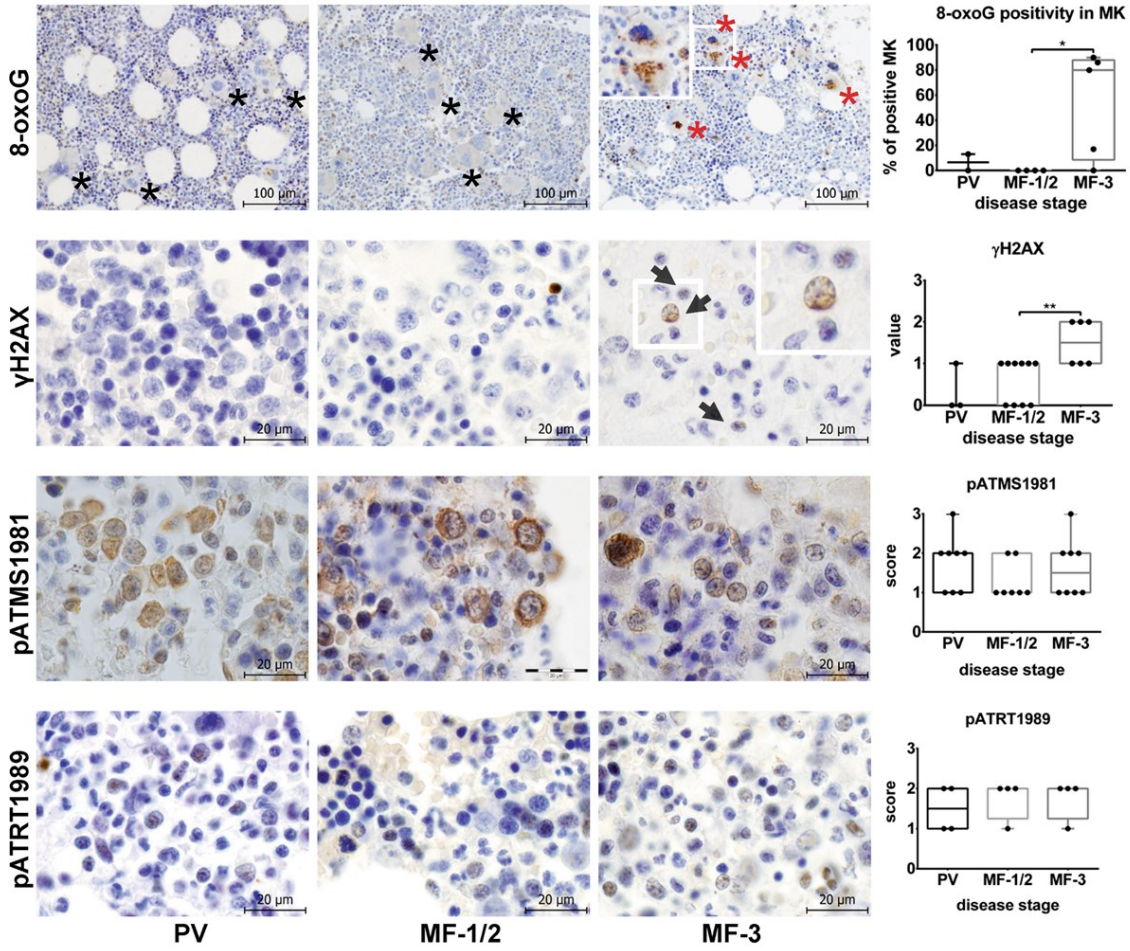

Figure 15: Representative Immunohistochemistry staining's of patient BM sections for DNA damage, oxidative stress and DDR markers along the progression of PV to MF-1/2 and post-PV MF-3. Red asterisks in 8-oxoguanine (8-oxoG) staining denote positive megakaryocytes (MKs), black asterisks mark negative MKs; scale bar, 100 µm. Inset in γH2AX staining magnifies cells stained positive for γH2AX nuclear foci; scale bar, 20 µm. pATMS1981 staining show cytoplasmic localization of antigen compared to pATRT1989 nuclear positivity; scale bars, 20 µm. Boxplots show score based on quantification of the number of cells expressing indicated markers. *P ≤ 0.05, **P ≤ 0.01, Mann–Whitney test.

We next examined whether we can also detect observed protection against DNA damage accumulation in HSCs and early progenitors of our *JAK2* wt and V617F^{+} CD34^{+} P-ECs. In line with *in vivo* results, immunostaining of embryoid bodies from CD34^{+} P-ECs embedded into paraffin revealed absence of mutagenic 8-oxoG in V617F^{+} EBs even after treatment with inflammatory cytokines, while *JAK2* wt EBs accumulated cells positive for this marker upon treatment (Figure 16).

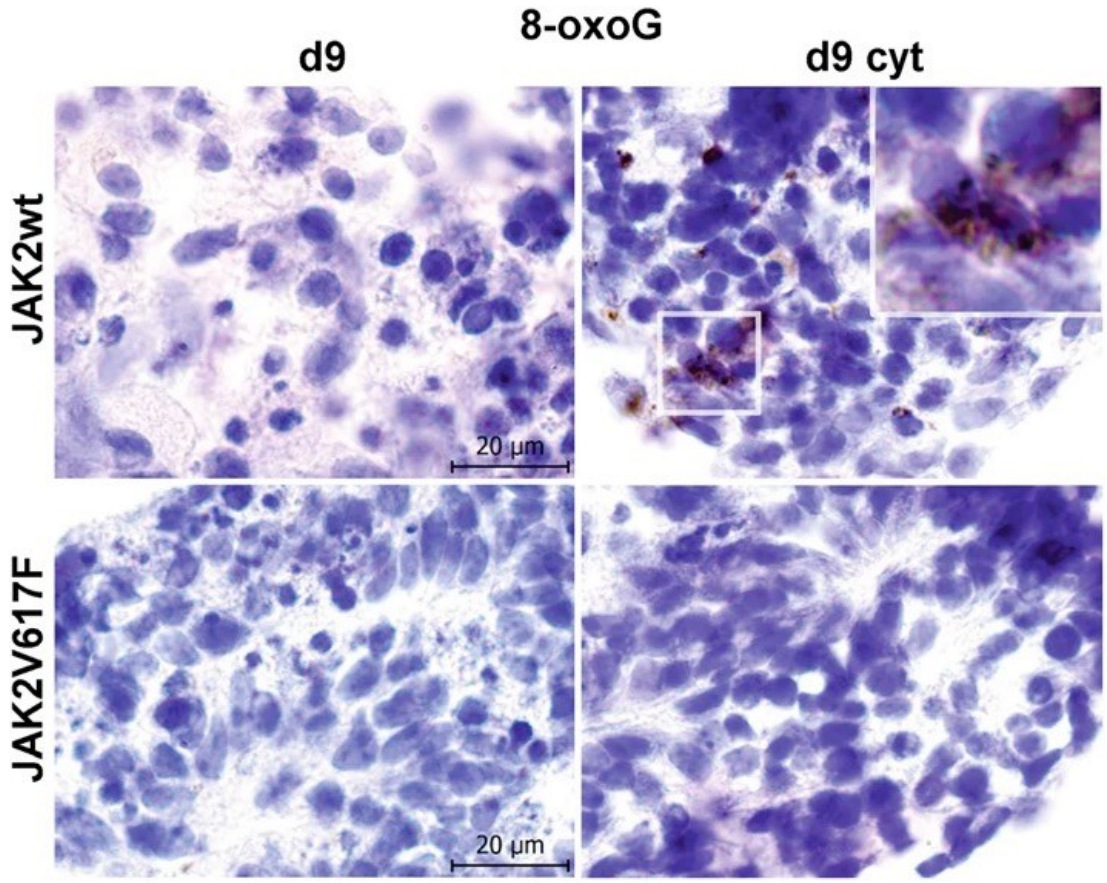

Figure 16: Immunocytochemistry staining for 8-oxoG on *JAK2* wt and V617F$^+$ CD34$^+$ P-ECs in agarose gel matrix saturated with paraffin; untreated in day 9 of differentiation (d9) or treated with inflammatory cytokines (d9 cyt). Inset magnifies positive cells for the antigen.

Further assessment of DDR by immunocytochemistry for γH2AX confirmed lack of excessive DNA damage accumulation (fewer γH2AX foci in nucleus) in the *JAK2* V617F$^+$ CD34$^+$ P-ECs treated with various combinations of inflammatory cytokines, compared with *JAK2* wt cells (Figure 17). Excessively used homologous recombination (HR), denoted by increased RAD51 foci presence, have been previously demonstrated on *hEPO*$^+$ V617F$^+$ Ba/F3 cell line. As HR, might provide essential support for highly-replicating cells in inflammatory BM micromilieu, these results prompted us to test if our *JAK2* V617F$^+$ CD34$^+$ P-ECs use HR to higher extent than wt cells. In our dual staining for nuclear γH2AX/RAD51, with sequential primary-Abs staining (Bennett et al., 2009) assessment of RAD51 recruitment to DNA damage sites, marked by γ-H2AX foci as a readout of HR efficiency have not showed significantly altered RAD51 recruitment to these sites (Figure 17). Rather RAD51 foci presence followed the trends of γH2AX

accumulation after treatment by inflammatory cytokines, suggesting intact regulation of HR.

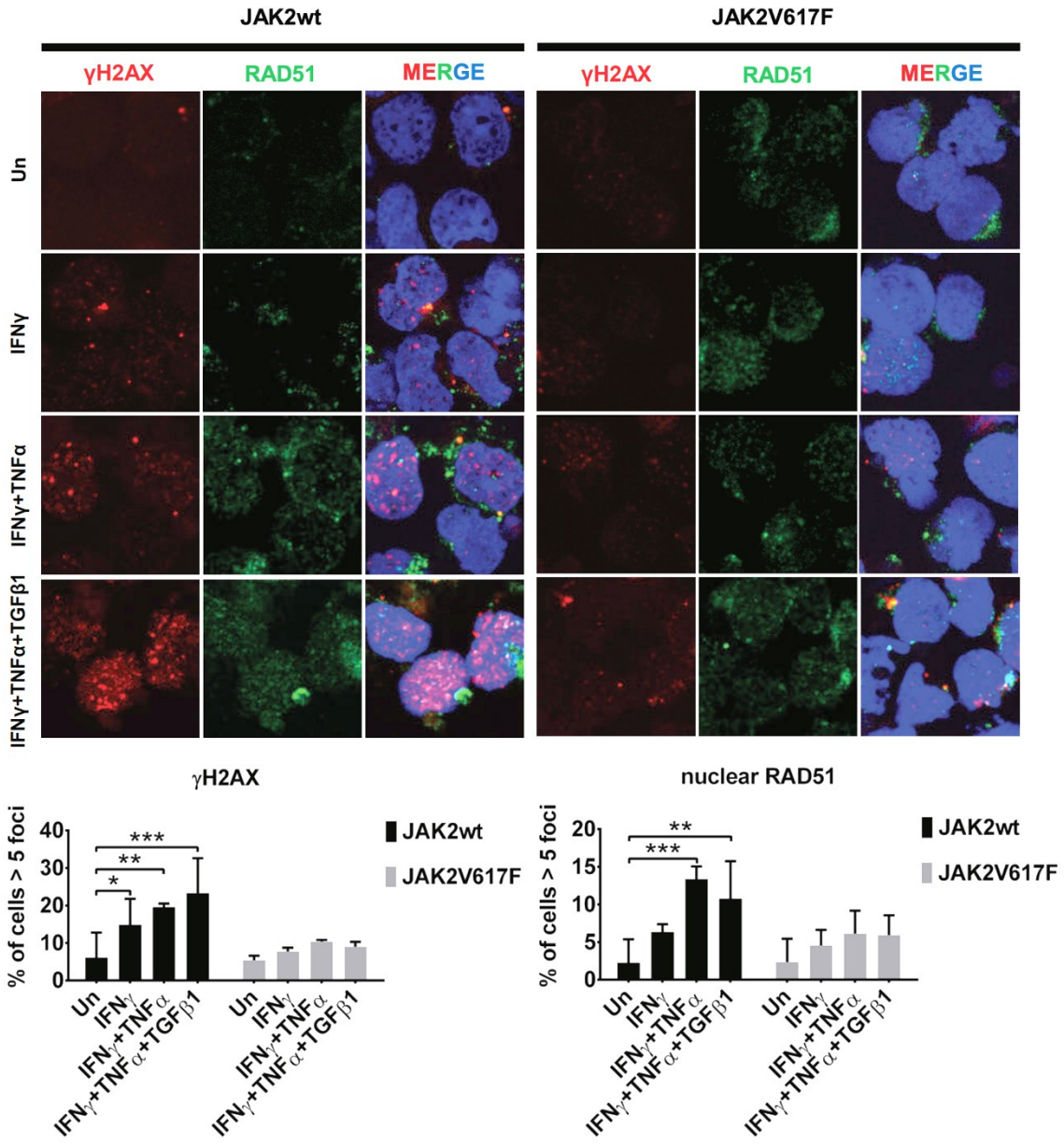

Figure 17: Immunocytochemistry staining for DNA damage marker γH2AX (red) and DDR marker RAD51 (green) on day 9 *JAK2* wt and *JAK2* V617F$^+$ CD34$^+$ P-ECs, either untreated (Un) or treated with various combinations of inflammatory cytokines. Charts show percentage of cells ± SD (n=3) with more than five γH2AX or RAD51 foci per cell in nucleus. **P≤0.05, **P ≤ 0.01*, ****P ≤ 0.001,* two-way ANOVA

To determine if the inflammatory-primed *JAK2* V617F$^+$ CD34$^+$ P-EC cells can also induce bystander DNA damage by secreted factors to *JAK2* wt cells and thus possibly promote clonal dominance of *V617F*$^+$ cells *in vivo*, we have collected conditioned media from *JAK2* V617F$^+$ CD34$^+$ P-ECs and used it for cultivation of *JAK2* wildtype cells for 24 hours,

with subsequent measurement of γH2AX and RAD51 foci presence. Even though not statistically significant due to variations of γH2AX/RAD51 foci basal levels, we have observed increase in γH2AX and RAD51 foci in JAK2 wt cells after treatment with conditioned media in each experimental replicate (Figure 18). These data indicate further increase in relative growth advantage of *JAK2* V617F^{+} cells over *JAK2* wt cells not only through increase in oncogene-dependent proliferation but also through cell-extrinsic inflammation-evoked mechanisms.

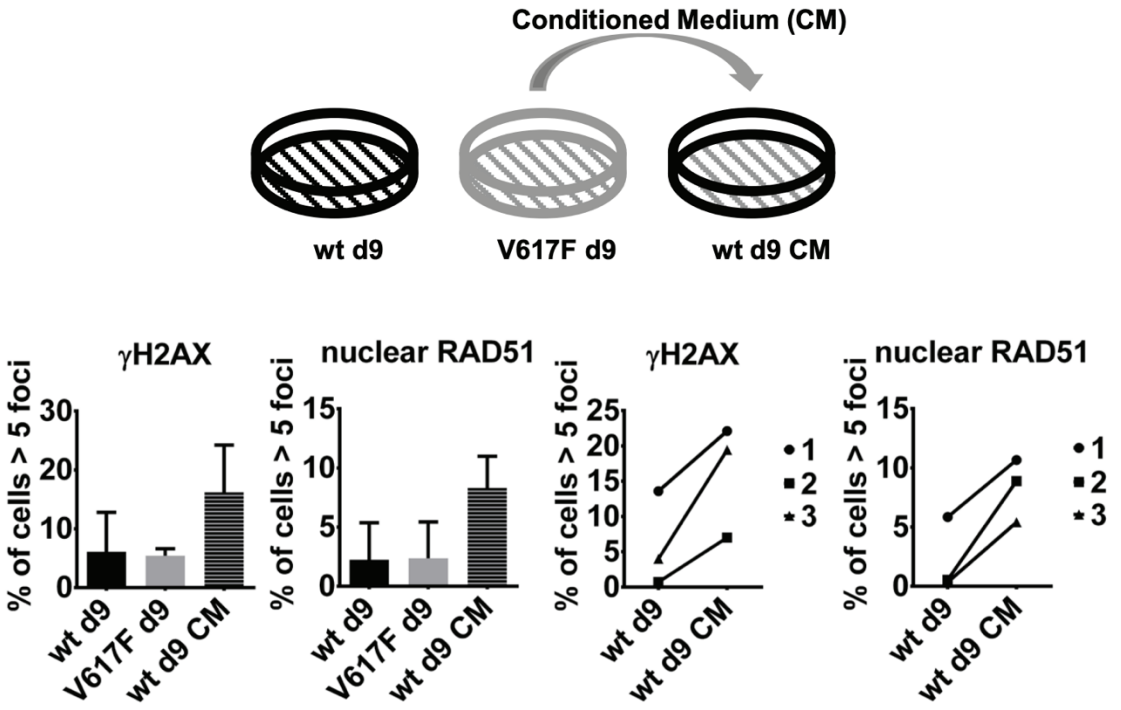

Figure 18: *JAK2* V617F^{+} CD34^{+} P-ECs (V617F d9) induce paracrine DNA damage through conditioned medium (CM) used for treatment of day9 *JAK2* wt CD34^{+} P-ECs (wt d9) for 24 h. Bar charts and before-after graphs present percentages of cells ± SD (n=3) with more than five γH2AX or RAD51 foci per cell in nucleus.

To study how is the protection against DNA damage accumulation reflected on the global regulation, we have analyzed expression of DNA damage response gene set and associated DDR categories (Pearl et al., 2015). We have found statistically significant decrease in expression of single-strand break repair genes in *JAK2* V617F^{+} CD34^{+} P-ECs (Figure 19A,B), pointing towards protection up-stream of these genes, most likely with contribution of increased ROS buffering system activity.

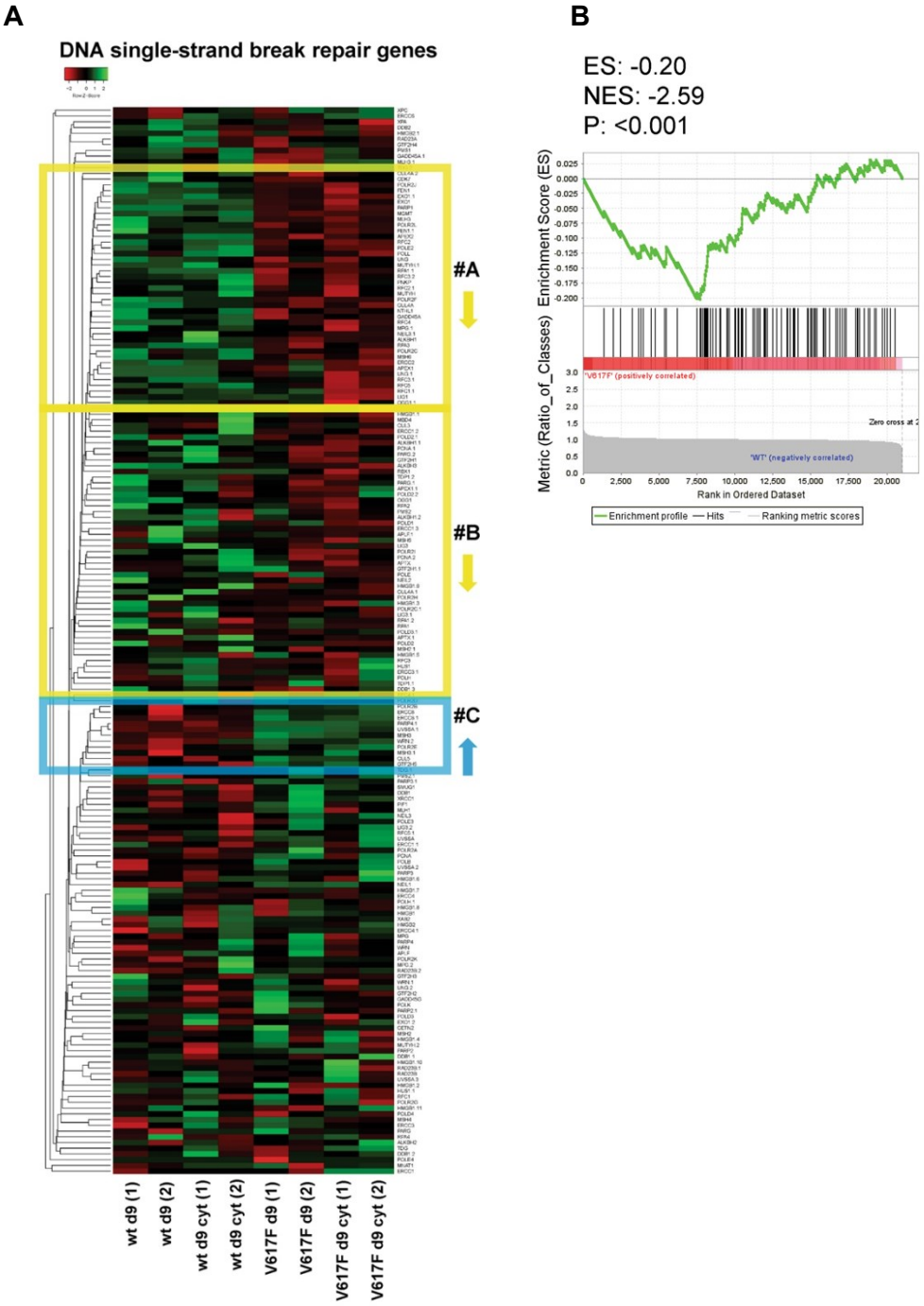

Figure 19: **A** Heatmap of single-strand repair gene set (Pearl et al., 2015) expression in day 9 *JAK2* wt and *JAK2* V617F$^+$ CD34$^+$ P-ECs, untreated (d9) or treated with inflammatory cytokines (d9 cyt). Two biological replicates (1, 2) were used for each condition. Clusters of differentially downregulated genes in V617F$^+$ samples are highlighted by two yellow boxes with low variance between experimental duplicates (#A) and higher variance (#B). Cluster of genes upregulated between experimental duplicates in V617F$^+$ samples with low variance is delineated by blue box (#C). **B** Gene set enrichment (GSEA) plot of single-strand repair genes from d9 cyt *JAK2* V617F$^+$ and *JAK2* wt CD34$^+$ P-ECs.

Absence of significant DDR upon oncogenic signaling in the presence of inflammatory factors in *JAK2* V617F$^+$ HSCs of CD34$^+$ P-ECs and patient BM sections suggest creation of a barrier preventing checkpoint signaling and cell cycle arrest. Therefore, to study how are sub-threshold levels of DNA damage relayed to cell cycle machinery, we have decided to use dual pulse labelling with propidium iodide and BrDU incorporation on synchronized *JAK2* V617F$^+$ and wt CD34$^+$ P-ECs cells by 12 hours growth factors withdrawal (experimental set-up and time course is further described in materials and methods and Figure 20A). As presented in Figure 20B, *JAK2* V617F$^+$ cells have higher proliferation rate, compared to wt cells, demonstrated by significantly lower percentage of cells in G0/G1 phase and more cells in S-phase as a result of oncogene driven propagation. Treatment with inflammatory cytokines decreased number of cells undergoing S-phase more significantly in wt cells, compared to V617F$^+$ cells, with concomitant increase in G2/M populations (Figure 20B). Moreover, we have harvested protein lysates from each biological replicate used for cell cycle analysis which showed reduced activation of important checkpoint signaling nodes in *JAK2* V617F$^+$ CD34$^+$ P-ECs, as evidenced by lack of p53 and Chk1 activation, compared to robust *JAK2* wt responses (Figure 21). These results complement our data on low ATR/ATM signaling in PV patient BMs, suggesting that inflammatory factors induce only moderate degree of oxidative stress (buffered by ROS buffering system) and DDR signaling in *JAK2* V617F$^+$ cells, compatible with more dynamic cell cycle progression of PV cells in the latent proliferative stage, protecting cells from signaling that could eventually trigger cell cycle arrest and senescence.

A

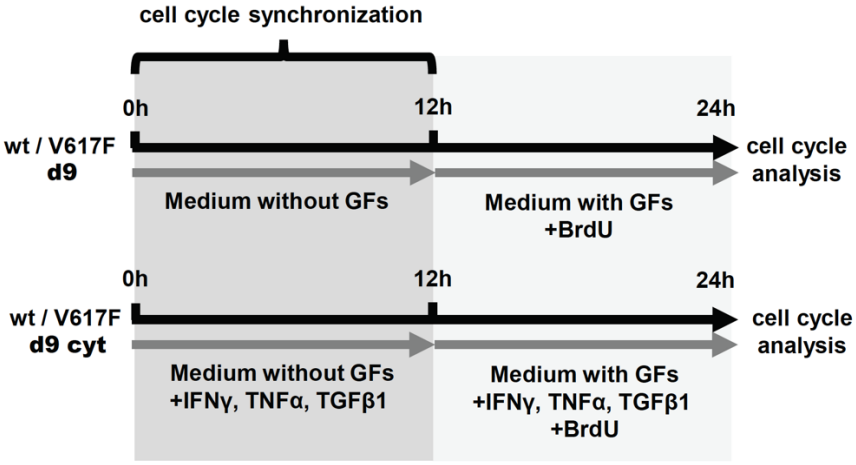

B

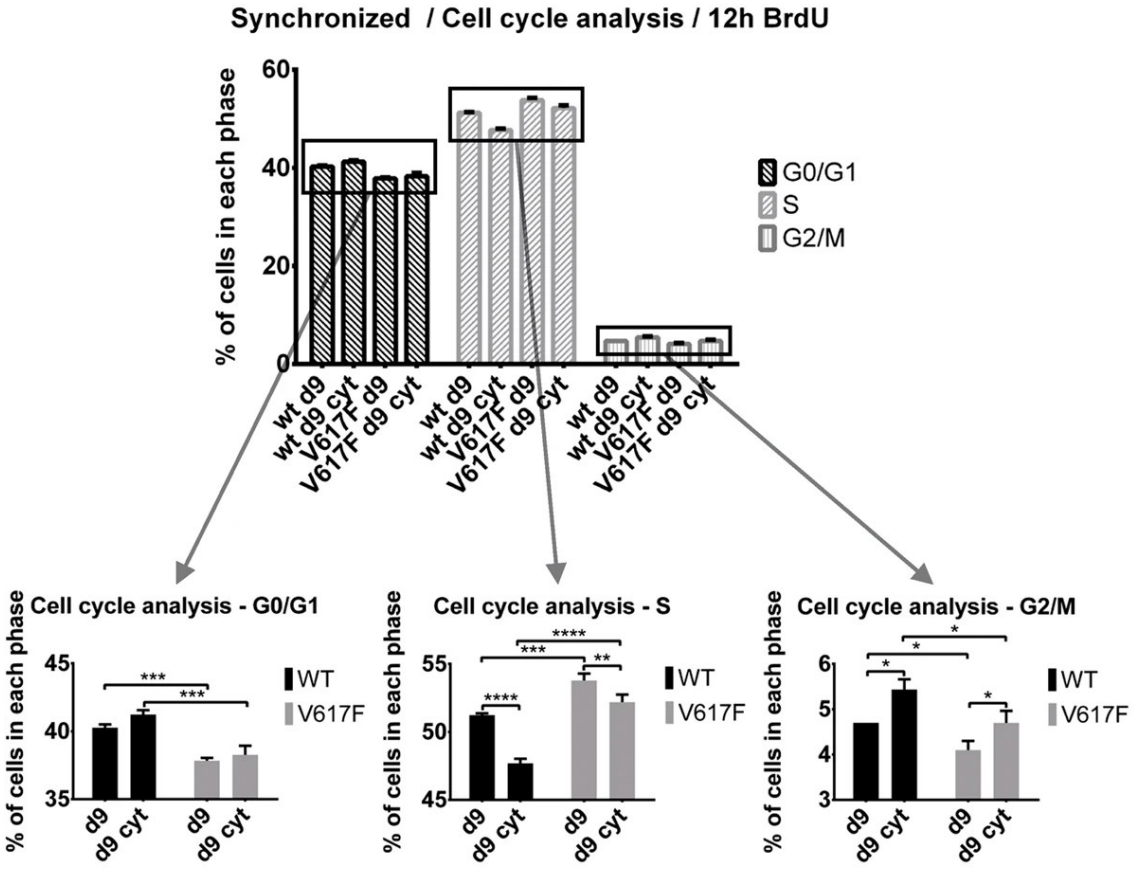

Figure 20: **A** Time course scheme for CD34⁺ P-EC cell cycle synchronization. Growth factors (GFs) were (*top*) / were not (*down*) removed from medium, followed by dual pulse chase labelling with propidium iodide and BrdU incorporation. **B** Cell cycle analysis of synchronized cells by dual pulse labelling with propidium iodide and BrDU incorporation. Charts showing percentage ± SD (n=3) of *JAK2* wt (WT) and *JAK2* V617F⁺ (V617F) CD34⁺ P-ECs cells in each phase of cell cycle, either untreated (Un) or after treatment with inflammatory cytokines (Cyt). *P≤0.05, **P ≤ 0.01, ***P ≤ 0.001, ****P ≤ 0.0001.

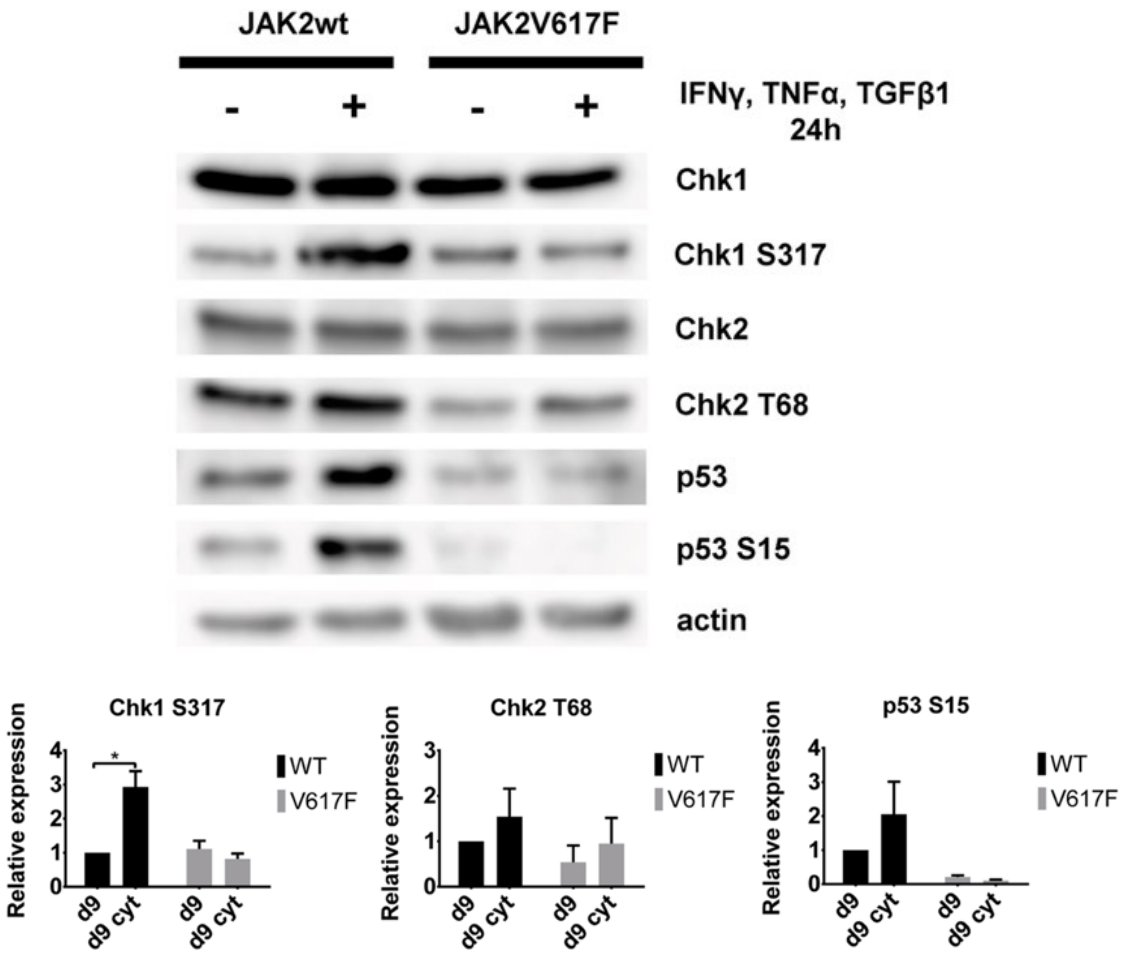

Figure 21: Representative western blots of checkpoint proteins, either total or phosphor-form/active from protein lysates of synchronized day 9 differentiated *JAK2* wt and *JAK2* V617F^{+} CD34^{+} P-ECs. Charts show relative expression (mean ± SD, n = 2) of proteins phosphor-form normalized to actin. *P ≤ 0.05, two-way ANOVA.

Overexpression of DUSP1 facilitates survival and proliferation of *JAK2* V617F^{+} cells in inflammatory conditions

Essential signaling junction governing cellular responses upon inputs from DDR and inflammatory signaling involves stress-activated protein kinases (SAPKs) from MAPK superfamily (Lee et al., 2018). Main SAPKs components, Jun kinases (JNKs) and p38MAPK, maintain balance of survival versus senescence and apoptosis based on amount of signaling inputs in inflammatory microenvironment (Arthur and Ley, 2013; Iwasa et al., 2003; Karigane et al., 2016), vital even in MPN hematopoiesis (Lu et al., 2010). We have, therefore, hypothesized that observed intrinsic protection of the PV

progenitors against inflammation-evoked DNA damage involves suppression of SAPKs signaling.

We have detected differential and global transcriptional overexpression of Dual-specificity MAPK phosphatases (MKPs or DUSPs) in our *JAK2* V617F^{+} CD34^{+} P-ECs (Figure 22), which dephosphorylate and thus inactivate different MAPK isoforms (Kidger and Keyse, 2016). This included key spatiotemporal modulators of p38MAPK/JNK pathway activity, DUSP1, 8 and 16 (Kidger and Keyse, 2016), present in intrinsically upregulated cluster of genes (cluster #A; Figure 22) of *JAK2* V617F^{+} CD34^{+} P-ECs. Among those *DUSP1*, known NF-κB target (Zhou et al., 2003), was already published to have important prosurvival roles in CML pathogenesis and resistance to TKIs and was suggested to play pivotal role also in protection of V617F compartment (Kesarwani et al., 2018, 2017).

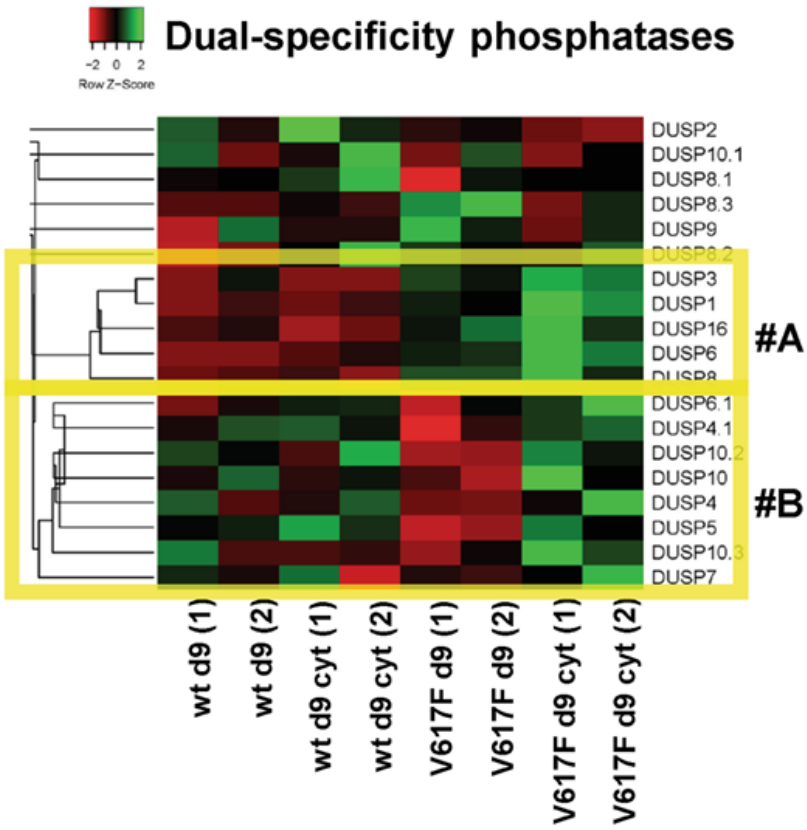

Figure 22: Heatmap representation and accompanied cluster analysis of dual-specificity phosphatase (DUSP) family genes expression in untreated (d9) and inflammatory cytokine treated (d9 cyt) *JAK2* wt and *JAK2* V617F^{+} CD34^{+} P-ECs (n=2 per group). Cluster #A consists of intrinsically upregulated DUSPs, while cluster #B contains DUSPs upregulated in d9 cyt *JAK2* V617F^{+} CD34^{+} P-ECs. Heatmap was clustered by using Kendall's Tau Distance Measurement Method and Centroid Linkage Clustering Method.

We have therefore sought to further investigate intrinsic and induced overexpression of DUSP1 at the protein level, where we confirmed overexpression of DUSP1 in *JAK2* V617F^{+} CD34^{+} P-ECs, further increased upon treatment with inflammatory cytokines (Figure 23A), and detected constitutive presence of DUSP1 in PV patient BMs across disease stages (Figure 23B).

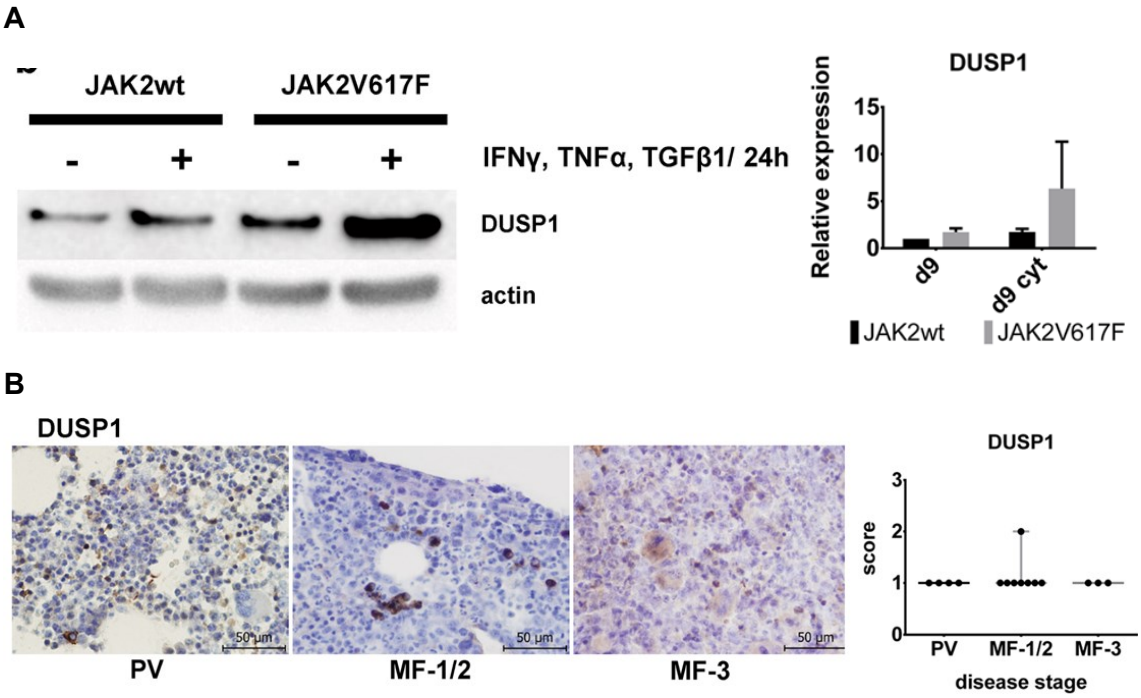

Figure 23: **A** Representative western blot of DUSP1 from lysates of untreated (d9) or inflammatory cytokine treated (d9 cyt) *JAK2* wt and *JAK2* V617F^{+} CD34^{+} P-ECs. Bar graph shows relative expression of DUSP1 protein normalized to actin (n=3). **B** Representative IHC staining of DUSP1 on patient BM sections along the progression of PV. Scale bar, 50 µm. Boxplot shows quantification of the DUSP1 expressing cells.

In order to functionally probe the role of DUSP1 in *JAK2* V617F^{+} cells, my colleague Dr. Lucie Láníková (Department of Biology, Faculty of Medicine and Dentistry, Palacky University Olomouc and Laboratory of Cell and Developmental Biology, Institute of Molecular Genetics of the ASCR) generated corrected/edited HEL cell line (*JAK2* wt) from parental *JAK2* V617F^{+} HEL cells (human erythroleukemia cell line; HELV617F; kind gift of T. Stopka lab, 1st Faculty of Medicine, Charles University Prague), which was repaired by homologous recombination using CRISPR/Cas9 system (CRISPR construct pXPR_001 plasmid (Addgene plasmid #49535). To functionally compare HEL-edited cells to their parent counterparts, a luciferase assay was performed by electroporating the clones with pGRR4-Luc luciferase reporter and the transfection control Renilla. HEL-edited cells exhibited statistically significant decrease of JAK2 mRNA and protein

expression compared to the parental clone (Figure 24). As a result, STAT5 was phosphorylated less while the total amount of STAT5 remained the same as shown by immunoblotting (Figure 24).

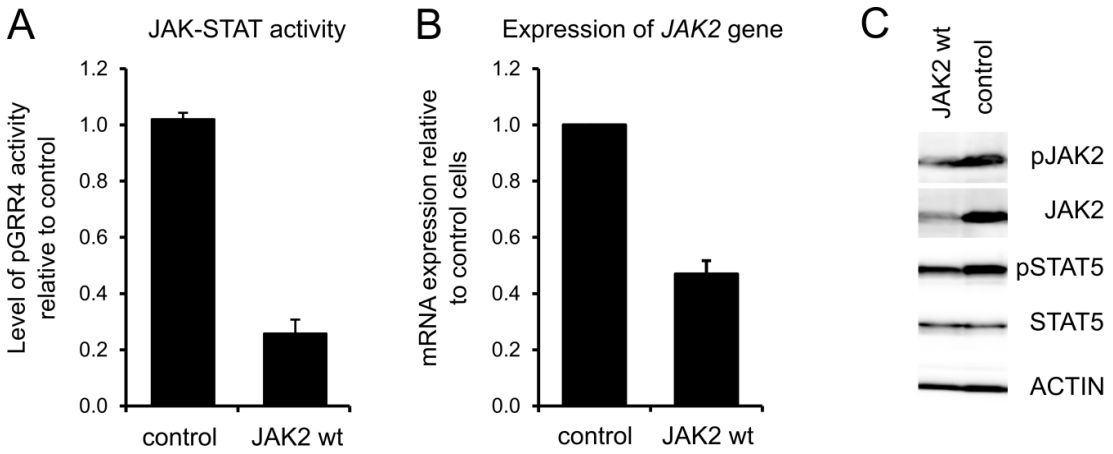

Figure 24: Functional characterization of HELV617F (*JAK2* V617F^{+}; control) and HEL-edited cells (*JAK2 wt*). **A** Bar graph showing luciferase assay readout after electroporating the HELV617F (control) and HEL-edited cells (*JAK2 wt*) with pGRR4-Luc luciferase reporter and the transfection control - Renilla. **B** Bar graph showing relative mRNA expression of *JAK2* in HELV617F and HEL-edited cells **C** Representative western blot of phosphorylated and total JAK2 protein and its downstream target STAT5 in HELV617F (control) and HEL-edited cells (*JAK2 wt*).

Upon correction of *JAK*2 allele to the wt constitution HEL cells exhibited reduced intrinsic and inflammatory factors-induced expression of DUSP1 compared to the parental HELV617F cells (Figure 25). This prompted us to test dual-specific inhibitor BCI ((E)-2-benzylidene-3-(cyclohexylamino)-2,3-dihydro-1H-inden-1-one), which was previously published to target DUSP1 and DUSP6 (Molina et al., 2009) on HELV617F and HEL-edited cells. We have also measured expression of other BCI target DUSP6 in HEL cells, and even though we have detected more elevated DUSP6 in the HELV617F cells compared with the HEL-edited *JAK2* wt cells, DUSP6 expression after cytokine treatment significantly decreased, compared to further increase in DUSP1 expression (Figure 25). These results suggested that DUSP1 is the main target of the BCI inhibitor in these cells.

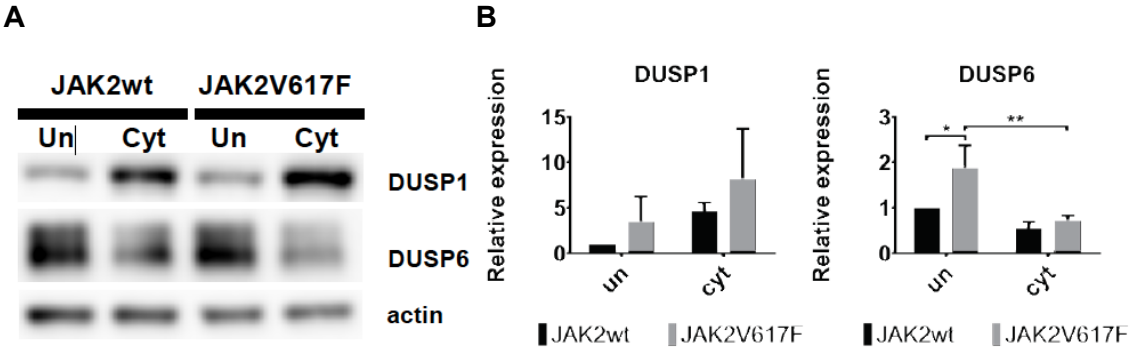

Figure 25: Representative western blot of DUSP1 and DUSP6 protein expression in HELV617F (JAK2V617F) and HEL-edited (JAK2wt) cells, which were either untreated (un) or treated with inflammatory cytokines (cyt). Accompanied bar graphs show DUSP1 and DUSP6 relative expression normalized to actin (mean ± SD, n = 3). *P ≤ 0.05, **P ≤ 0.01, two-way ANOVA.

Given the oscillatory nature of p38MAPK signaling (Zhang et al., 2017), we have first conducted extensive time-course analysis of BCI effects on p38MAPK/JNK signaling and DDR marker γH2AX accumulation in HELV617F and HEL-edited cells, which helped us to set a time-point post-BCI treatment for 1h, when we observed most extensive effects on parameters measured (Figure 26).

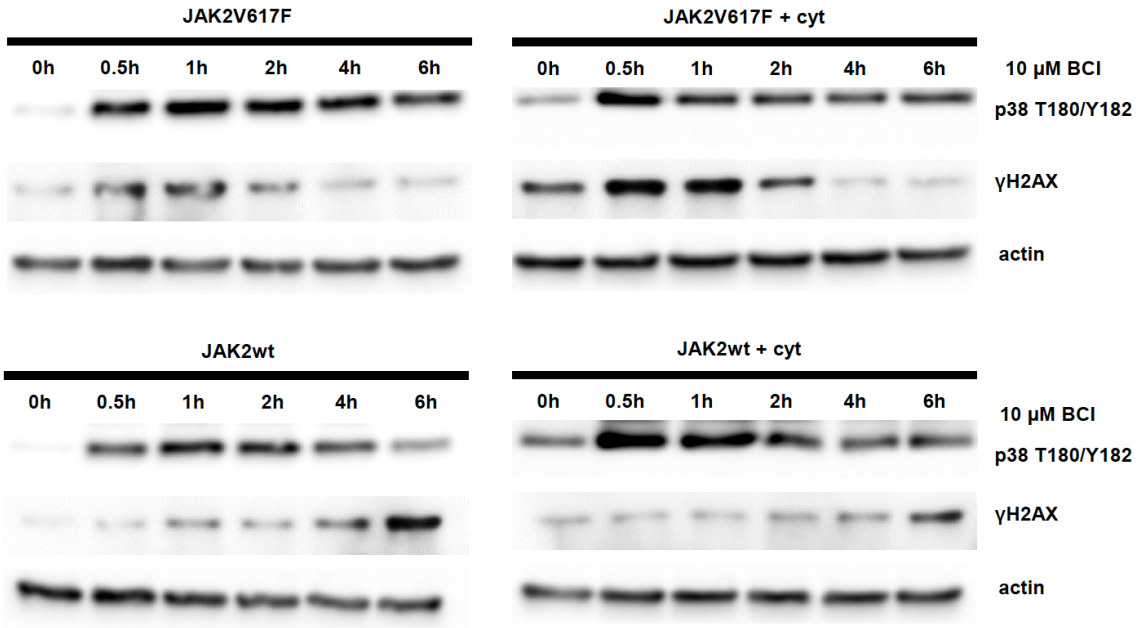

Figure 26: Representative western blot of γH2AX and Thr 180/Tyr 182-phosphorylated p38MAPK (p38 T180/Y182) in HELV617F (JAK2V617F) and HEL-edited cells (JAK2wt), either untreated or treated with inflammatory cytokines (cyt) upon exposure to 10 μM DUSP 1/6 inhibitor in various time points.

As previously published (Molina et al., 2009) and seen on our preliminary time course analysis of BCI effects (Figure 26), Thr180/Tyr182-phosphorylated p38MAPK (p38 T180/Y182) and Thr183/Tyr185-phosphorylated JNK (JNK T183/Y185) sharply increased after BCI treatment in both HELV617F and HEL-edited cells, regardless of inflammatory cytokine treatment (Figure 27). However, we have detected differential effects of BCI-induced p38MAPK/JNK reactivation on global DDR marker, γH2AX expression. Remarkably, HELV617F cells treated with BCI were much more prone to express γH2AX, compared to completely unchanged γH2AX levels in HEL-edited cells, suggesting addiction of *JAK2* V617F^{+} cells towards DUSP1 activity (Figure 27). This was accompanied by analysis of cell cycle distribution and apoptosis, which revealed that increased p38MAPK/JNK activities in HELV617F cells solely after BCI treatment corresponded to significantly more cells in G1 phase and increased apoptosis, suggesting unresolved G1 checkpoint activation (Figure 27). The HEL-edited cells accumulated DNA damage, marked by increase in γH2AX expression and increased proportion of apoptotic cells only when the BCI exposure was combined with inflammatory cytokine treatment (Figure 27).

As chemical inhibitors are known to have various disadvantages in off-targets and un-specific cytotoxicity, we have decided to verify our results from BCI treatment using validated siRNA knock-down of DUSP1 in HELV617F and HEL-edited cells. We have tested knock-down efficiency of our siRNA oligo, which proved to be efficient in significantly reducing DUSP1 expression on mRNA and protein levels (Figure 28A,B). In addition to reduced DUSP1 expression, our assessment of DDR and p38MAPK/JNK activity showed similar results to BCI inhibition with increase in p38MAPK/JNK activation, but increased DDR markers expression (γH2AX and KAP1 S824) only in HELV617F cells with accompanied G1 checkpoint activation and increase in apoptosis (Figure 28C,D).

Altogether, data from sections 2.3.1, 2.3.2 and 2.3.3 suggest that *JAK2* V617F induces cell-autonomous and non-cell autonomous IFNγ and NF-κB-associated inflammatory program, and, as a consequence, upregulates ROS antioxidant system and expression of DUSP1. Subsequently DUSP1 specifically targets JNK and p38MAPK activities to prevent accumulation of DNA damage, accelerated cell cycle arrest and apoptosis of *JAK2* V617F-positive cells. Therefore, we provide evidence that hyperactivated ROS buffering system and overexpression of DUSP1 in *JAK2* V617F-positive cells is a candidate mechanism keeping fast-cycling PV progenitors in proliferative phase despite the presence of DNA damaging inflammatory microenvironment.

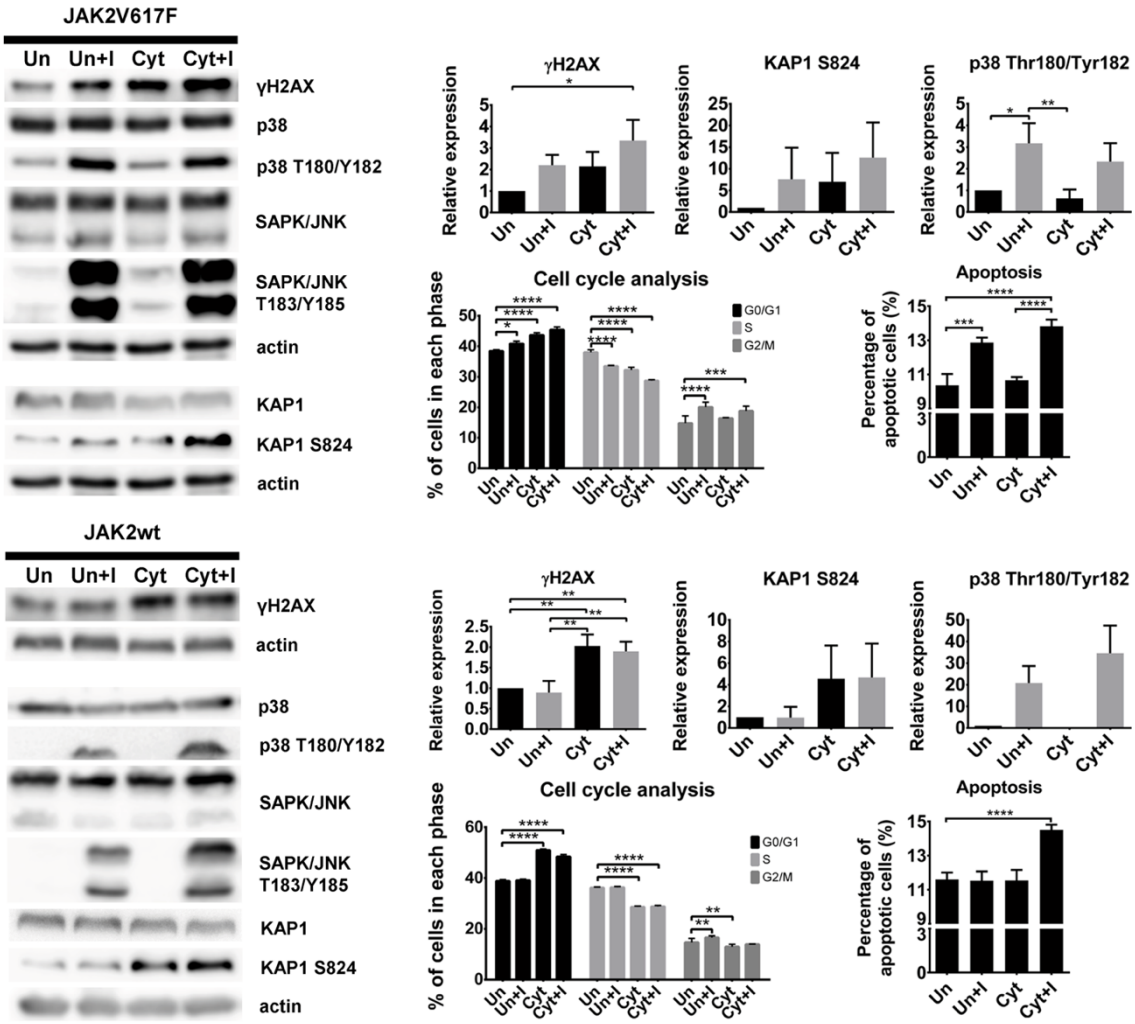

Figure 27: Western blotting of total and activated forms of DDR markers (γH2AX, KAP1) and SAPK (p38MAPK, JNK), cell cycle analysis with BrdU/PI staining and number of apoptotic cells for HELV617F cells (JAK2V617F; upper part) and HEL-edited cells (JAK2wt; lower part). HEL cells clones were either untreated (Un) or treated with inflammatory cytokines (Cyt); with or without BCI inhibitor (I). Charts show γH2AX, KAP1 S824 and p38 T180/Y182 relative expression (mean ± SD, n = 3) normalized to actin. Cell cycle analysis and apoptosis bar charts show percentage of cell numbers (± SD n=4) in each phase of cell cycle and percentage of apoptotic cells, respectively. *P ≤ 0.05, **P ≤ 0.01, ***P ≤ 0.001, ****P ≤ 0.0001, one-way (western blotting) and two-way (cell cycle and apoptosis) ANOVA.

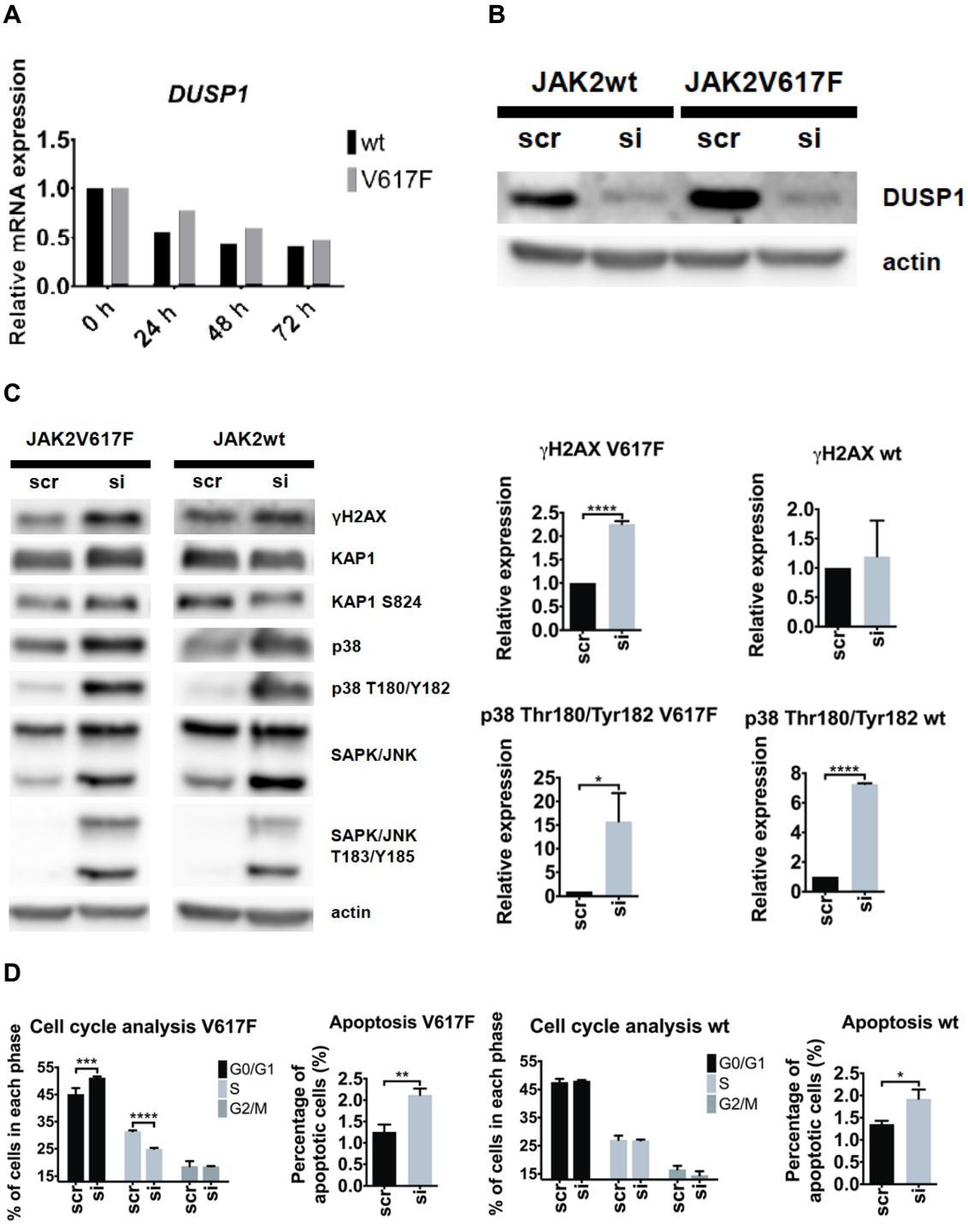

Figure 28: **A** Relative (mRNA) expression of *DUSP1* 24, 48 and 72 h-post DUSP1 siRNA transfection of HELV617F (V617F) and HEL-edited (wt) cells. **B** Representative western blot of DUSP1 protein 72 h after HELV617F (V617F) and HEL-edited (wt) cells were transfected with DUSP1 (si) or scrambled (scr) siRNA. **C** Western blot of DDR markers (γH2AX, KAP1) and SAPK (p38MAPK, JNK) in HELV617F cells (JAK2V617F) and HEL-edited cells (JAK2wt) 72h-post siRNA transfection with DUSP1 siRNA (si) and scrambled control (scr). Bar graphs show relevant γH2AX and p38 T180/Y182 protein expression

(mean ± SD, n = 3) normalized to actin. *P ≤ 0.05, ****P ≤ 0.0001, one-way ANOVA **D** Cell cycle distribution and apoptosis bar charts show percentage of cell numbers (mean ± SD; n=4) in each phase of cell cycle and percentage of apoptotic cells, respectively in HELV617F cells (JAK2V617F) and HEL-edited cells (JAK2wt) 72h-post siRNA transfection with DUSP1 siRNA (si) and scrambled control (scr).

Publications related to this aim:

Articles:

Stetka, J., Vyhlidalova, P., Lanikova, L., Koralkova, P., Gursky, J., Hlusi, A., Flodr, P., Hubackova, S., Bartek, J., Hodny, Z., Divoky, V., 2019. Addiction to DUSP1 protects JAK2V617F-driven polycythemia vera progenitors against inflammatory stress and DNA damage, allowing chronic proliferation. Oncogene 38, 5627–5642. https://doi.org/10.1038/s41388-019-0813-7

Abstracts:

Stetka, J., Luzna, P., Lanikova, L., Bartek, J., Divoky, V., 2015. Inflammatory response of hematopoietic progenitors differentiated from polycythemia vera patient-specific induced pluripotent stem cells. International Conference on the tumour microenvironment in the haematological malignancies and its therapeutic targeting, 2015, Lisbon, Portugal, abstracts, poster 24

Stetka, J., Luzna, P., Lanikova, L., Bartek, J., Divoky, V., 2015 Inflammatory response of polycythemia vera hematopoietic progenitors differentiated from patient-specific induced pluripotent stem cells. Olomouc Hematological Days, 2015, Olomouc, abstracts, ISBN 978-80-244-4697-4, page 6

Raskova Kafkova, L., Somikova, Z., Kucerova, J., Calabkova, L., Luzna, P., Stetka, J., Simkova, D., Dolezal, D., Divoky, V., 2015. Iron Chelation Reinforces DNA Damage Response and Leads to G2/M Checkpoint Activation and Autophagy in Myeloid Bone Marrow Cells of Preleukemia Mouse Model. Blood 126, 3351–3351. https://doi.org/10.1182/blood.V126.23.3351.3351

Stetka, J., Luzna, P., Lanikova, L., Koralkova, P., Hodny, Z., Prchal, J., Bartek, J., Divoky, V., 2016. JAK2 V617F progenitors exhibit intrinsic inflammatory signaling and protection against inflammation induced DNA damage. ESH 7th International Conference on MYELOPROLIFERATIVE NEOPLASMS, 2016, Estoril, Portugal, abstracts, poster 21

Stetka, J., Luzna, P., Lanikova, L., Koralkova, P., Hodny, Z., Bartek, J., Divoky, V., 2016. JAK2 V617F progenitors exhibit intrinsic inflammatory signaling and protection against inflammation induced DNA damage. Olomouc Hematological Days, 2016, Olomouc, abstracts, ISSN 1213-5763, page 28-29

Stetka, J., Luzna, P., Lanikova, L., Koralkova, P., Hodny, Z., Bartek, J., Divoky, V., 2016. JAK2 V617F progenitors exhibit intrinsic inflammatory signaling and protection against inflammation induced DNA damage. 12th International Congress of Cell Biology in Prague, 2016, Praha, abstracts, page 110

Stetka, J., Luzna, P., Lanikova, L., Koralkova, P., Gursky, J., Hodny, Z., S., Bartek, J., Divoky, V., 2017. JAK2 V617F Progenitors Utilize Adaptations to Cell-Autonomous and Microenvironment-Dependent Inflammatory Stress in Polycythemia Vera, Likely Exhibiting Barrier Against Rapid Transformation to Myelofibrosis. Blood 130, (Supplement 1): 1667

Aim 4 Investigate the role of interferon signaling on hematopoietic stem cells heterogeneity in MPN mouse model.

Recent studies showed that HSC compartment can be subdivide into functionally heterogeneous populations. In particular, testing functionality of individual HSCs through transplantation assays and *in vivo* fate mapping showed selective linage bias or restriction of various subpopulation (Carrelha et al., 2018). Furthermore, the composition of HSC pool is significantly changed with aging towards increase in megakaryocyte-biased (Mk-biased) HSC frequencies and platelets production, with decrease in lymphoid lineage output (Grover et al., 2016). However, how are these subpopulations related to long-term engraftment, stemness and eventually modulated by oncogene and inflammatory conditions had been so far unexplored.

In a recent paper on which I had an opportunity to collaborate, we have explored the functional role of Mk-biased HSCs in *JAK2* V617F^{+} MPN mouse model. Currently, pegylated IFN alpha (pegIFNα) therapy is the only treatment for MPNs, which is able to directly target and reduce *JAK2* V617F^{+} HSC pool. Thus, we have also assessed impact of long-term treatment with pegIFNα on composition of MPN HSC pool.

I have participated in part or full in transplantations for repopulation with *JAK2* V617F (*VF*) subsets of HSCs and treatment of MPN mouse models and *WT* mice intended for treatments with saline as a control, polyinosinic:polycytidylic acid (pIpC), pegIFNα, thrombopoietin (TPO) and all the downstream experiments intended to resolve long-term HSC subpopulations in bone marrow and spleen. To keep the dataset understandable, I have included necessary minimum of the data from my colleague Nageswara Rao Tata (Radek Skoda lab, University Hospital and University Basel, Switzerland). This involves single cell liquid cultures of FACS sorted HSCs.

Functionally impaired Mk-biased HSCs frequencies are increased in *JAK2* V617F MPN mouse model

As Mk-biased HSCs were described to have high surface expression of CD41 (CD41^{hi} , (Gekas and Graf, 2013, p. 41; Sanjuan-Pla et al., 2013)) we determined the HSC frequencies of CD41^{hi} and CD41^{lo} (CD41 low expression) in the Cre-inducible mice expressing the human *JAK2* V617F transgene. We show in Figure 29, that compared to wildtype (*WT*) littermates the *VF* mice have significantly expanded CD41^{hi} HSCs frequencies in absolute (‰ out of total) and relative (% out of HSCs) numbers (Figure 29A,B). This expression was inversely correlated to Epcr expression

(Figure 29D), well-described stemness and quiescence marker of HSCs (Balazs et al., 2006; Iwasaki et al., 2010; Zhou et al., 2016). Furthermore, as my colleague Nageswara Rao Tata shows in his submited paper (Tata et al., 2020, *Manuscript submitted in Blood*) CD41^{hi} and Epcr^{lo} HSCs also showed increased Mk differentiation potential in single cell liquid cultures of FACS sorted CD41^{hi} or CD41^{lo} HSCs (Figure 29C,E).

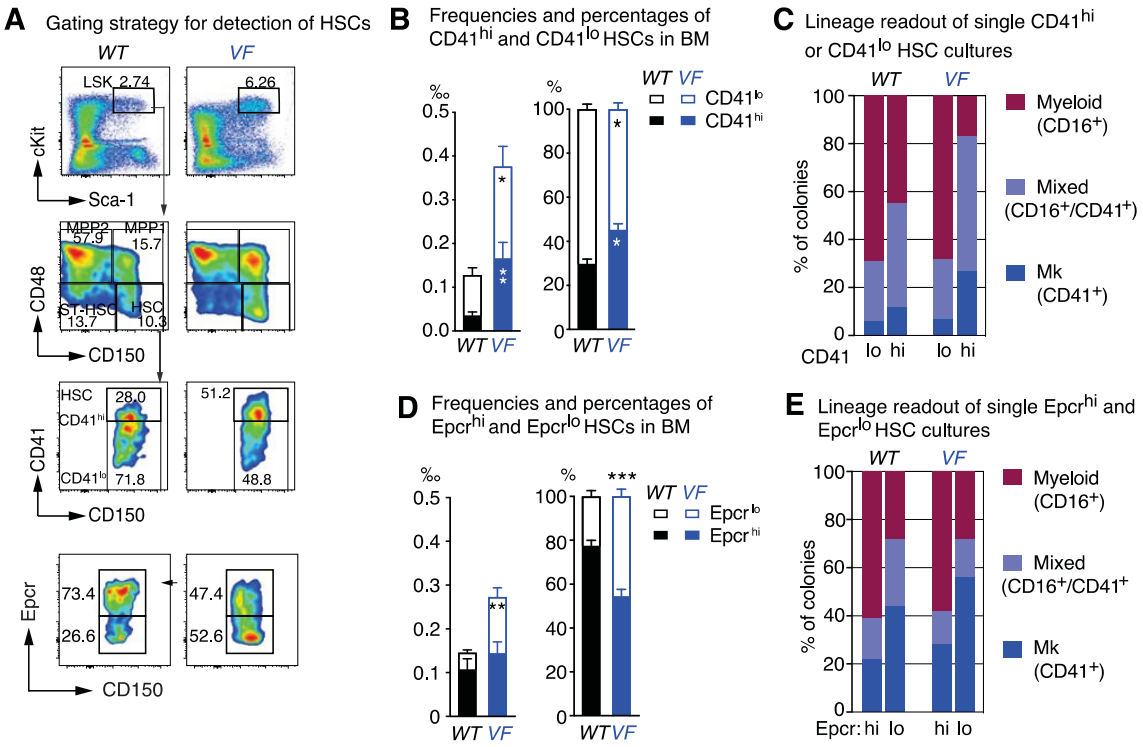

Figure 29: A Gating strategy for CD41 and Epcr surface expression in the long-term HSC (Linage^{-}, c-Kit^{+}, Sca-1^{+}, CD48^{+}, CD150^{+}) compartment of the bone marrow. **B** Stacking bar graphs showing frequencies (left panel) and the percentages (right panel) of CD41^{hi} and CD41^{lo} HSCs. The genotypes are indicated (n=7 mice per genotype). **C** Analysis of colonies grown from FACS sorted single CD41^{hi} or CD41^{lo} HSCs in liquid culture. Bar graph shows the percentages of colonies containing Mk (CD41^{+}), myeloid (CD16^{+}), or mixed (Mk and myeloid, CD41^{+}/CD16^{+}) cells after 10 days of culture. **D** Stacking bar graphs showing frequencies (left panel) and the percentages (right panel) of Epcr^{hi} and Epcr^{lo} HSCs. The genotypes are indicated (n=7 mice per genotype). **E** Analysis of colonies grown for 10 days in liquid culture from FACS sorted single Epcr^{hi} or Epcr^{lo} HSCs. Bar graph shows the percentages of colonies containing Mk (CD41^{+}), myeloid (CD16^{+}), or mixed (Mk and myeloid, CD41^{+}/CD16^{+}) cells.

To examine long-term hematopoietic repopulation capacity and thus functionality, 50 FACS-sorted *VF* or *WT* CD41^{hi} and CD41^{lo} HSCs (GFP^{+}) were transplanted into lethally irradiated recipients with one million *WT* competitor cells. After follow-up (12 weeks)

CD41^{hi} HSCs, compared to CD41^{lo} showed decreased functionality shown by less efficient hematopoiesis reconstitution, unable to outcompete *WT* HSCs (Figure 30).

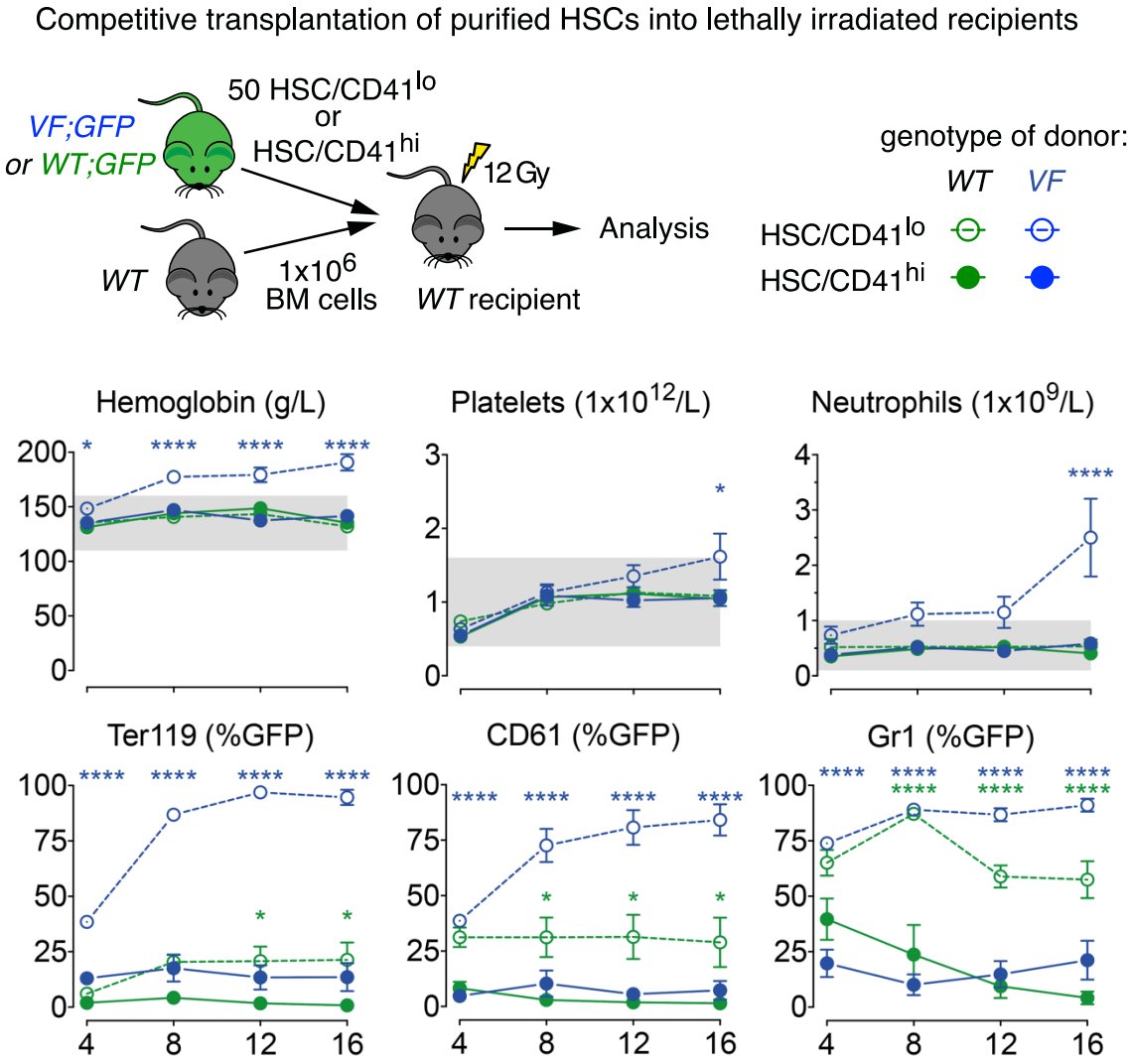

Figure 30: Scheme of transplantation setup with FACS-sorted CD41^{hi} or CD41^{lo} HSC into lethally irradiated recipients (n=12 mice per cell type; two independent donors were used). Blood counts, spleen weight (*upper* part) and donor chimerism (*lower* part) are shown. Two-way ANOVA test. All data shown are mean ± SEM. ∗p <0.05; ∗∗∗p < 0.001;∗∗∗∗p < 0.0001.

JAK2 and IFN signaling drives expansion of CD41^{hi} HSCs in MPN mouse model

To investigate the role of short-term and chronic IFN signaling on CD41 subsets of HSCs *in vivo*, we treated *VF* and *WT* mice either with pIpC, an IFN-inducing agent

(Baldridge et al., 2010; Essers et al., 2009; Pietras et al., 2014) for 24 hours (Figure 31A) or pegIFNα for 22 weeks (Figure 33).

VF and *WT* mice treated with single injection of pIpC for 24 hours significantly increased percentages of $CD41^{hi}$ HSCs within the pool of HSCs (Figure 31B). Consistently with previous data, pIpC treatment had converse effects on Epcr positivity within this pool, decreasing the percentages of $Epcr^{hi}$ HSC subsets in both *VF* and *WT* mice (Figure 31B). We have also explored, if the observed increased baseline of $CD41^{hi}$ HSCs subfractions in *VF* mice are specific to JAK2 mutant signaling or to constitutive JAK-STAT signaling in general. To address this issue, we treated *WT* and *VF* mice with recombinant mouse TPO and assessed the percentages of $CD41^{hi/lo}$ HSCs and $Epcr^{hi/lo}$ HSCs in the bone marrow (Figure 31B). A single dose of recombinant TPO increased the percentages of $CD41^{hi}$ HSCs in *WT* mice to levels similar as the baseline (saline) in *VF* mice, but to lower levels than pIpC in *WT* mice (Figure 31B). In *VF* mice, TPO treatment increased the percentages of $CD41^{hi}$ HSCs to higher levels than in *WT* mice, in fact the $CD41^{hi}$ HSCs reached the same levels as VF mice treated with pIpC (Figure 31B), suggesting that TPO signaling through *JAK2* V617F is amplified and elicits a stronger signal than through wildtype *Jak2*. Thus, activating JAK-STAT signaling by TPO is able to induce a rapid increase in $CD41^{hi}$ HSCs, demonstrating that the phenotypic shift to $CD41^{hi}$ is not specific to the mutant JAK2.

Interestingly and contrary to expectations, TPO in the same experiment did not reduce the percentages of $Epcr^{hi}$ HSCs in *WT* or *VF* mice, while pIpC led to the expected substantial decrease of $Epcr^{hi}$ HSCs in both *VF* and *WT* mice (Figure 31B). These data show that CD41 and Epcr subpopulations of HSCs do not always behave reciprocally. As TPO was shown to increase the expression of Epcr (Kohlscheen et al., 2019), It remains to be determined whether Epcr is just a marker for quiescence, or if increased expression may also exert functional effects on HSCs on its own.

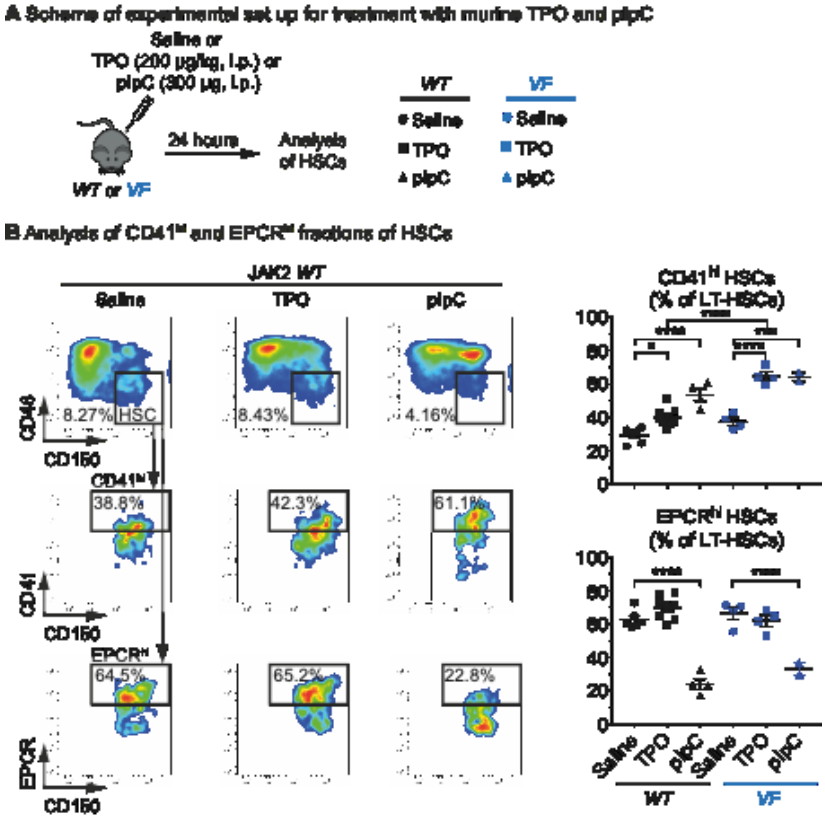

Figure 31: Effects of mouse TPO and pIpC on percentages of bone marrow CD41^{hi} and Epcr^{hi} HSCs in *WT* and *VF* mice. **A** Schematic showing *in vivo* TPO (200µg/kg; i.p.) or pIpC (300µg/mouse i.p.) stimulation and assessment of CD41^{hi} HSCs in *WT* and *VF* mice. **B** Graph showing the percentages of CD41^{hi} and Epcr^{hi} HSCs in *WT* and *VF* mice treated with saline or TPO or pIpC. One-way ANOVA test. All data shown are mean ± SEM. ∗p <0.05; ∗∗∗p < 0.001;∗∗∗∗p < 0.0001.

Since expression of Sca-1, as one of the interferon responsive genes, varies upon interferon treatment (Dumont et al., 1986); we needed to verify if the gating strategy of CD41^{hi} HSCs (CD48^{-}, CD150^{+}, CD41^{hi}) from the LSK (Linage^{-}, c-Kit^{+}, Sca-1^{+}) compartment is correct. This is mainly due to possible contamination of megakaryocyte progenitors (MkPs: Linage^{-}, c-Kit^{+}, Sca-1^{-}, CD150+, CD41^{hi}), which might become Sca-1^{+} after activation of IFN-responsive programe and ending up in LSK gate.We have therefore conducted additional experiments to check the purity of CD41$^{lo/hi}$ HSCs by adding an alternative HSC marker absent on MkPs, Esam1 (Lisa Ooi et al., 2009).
We found that virtually all CD41^{lo} and CD41^{hi} HSC subsets were Esam-positive both in control (saline) and pIpC treated *WT* and *VF* mice (Figure 32A). Likewise, assessment of Epcr^{lo} and Epcr^{hi} HSC subsets showed a similar Esam1 expression pattern in both in control (saline) and pIpC treated *WT* and *VF* mice (Figure 32B). Together, these data

indicate that CD41$^{lo/hi}$ HSCs are not contaminant of progenitor cells expressing CD41, and further validate the appropriateness of our FACS gating strategy.

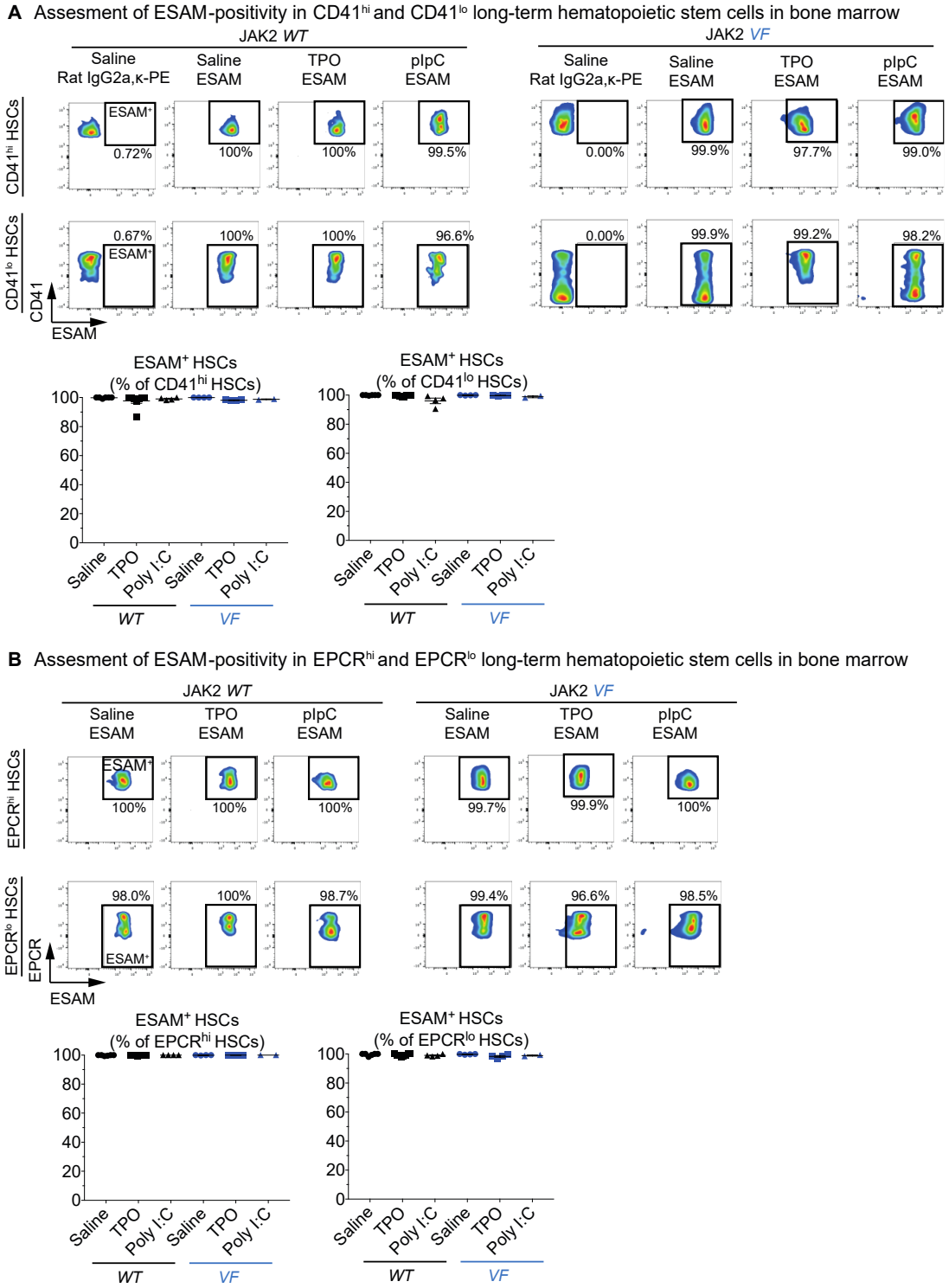

Figure 32: **A** Esam1 expression on CD41$^{lo/hi}$ HSCs. Esam1 expression on CD41^{hi} (*upper* panel) and CD41^{lo} HSCs (*lower* panel) in the bone marrow of control (saline), Tpo and pIpC treated *WT* and *VF* mice. The percentages of Esam^{+} HSCs within the CD41^{hi} HSCs (*left*) and Esam^{+} HSCs within the CD41^{lo} HSC fraction are shown below. **B** Esam1 expression on Epcr^{hi} (*upper* panel) and Epcr^{lo} HSCs (*lower* panel) in the bone marrow of mice. Graphs showing the percentages of Esam1+ HSCs within the Epc^{rhi} HSCs (*left*) and Esam1^{+} HSCs within the Epcr^{lo} HSC fraction are shown below.

Finally, to model effects of pegIFNα therapy in MPN we have transplanted *VF* mice bone marrow in 1:1 ratio with *WT* competitor bone marrow cells into lethally irradiated recipients (Figure 33A). 6 weeks post-transplantation we have randomized engrafted mice and commenced the treatment with pegIFNα injections weekly for 22 weeks. After complete hematological response marked by normalized blood counts and spleen weight (Figure 33A) we have terminated the experiment and analyzed the HSC subfractions (Figure 33B). We have observed reduction of mutant *VF* HSCs in total numbers with significant increase of CD41^{hi} HSCs in residual mutant HSC pool.

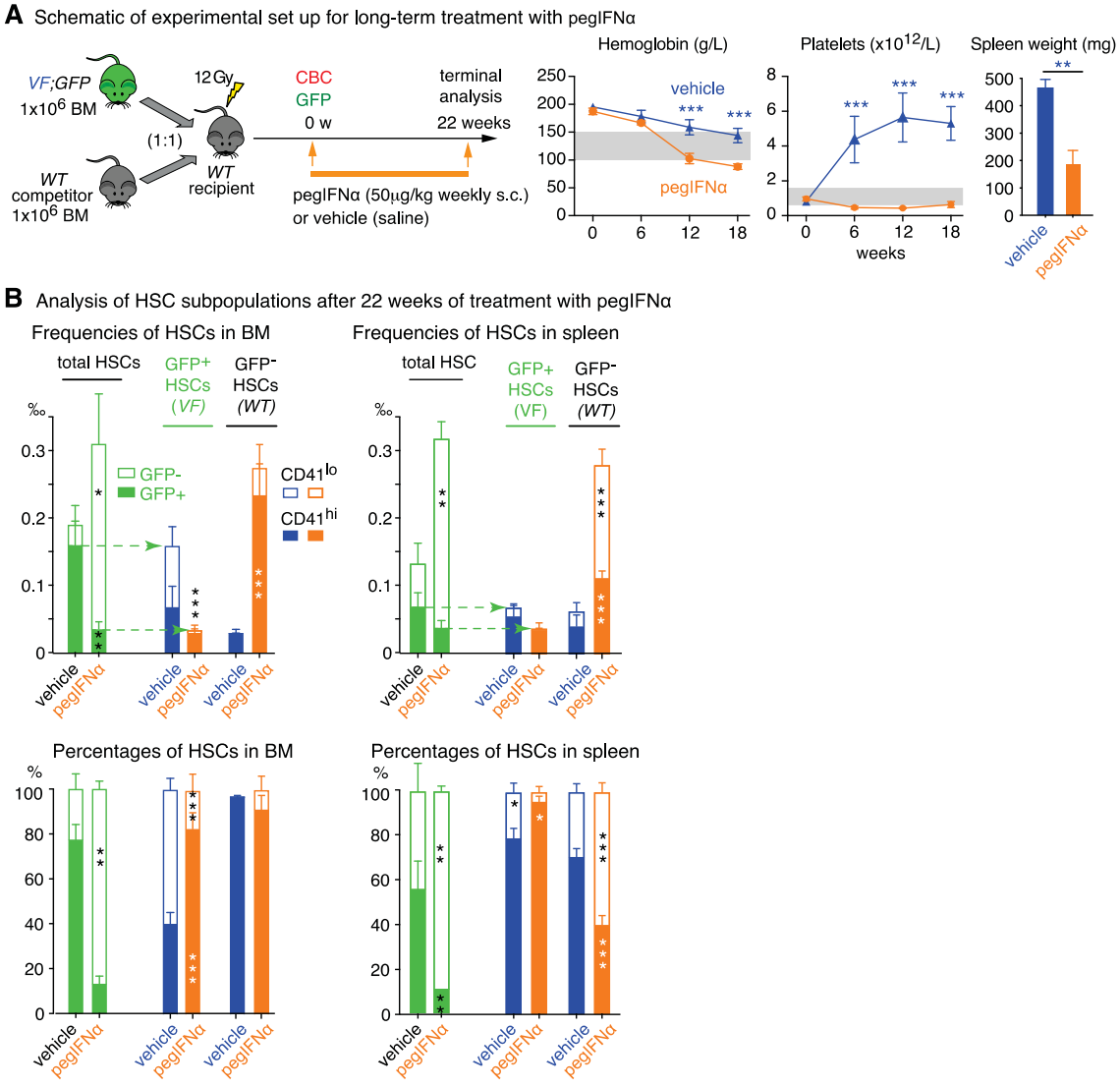

Figure 33: **A** Scheme of competitive transplantation and pegIFNα regimen (*left*) together with observed reduction in hemoglobin, platelets and spleen weight (*right*) **B** Analysis of GFP-positive and GFP-negative subpopulations of HSCs after 22 weeks of treatment with pegIFNα. The frequencies per 1x10^3 bone marrow cells and the percentages of donor derived (GFP+) HSC subsets in recipient mice treated with pegIFNα or vehicle are shown (n=5 mice per group). All data shown are mean ± SEM. ⁎p < 0.05; ⁎⁎p <0.01; ⁎⁎⁎p < 0.001; ⁎⁎⁎⁎p < 0.0001. Two-way ANOVA tests were performed

Overall, these data suggest the apparent expansion of the $CD41^{hi}$ subset occurred because $CD41^{lo}$ HSC were more sensitive to IFN signaling (shown by short-term treatment with pIpC), and while responding they converted to $CD41^{hi}$. This would fit with the higher expression of IFNα response pathway genes in $CD41^{lo}$ HSCs shown by Rao et al. in his RNAseq analysis of these two distinct subpopulations (data not shown). Consistently, long-term treatment with pegIFNα decreased the frequencies of the *VF* HSCs and within the *VF* HSCs (GFP^{+}) the proportion of $CD41^{hi}$ HSCs was increased (Figure 37B), suggesting that continuous conversion of $CD41^{lo}$ to the $CD41^{hi}$ HSC subset might be a mechanism of how IFNα preferentially targets and exhausts the JAK2 mutant clone.

Publications related to this aim:

Articles:

Rao, T.N., Hansen, N., Stetka, J., Kalmer, M., Hilfiker, J., Endele, M., Kubovcakova, L., Rybarikova, M., Hao-Shen, H., Geier, F., Beisel, Ch., Dirnhofer, S., Schroeder, T., Brümmendorf, T., Wolf, D., Koschmieder, S., Skoda, R.C., 2020. Interferon-α achieves molecular remission in myeloproliferative neoplasms by inducing megakaryocyte-biased stem cells. *Manuscript submitted in Blood*

Aim 5 Explore role of iron availability on MPN phenotype manifestation.

As previously discussed, MPN patients with *JAK2* V617F mutation can manifest as PV with significant expansion of erythropoiesis, ET with increased production of megakaryocytes and platelets, or PMF with extramedullary hematopoiesis in spleen (Arber et al., 2016; Levine and Gilliland, 2008). In contrast, MPN patients with mutations in *JAK2 exon 12* invariably display PV phenotype with predominant erythrocytosis (Passamonti et al., 2011; Scott et al., 2007).

The molecular mechanisms of the variable phenotype in patients with *JAK2* mutations are unknown. Iron strongly affects erythropoiesis since in normal subjects majority of circulating iron is consumed for hemoglobin production (Camaschella and Pagani, 2018). To maintain the high hemoglobin levels of PV, iron homeostasis has to be adjusted: to increase plasma iron, the production of the iron regulatory peptide hepcidin that inhibits iron absorption and recycling (Nemeth et al., 2004) is suppressed (Ginzburg et al., 2018). This process is mediated by erythroferrone, a molecule released from maturing erythroblasts that inhibits hepcidin expression (Kautz et al., 2014) by sequestering the hepcidin activating Bone Morphogenetic Proteins (Lim et al., 2019). This adjustment does not occur equally in all MPNs. Previous data in MPN animal models showed that hepcidin suppression and iron acquisition are stronger in *JAK2* E12 as compared with *JAK2* V617F mice (Grisouard et al., 2016) suggesting a potential role of iron in favoring PV vs ET phenotype.

Thus, I investigated the functional role of iron on MPN phenotype by inducing either iron deficiency in models of PV or increasing total body iron by parenteral iron injection in models of ET and PV. The results of these opposite approaches converge on the essential role of iron in the alternative phenotype presentation caused by mutated *JAK2*.

Iron deficiency induced a switch from PV to ET-like phenotype in *JAK2* mutant mouse models of MPN

First, we examined the effects of iron deficiency *in vivo* in MPN models of PV. To generate sufficient numbers of *JAK2*-mutant mice for exposure to iron deficiency *in vivo*, we performed bone marrow transplantations into lethally irradiated wildtype recipient mice (Figure 34A). *SclCre^{ER};Jak2*-V617F (*Ki*), or *SclCre^{ER};JAK2 exon12* mutant *(E12)* mice were induced by tamoxifen and sacrificed as bone marrow donors 8 weeks later when they displayed PV phenotype. Wildtype donor mice (*WT*) treated with tamoxifen served as controls. Four weeks after transplantation, blood counts were performed in the

recipients (time point 0). The *Ki* and *E12* mice already displayed elevated hemoglobin levels and were randomized in groups to be either placed on iron deficient diet (5mg iron/kg food) or iron deficient diet combined with phlebotomy, or on control diet supplemented with iron (200mg iron/kg food). We noted that the mice initially had difficulties with the switch to iron deficient diet, which resulted in a drop in body weight in the first 2 weeks, followed by normalization to the initial values after the mice became adapted to the new chow (Figure 34B).

Ki mice developed thrombocytosis within 8 weeks after transplantation, while *E12* and *WT* mice, as expected, maintained platelet counts in the normal range (Figure 34C). Iron deficient diet increased platelet counts and megakaryocyte numbers in bone marrow in mice of all three genotypes compared with control diet, and this increase was further accentuated by additional phlebotomy (Figure 34C and 34D, left panel). The increase in platelet counts and megakaryocyte numbers in *WT* and *E12* mice inversely correlated with decrease in Tpo concentrations in bone marrow (Figure 34D, right panel). In contrast, *Ki* mice maintained low Tpo irrespective of the treatment group, which is explained by very high baseline platelet and megakaryocyte numbers already on control diet.

Mice on iron deficient diet also showed the expected decrease in hemoglobin and red cell parameters in peripheral blood (Figure 34E). On iron deficient diet combined with phlebotomies, anemia developed in all three genotypes, but was most severe in *Ki* mice and therefore, this group had to be terminated already after 8 weeks of treatment. *E12* mice were more resistant to iron deficient diet and after 12 weeks still maintained normal hemoglobin levels. The very low erythrocyte indexes, i.e., mean corpuscular volume (MCV) and mean corpuscular hemoglobin (MCH), show that even on control diet, with 200 mg iron/kg food, both MPN models became iron deficient after MPN hematopoiesis engrafted and erythropoiesis fully expanded. In *Ki* mice, MCV and MCH further decreased when exposed to diet plus phlebotomy, whereas *E12* mice showed only minimal decrease in MCH (Figure 34E. lower panel).

Analysis of iron parameters and regulatory cytokines is shown in Figure 34F. *WT* mice after 12 weeks on iron deficient diet showed the expected decrease in liver iron, an indicator of total body iron, and lower serum iron levels, accompanied by increase in total iron binding capacity (TIBC) and decrease in transferrin saturation (Figure 34F). *Ki* mice on control diet already showed depletion of liver iron stores, but serum iron decreased only on iron deficient diet plus phlebotomy, in parallel with decrease in MCV and MCH. *E12* mice maintained almost normal liver iron levels and high hemoglobin on control diet, but on iron deficient diet ± phlebotomy showed depletion of liver iron stores accompanied by decrease in hemoglobin. As expected for PV, Epo levels were low and suppressed in

Ki and *E12* mice on control diet, but Epo increased in response to lowering hemoglobin levels on iron deficient diet ± phlebotomy. Erythroferron levels in *Ki* and *E12* mice on control diet were elevated despite low Epo serum levels, likely due to increased Epo-receptor signaling in erythroid progenitors expressing the mutant *JAK2*. As a consequence, Hepcidin levels were suppressed in *Ki* and *E12* mice irrespective of the diet, while in *WT* mice increase in erythroferrone and decrease in Hepcidin was only seen on iron deficient diet ± phlebotomy. Hemoglobin was lower and erythropoiesis expansion more limited in *Ki* mice compared to *E12*, indicating a remarkable ability to compensate iron deficiency by *E12* mice. Overall, iron deficiency induced reciprocal increase in platelet counts and decrease in hemoglobin levels in *Ki* and in *E12* mice. These results are compatible with the concept of iron-dependent switch towards an ET-like phenotype in MPN.

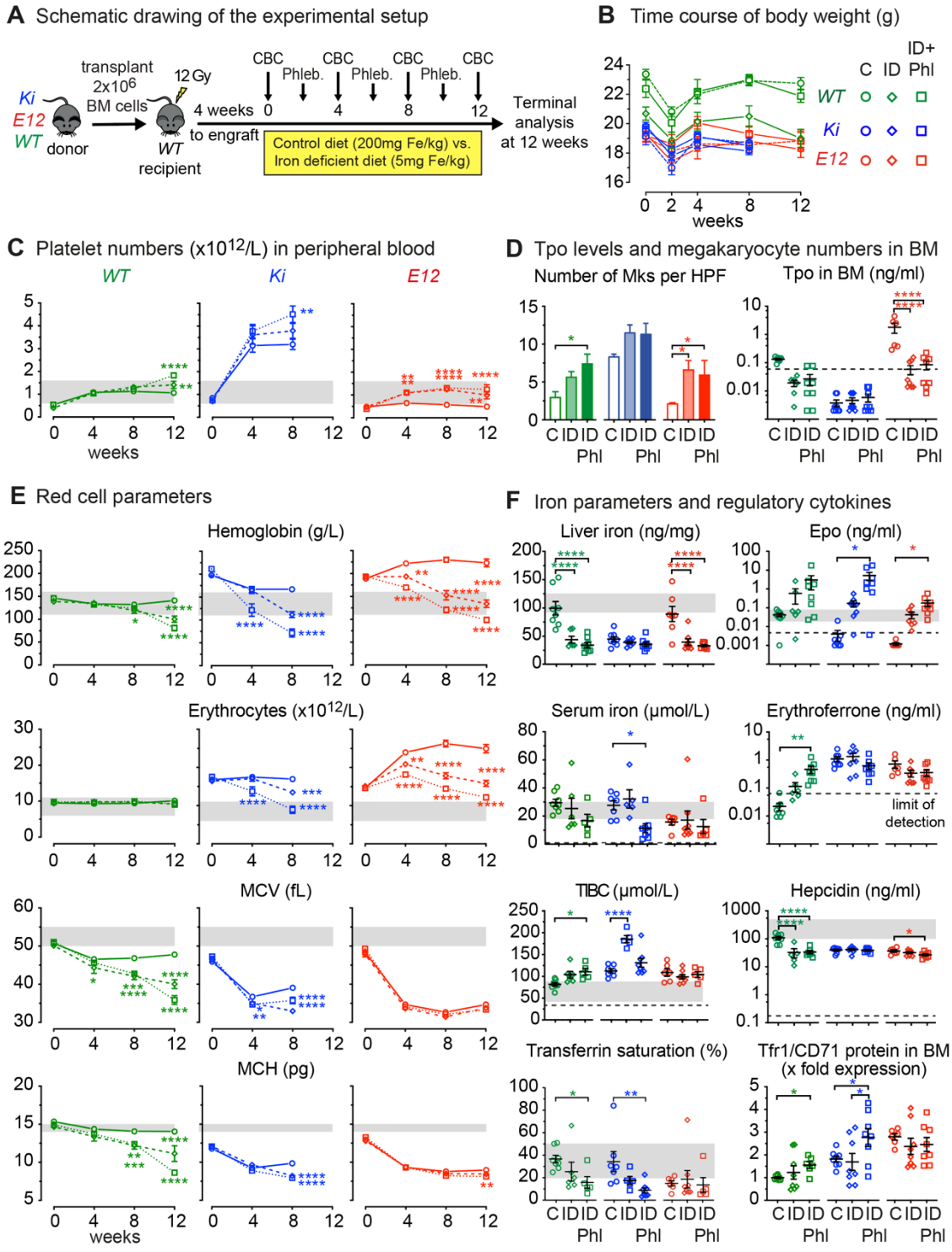

Figure 34: **Figure 1. Effects of iron deficiency on MPN phenotype.** (**A**) Schematic drawing of the experimental setup for the bone marrow transplantations and iron deficient regimens. (**B**) Time course of body weight. C, control diet; ID, iron deficient diet; ID+Phl, iron deficient diet plus phlebotomy. (**C**) Platelet counts of recipient mice (n = 8 mice per genotype) are shown at the indicated times. (**D**) Left panel shows numbers of megakaryocytes (Mks) per 10 high power fields (HPF) counted in sternum sections of mice at 40x magnification. N = 3 mice per genotype and treatment group. Right panel

shows thrombopoietin (Tpo) concentration in bone morrow (BM) lavage (one femur and one tibia) determined at terminal workup 8-12 weeks after start of the treatment. Dotted line indicates the limit of detection of the assay. **(E)** Red blood cell paramethers (n = 8 mice per genotype) are shown at the indicated times. (**F**) Iron parameters and regulatory cytokines. Group size was n= 4-8 mice per genotype and treatment group. Erythropoietin (Epo), Erythroferrone and Hepcidin levels were determined in serum. Two-way analyses of variance (ANOVAs) with subsequent Dunnett posttest (C, E) or Tukey's test (D,F) were used for multiple-group comparisons. *P < .05, **P < .01, ***P < .001, ****P < .0001. CBC, complete blood count; Phleb., phlebotomy.

Effects of parenteral administration of iron dextran on the phenotype of *JAK2* mutant MPN mice

We next examined whether parenteral iron supplementation can have the opposite effect on megakaryopoiesis and erythropoiesis in *JAK2* V617F mice. In addition to *Ki* mice we also examined *VavCre;FF1* mice (*VaF*) that express the human *JAK2*-V617F and display pure ET phenotype with very high platelet count and normal hemoglobin values, and *SclCre^{ER};FF1* mice *(ScF)* that display PV phenotype with very high platelets. To generate sufficient numbers of *JAK2*-mutant mice, we again performed bone marrow transplantations into lethally irradiated wildtype recipient mice (Figure 35A). Iron dextran was administered intraperitoneally at week 1 and week 4 post transplantation (Figure 35A). Body weight was unchanged in the treatment groups, except in *Ki* mice injected with iron that lost weight (Figure 35B). Iron injections also decreased platelet counts in *Ki*, *ScF* and *WT* mice, but did not alter thrombocytosis in *VaF* mice (Figure 35C). Spleen weight increased in Ki and ScF mice upon iron injections, but not in *VaF* and *WT* mice (Figure 35D).

Ki and *ScF* mice injected with iron maintained a strong PV phenotype and did not show a decrease in hemoglobin and red cell red cell numbers at 8 weeks post transplantation, contrary to the vehicle treated mice (Figure 35E). MCV and MCH values were higher in *Ki* mice that received iron injections compared to vehicle, but at 8 weeks post transplantation, *Ki* mice that received iron injections were visibly impaired and had to be sacrificed prematurely. *VaF* mice displayed no changes in hemoglobin or red cell parameters except a small increase in in MCV and MCH.

Liver iron in vehicle treated in *Ki* and *ScF* mice was decreased, but *VaF* displayed iron content similar to *WT* mice (Figure 35F). Upon iron injections, liver iron strongly increased in all genotypes, but *Ki* mice sacrificed at 8 weeks had significantly lower liver iron stores than *ScF* mice after 14 weeks (Figure 35F, right panel). Serum iron increased in *WT* and

VaF mice, but decreased in *Ki* and *ScF* mice injected with iron, reflecting increased demand in the latter mice due to massively increased erythropoiesis. Accordingly, erythroferrone was elevated in *Ki* and *ScF* mice and hepcidin suppressed in *Ki* mice but not in ScF mice, suggesting that *Ki* mice displayed the highest demand for iron to support erythropoiesis. TIBC and transferrin saturation was lower in *Ki* and *ScF* mice injected with iron, whereas *WT* and *VaF* mice showed the expected increase in transferrin saturation. Tfr1 protein expression levels were highest in *Ki* mice, but lower than *WT* in *ScF* mice and Tfr1 expression decreased upon iron injections in WT mice.

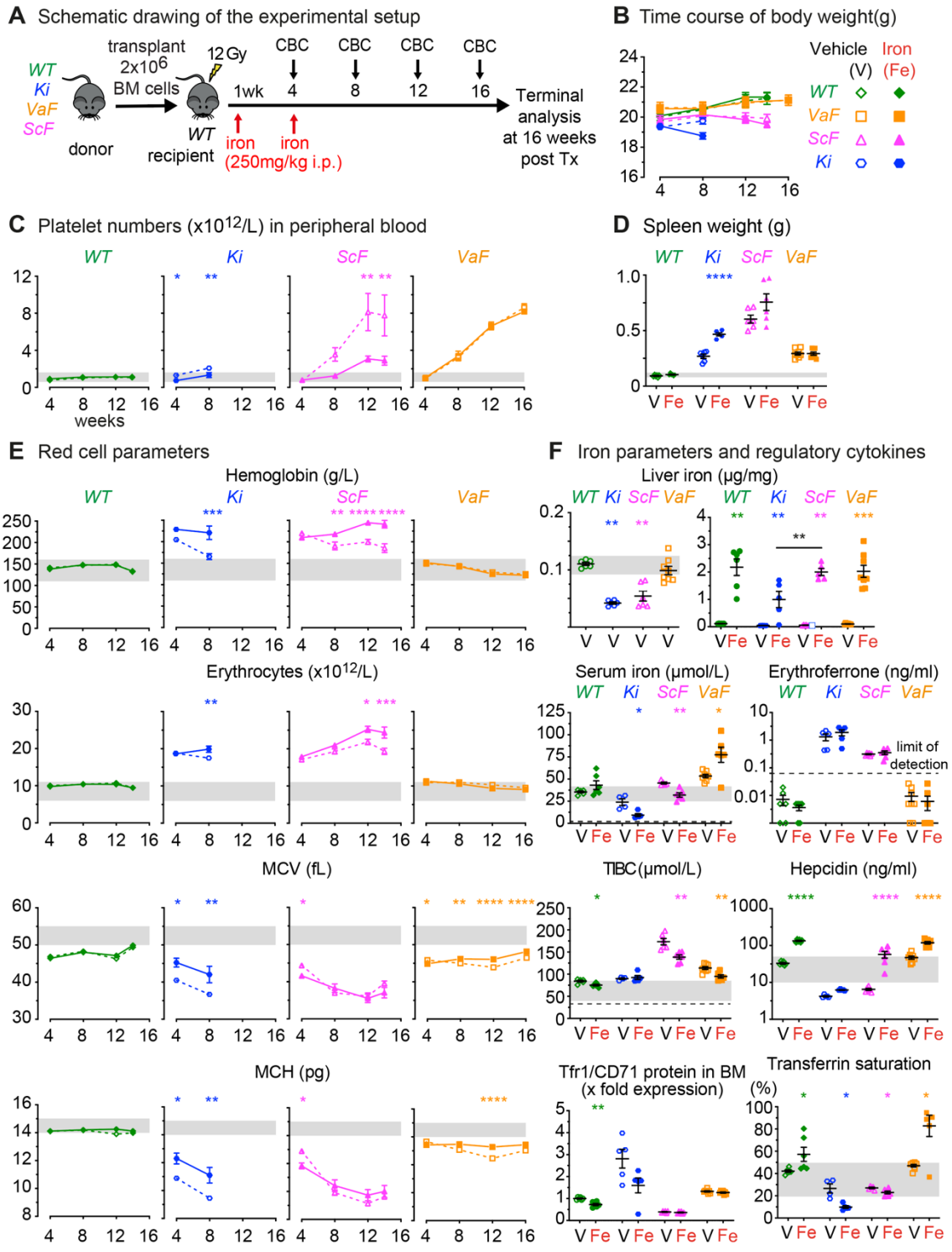

Figure 35: Effects of parenteral iron injections on platelet and red cell production in MPN mouse models with very high platelet counts. (**A**) Schematic drawing of the experimental setup for the bone marrow transplantations and iron injections. (**B**) Time course of body weight. (**C**) Time course of platelet counts (n= 6-8 mice per genotype and treatment group) **(D)** Spleen weight at terminal analysis. (**E**) Time course of red blood cells parameters. N= 6-8 mice per genotype and treatment group (**F**) Iron parameters and regulatory cytokines. Group size was n= 4-8 mice per genotype and treatment group.

All data are presented as mean ± standard error of the mean. Two-way analyses of variance (ANOVAs) were used for multiple-group comparisons. *P < .05, **P < .01, ***P < .001, ****P < .0001.

Hematopoietic progenitor and stem cell frequencies were determined at terminal workup (Figure 36). Iron injections had no effect on the frequencies of LT-HSCs in bone marrow and spleen. Also, the percentages of $CD41^{hi}$ HSCs did not change upon iron injections, except for a trend towards lower $CD41^{hi}$ HSCs in *Ki* mice injected with iron. *VaF* mice had substantially higher frequencies of LT -HSCs and CMPs than any of the other genotypes (Figure 36A, insert with higher frequency range). Within the CMPs progenitors, *VaF* mice also displayed the highest percentages of the $CD41^{hi}$ subset both in bone marrow and spleen. Iron injections decreased the frequencies of MEPs, pre-MegE, and MkPs in spleen of *Ki* and *ScF* mice, whereas an increase was noted in MEPs, pre-MegEs and CFU-E in spleen of *WT* mice. Detailed analysis of erythroid maturation showed increase in terminally differentiated erythroid cells (stage 5) in *Ki* and *ScF* mice upon iron injection, whereas no change was observed in *WT* and *VaF* mice (Figure 36B).

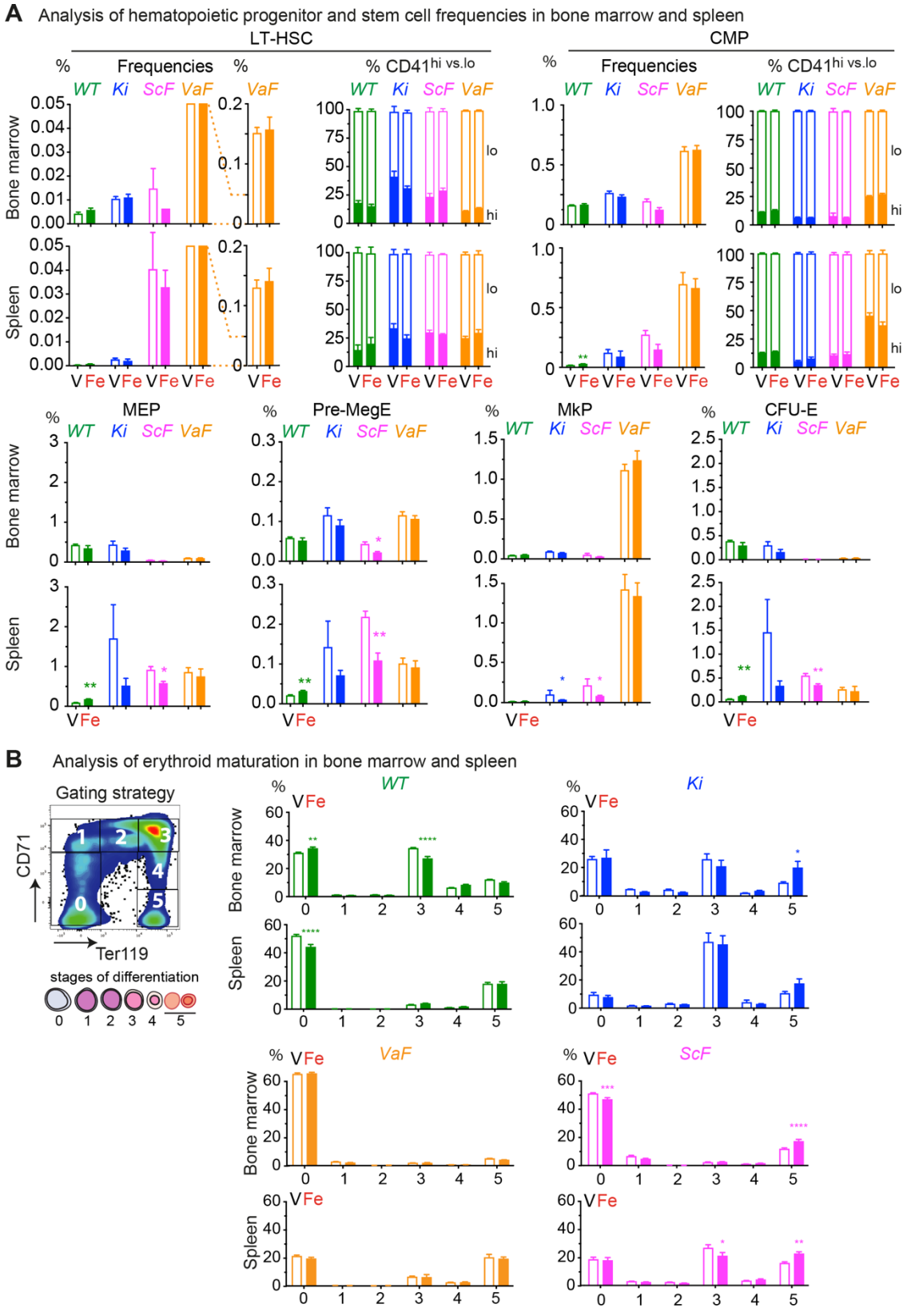

Figure 36. Effects of parenteral iron injections on hematopoietic progenitor and stem cells at terminal workup. (**A**) Analysis of hematopoietic progenitor and stem cell frequencies in bone marrow and spleen at 16 weeks. Bar graphs show frequencies of hematopoietic stem cells and progenitors in bone marrow and spleen. V, vehicle; Fe,

iron treatment. For long-term hematopoietic stem cells (LT-HSC) and common myeloid progenitors (CMP), the total frequencies (left panel) and the percentages of $CD41^{hi}$ (filled bars) versus $CD41^{lo}$ (open bars) subsets of LT-HSC are shown (right panel). (**B**) Analysis of erythroid maturation. All data are presented as mean ± standard error of the mean. Unpaired 2-tailed *t*-test with Welsch's correction (A) or two-way analyses of variance (ANOVAs) with subsequent Sidak (A - Percentages of $CD41^{hi/lo}$ HSCs) posttest were used. *P < .05, **P < .01, ***P < .001, ****P < .0001.

Collectively these results show that iron supplementation in *Ki* and *ScF* mouse models induces shift in hematopoiesis towards production of red blood cells at the expense of platelets. However, *VaF1* mice appear to be non-responsive to iron, as their erythropoiesis is less driven by the mutant *JAK2* (Tiedt et al., 2008). *VaF* mice appear to primarily use the $CD41^{hi}$ subset of CMPs to increase the production of MkPs, avoiding iron-responsive bipotent MEP progenitors resulting in massive thrombocytosis that is unaffected by iron injections.

Publications related to this aim:

Articles:

Stetka, J., Rai, S., Usart, M., Hao-Shen, H., Dirnhofer, S., Silvestri, L., Nai, A., Camaschella, C., Skoda, R.C., 2020. Iron-dependent steps in defining the phenotypes of *JAK2*-mutant myeloproliferative neoplasms. *Manuscript prior submission to Blood.*

4. Materials and methods

The Materials and methods section contains detailed information about experiments I performed at the Department of Biology, Faculty of Medicine and Dentistry, Palacky University Olomouc. The methods involving mouse models were performed during my stay at the Department of Biomedicine, Experimental Hematology, University Hospital Basel and University of Basel. All the other experiments, done by coauthors, are presented only in brief and cited accordingly.

4.1 Laboratory equipment and software

Irradiator RS Research Cabinet (Xstrahl, Camberley, UK); Amaxa Nucleofector system (Lonza, Visp, Switzerland); Agilent 2100 Bioanalyzer (Agilent Technologies, Santa Clara, USA); HumanHT-12 v4 Expression BeadChips (Illumina, San Diego, USA); Genome Studio software (version 1.9.0.24624; Illumina); Bioconductor software (version 3.8; (Carvalho and Irizarry, 2010; Gentleman et al., 2004; Smyth, 2004); Heatmapper software (Babicki et al., 2016); ConsensusPathDB software tool (Release 34 (15.01.2019); Max-Planck-Institut für molekulare Genetik, Berlin, Germany); Real-time thermocycler LightCycler 480 (Roche, Basel, Switzerland) LightCycler 480 software (Roche); Cytometer Cytomics FC 500 (Beckman Coulter, Brea, USA); cytometer data processing CXP software (Beckman Coulter); spectrophotometer Infinite 200 Nanoquant (Tecan, Männedorf, Switzerland); microtome (Leica, Wetzlar, Germany); microwave histoprocessor (Histos 3, Milestone, Shelton, USA); Olympus BX51 inverted microscope equipped with ColorViewIII digital CCD camera (Olympus, Tokio, Japan); Axio Observer.Z1/Cell Observer Spinning Disc microscopic system (Yokogawa, Tokyo, Japan and Zeiss, Oberkochen, Germany) equipped with an Evolve 512 (Photometrix, Tucson, USA) EMCCD camera; ScanR imaging workstation software (Olympus, Tokyo, Japan); ScanR image analysis software (Olympus); Bio-Rad PowerPack (Bio-Rad Laboratories, Hercules, USA); Odyssey Imaging System (LI-COR Biosciences, Lincoln, USA); Prism statistical software (version 6.0, GraphPad Software, San Diego, USA)

4.2 Biological material

Human BM bioptic samples were obtained from the Department of Clinical and Molecular Pathology, University Hospital Olomouc (UHOL), Olomouc, Czech Republic. The original examinations were obtained with the approval of the IRB committee of the UHOL and according to the Declaration of Helsinki.

4.3 Other chemicals, cytokines and reagents

Mitomycin C (Sigma Aldrich, St. Louis, USA); Dulbecco's modified eagle medium (DMEM; Thermo Fisher Scientific, Waltham, USA); Fetal bovine serum (FBS, Thermo Fisher Scientific); Gelatin powder (Sigma Aldrich); Phosphate-Buffered Saline (PBS, Thermo Fisher Scientific); DMEM with Nutrient Mixture F-12 (DMEM/F-12, Thermo Fisher Scientific); knockout serum replacement (Thermo Fisher Scientific); L-glutamine (Thermo Fisher Scientific); non-essential amino acids (Thermo Fisher Scientific); penicillin-streptomycin (Thermo Fisher Scientific); 2-mercaptoethanol (Sigma Aldrich); recombinant human fibroblast growth factor-basic (FGF-Basic; Prospec, Rehovot, Israel); Collagenase B (Roche); TrypLE select (Thermo Fisher Scientific); TrypLE express (Thermo Fisher Scientific); StemPro-34 SFM (Thermo Fisher Scientific); bone morphogenetic protein 4 (BMP-4; Prospec); Holo-transferrin (Prospec); L-ascorbic acid (Sigma Aldrich); monothioglycerol (Sigma-Aldrich); Activin A (Prospec); vascular endothelial growth factor (VEGF; Prospec); dickkopf-related protein 1 (DKK-1; Prospec); interleukin 6 (IL-6; Prospec); Insulin-like growth factor 1 (IGF-1; Prospec); interleukin 11 (IL-11; Prospec); stem cell factor (SCF; Prospec); erythropoietin (EPO; Prospec); thrombopoietin (TPO; Prospec); murine thrombopoietin (TPO; Peprotec); interleukin 3 (IL-3; Prospec); Fms-related tyrosine kinase 3 ligand (FLT3LG; Prospec); interferon gamma (IFNγ; Prospec); tumor necrosis factor alpha (TNFα; Prospec); transforming growth factor beta 1 (TGFβ1, Thermo Fisher Scientific); TRI Reagent (Sigma-Aldrich); TURBO DNA-free DNase (Thermo Fisher Scientific); 5-Bromo-2′-deoxyuridine (BrdU, Sigma-Aldrich); 2N HCL (Sigma Aldrich); Triton X100 (Sigma Aldrich); anti-BrdU-FITC antibody (Roche); eBioscience Propidium Iodide Staining Solution (Thermo Fisher Scientific); RNase A (Qiagen, Hilden, Germany); bovine serum albumin (BSA, Sigma Aldrich); FITC tagged anti-CD34 antibody (Thermo Fisher Scientific); APC conjugated anti-CD43 (Thermo Fisher Scientific); anti-CD41a-PerCP-5.5 antibody (BD Biosciences, San Jose, USA); RIPA buffer (Sigma Aldrich); 4% neutral-buffered formaldehyde (Sigma Aldrich); low-melting seaplaque agarose (Lonza); xylene (Sigma Aldrich); ethanol (VWR, Radnor, USA); 10mM citrate buffer (Sigma Aldrich); goat anti-rabbit Alexa Fluor 488 antibody (Thermo Fisher Scientific); goat anti-mouse Alexa Fluor 568 conjugated secondary antibody (Thermo Fisher Scientific); DAPI (Sigma-Aldrich); MOWIOL 4-88 solution (Sigma-Aldrich); paraformaldehyde (Sigma Aldrich); Methanol (VWR); 10% goat serum (Sigma Aldrich); Tween20 (Sigma Aldrich); Glycine (Sigma Aldrich); Vectashield mounting reagent (Vector Laboratories, Peterborough, UK); DUSP 1/6 Inhibitor (Merck, Darmstadt, Germany); IP buffer (Thermo Fisher Scientific); phosphatase inhibitor cocktail (Sigma Aldrich); loading buffer (Bio-Rad Laboratories); 10% precast SDS-PAGE

gel (Bio-Rad Laboratories); PVDF membrane (Merck Millipore, Burlington, USA); HRP-conjugated anti-rabbit secondary antibody (Sigma Aldrich); HRP-conjugated anti-mouse secondary antibody (Sigma Aldrich); non-fat dry milk (kindly donated by OLMA, Olomouc, Czech republic); Tris-HCl (Sigma Aldrich); hematoxylin (Sigma Aldrich); 4-hydroxytamoxifen (Sigma Aldrich); Polyinosinic polycytidylic acid (Sigma-Aldrich);

4.4 Commercial Kits

CRISPR construct pXPR_001 plasmid (Addgene, Watertown, USA); pGEM-T easy vector (Promega, Madison, USA); Cell Line Nucleofector Kit V (Lonza); Illumina TotalPrep RNA Amplification Kit (Ambion; Thermo Fisher Scientific); Transcriptor First Strand cDNA Synthesis Kit (Roche); LightCycler 480 SYBR Green I Master kit (Roche); CellROX Green Flow Cytometry Assay Kit (Thermo Fisher Scientific); SuperSignal HRP Chemiluminescent Substrates (Thermo Fisher Scientific); Dako EnVision + Dual Link System-HRP (DAKO, Glostrup, Denmark); Liquid DAB + Substrate Chromogen System (DAKO);

4.5 Culture of undifferentiated iPSCs

Human iPSC line clone generated from female PV patient with *JAK2 V617F* genotype (PVB1.4) used in our study was described in detail previously (Smith et al., 2015; Ye et al., 2014). Gender-matched, control iPSC line with wildtype *JAK2* genotype (*JAK2 wt*, BXS0116) was obtained from ATCC (Manassas, USA). iPCSs were grown on mouse embryonic fibroblasts (MEFs) from day E13.5 post-coitus mouse embryos (Stemcell Technologies, Vancouver, Kanada), which were inactivated by incubation with mitomycin C (10ng/ml for 2 hours at 37°C) in dulbecco's modified eagle medium (DMEM) with 10% fetal bovine serum (FBS). Mitomycin C-inactivated MEFs were plated on culture dishes coated with 0.1% gelatin in harvested from porcupine skin in phosphate-Buffered Saline (PBS) and after 24 hours DMEM media was exchanged for DMEM with Nutrient Mixture F-12 (DMEM/F-12) supplemented with 15% knockout serum replacement, 1x L-glutamine, 1x non-essential amino acids, 1x penicillin-streptomycin, 55 µM 2-mercaptoethanol and 20 ng/ml of recombinant human fibroblast growth factor-basic (FGF-Basic). Cells were cultured in a 5% CO_2 humidified atmosphere at 37°C. For irradiation experiments, cells were irradiated with 2 gray of X-rays (RS Research Cabinet) and incubated 3 hours post-irradiation before harvesting.

4.6 iPSC hematopoietic differentiation

$CD34^+$ progenitor-enriched cultures ($CD34^+$ P-ECs) were generated from iPSCs through cytokine-induced hematopoietic differentiation of embryoid bodies (EBs) based on published protocol (Kennedy et al., 2012). To generate embryoid bodies (EBs), pre-split, iPSCs colonies were partially dissociated by incubating with Collagenase B solution (1 mg/ml in DMEM/F12) for 10 min at 37°C and 1 min by TrypLE select enzymatic solution. After removal of enzymes by washing plates two times with basal DMEM/F12 media, gently scraped, small colony fragments were resuspended in StemPro-34 SFM supplemented with bone morphogenetic protein 4 (BMP-4; 10 ng/ml), Holo-transferrin (150 mg/ml), 1x L-glutamine, 1x penicillin-streptomycin, L-ascorbic acid (1 mM), and monothioglycerol (4×10^{-4} M). Colonies fragments were then gently transferred to 6 well plate with Ultra-Low Attachment surface (Corning, New York, USA) to aggregate into EBs under hypoxic conditions (90% N2, 5% CO2 and 5% O2) at 37°C (day 0). Cytokines for directed hematopoietic differentiation were then added directly to the media as follows: day 1 - FGF-Basic (5 ng/ml); day 2 - Activin A (3 ng/ml); day 4 - medium exchange for fresh StemPro-34 SFM with Holo-transferrin (150 mg/ml), FGF-Basic (5 ng/ml), vascular endothelial growth factor (VEGF, 15 ng/ml), dickkopf-related protein 1 (DKK-1, 150 ng/ml), interleukin 6 (IL-6, 10 ng/ml), Insulin-like growth factor 1 (IGF-1, 25 ng/ml) and interleukin 11 (IL-11, 5 ng/ml); day 6 – stem cell factor (SCF, 50 ng/ml), erythropoietin (EPO, 2 U/ml final), thrombopoietin (TPO, 30 ng/ml), interleukin 3 (IL-3, 30 ng/ml), and Fms-related tyrosine kinase 3 ligand (FLT3LG, 10 ng/ml). $CD34^+$ P-ECs were cultivated until day 9 when they were harvested by centriguation for down-stream analysis. To test effects of inflammatory cytokines cultures in day 8 were supplemented with interferon gamma (IFNγ, 100 U/ml), tumor necrosis factor alpha (TNFα, 50ng/ml), transforming growth factor beta 1 (TGFβ1, 5 ng/ml) and cultivated until day 9.

4.7 Generation of *JAK2*-corrected (*JAK2* wt) HEL cell line

Generation of *JAK2*-corrected (*JAK2* wt) HEL cell line was carried out by my colleague Lucie Láníková, Ph.D. (Department of Biology, Faculty of Medicine and Dentistry, Palacky University Olomouc; Laboratory of Cell and Developmental Biology, Institute of Molecular Genetics of the ASCR, Prague; (Stetka et al., 2019)). Briefly, *JAK2* $V617F^+$ human erythroleukemia cell line (HEL cell line; kind gift of Prof. MUDr. Tomáš Stopka, Ph.D., 1st Faculty of Medicine, Charles University Prague) was repaired by homologous recombination using CRISPR/Cas9 system (CRISPR construct pXPR_001, plasmid #49535; Addgene)). A guide RNA sequence used for targeting of the *JAK2* gene was 5'-

ACGAGAGTAAGTAAAACTAC -3'. A homologous template carrying *JAK2* wt sequence was cloned into pGEM-T easy vector and wobbled (protospacer adjacent motif sequence mutated to prevent CRISPR cleavage *in vitro* while preserving the amino-acid sequence). HEL cells were electroporated using Amaxa Nucleofector system (according to manufacturer's protocol, Cell Line Nucleofector Kit V, program X-005). Cells were then single-cell sorted 48 hours post-electroporation based on their fluorescent status and single cell clones were expanded. Based on the screening test, clone 1 with *JAK2* wt genotype was selected.

4.8 Mice

Tamoxifen-inducible *Scl*Cre^{ER} mice (Göthert et al., 2005) were crossed with previously described conditional *JAK2*-V617F transgenic mice *(FF1)* (Tiedt et al., 2008), *JAK2 exon12* mutant mice (Grisouard et al., 2016) and *Jak2*-V617F conditional knock-in mice (Hasan et al., 2013). Cre^{ER} recombinase activity was induced by intraperitoneal injection of 2 mg tamoxifen for 5 consecutive days. To constitutively activate the *FF1* transgene in early hematopoietic stem cells and progenitors, *FF1* mice were also crossed with the *VavCre* strain (de Boer et al., 2003). All mice used in this study were on pure C57BL/6N background and were maintained under specific pathogen-free conditions and in accordance with Swiss federal regulations.

4.9 pIpC, pegIFNα, and TPO *in vivo* treatment

Polyinosinic polycytidylic acid (pIpC; P1530, Sigma-Aldrich) was injected intraperitoneally (300 µg per mouse) was injected subcutaneously once per week. For TPO treatment, a single dose of recombinant mouse thrombopoietin (Peprotech) was injected intraperitoneally (200 µg/kg per mouse).

4.10 Bone marrow transplantations

For competitive transplantation assays, FACS purified $CD41^{hi}$ or $CD41^{lo}$ HSC subsets (50 cells) from *VF* transgenic mice or wild type mice coexpressing GFP under UBC promoter were mixed with $1x10^6$ BM cells wildtype C57BL/6 competitors and injected intravenously (in 200µl PBS/mouse) into lethally irradiated (12 Gy) C57BL/6 recipient mice. Hematopoietic reconstitution was assessed in peripheral blood (PB) at indicated times post-transplantation by flow cytometry.

4.11 Microarray and data analysis

Biological duplicates per group were used for microarray analysis. Total RNA was isolated using TRI Reagent according to manufacturer's instructions and its integrity was tested by Agilent 2100 Bioanalyzer. All samples had RNA integrity number (RIN) above 9. RNA was amplified and labelled using Illumina TotalPrep RNA Amplification Kit and hybridized on HumanHT-12 v4 Expression BeadChips, according to manufacturers' protocols. Raw data was processed and analyzed using Genome Studio software (version 1.9.0.24624) and oligo and limma packages of the Bioconductor. Differentially expressed genes (DEGs) between the groups were detected by moderated t-test with two-fold gene expression change and Storey's q-values < 0.1 cut-off (Storey and Tibshirani, 2003). Processed data were deposited to the Array Express database (accession number: E-MTAB-7693). To visualize differences in gene expression, heatmaps were generated by Heatmapper software.

Enrichment of DEGs and generation of interaction network module maps based on gene regulatory interactions was carried out with the ConsensusPathDB software tool integrating 12 biological pathways repositories (Kegg, Reactome, Humancyc, Signalink, Ehmn, Pid, Wikipathways, Inoh, Netpath, Smpdb, Pharmgkb, Biocarta) to identify differentially regulated pathways in studied samples (Subramanian et al., 2005).

4.12 Quantitative Real-Time Polymerase Chain Reaction

Cells were pelleted at 250g for 5 min and thoroughly resuspended in TRI Reagent (1 ml of reagent per $5x10^6$ cells). Total RNA was isolated from TRI Reagent according to manufacturer's instructions and treated with TURBO DNA-free DNase for 20 min at 37°C. LightCycler 480 platform was used for reverse transcription (Transcriptor First Strand cDNA Synthesis Kit, LightCycler 480), real-time PCR with cycling conditions: 10 min 95°C, 40 cycles: [10 s 95°C, 20 s 63°C, 30 s 72°C] (LightCycler 480 SYBR Green I Master kit) and relative quantification of gene expression (LightCycler 480 software, ΔΔct-method, Roche) of all candidate genes. *RPLP0* was used as a most stable reference gene in our experimental conditions (out of candidate reference genes *YWHAZ, RPLP0* and *HPRT1*).

4.13 Flow cytometry analysis

To obtain single cell suspension from $CD34^+$ P-ECs for flow cytometry, EBs were dissociated by TrypLE Express for 10 min at 37°C, followed by 2 min of extensive pipetting with 1ml pipette tip to further release cells from EBs. Cell suspension was washed afterwards twice with ice-cold 1% BSA in PBS and flown through 40 µm cell strainer to remove cell aggregates.

For cell cycle distribution analysis, $CD34^+$ P-ECs were synchronized in basal StemPro-34 SFM media without any cytokines for 12 hours and afterwards pulse-labelled with 10µM 5-Bromo-2′-deoxyuridine (BrdU) in complete differentiation media for 12 hours. For group of samples treated with inflammatory cytokines, IFNγ, TNFα and TGFβ1 were added in both basal media for synchronization and to complete media for pulse labeling with BrdU (Σ 24 hours). Cells were then pelleted by 250g for 5 min and resuspended in 1ml of 2N HCL with 0.1% Triton X100. After 30 min incubation at room temperature, cells were washed twice with PBS-T/1%FBS (PBS containing 0.1% Tween20 and 1% FBS) and resuspended in PBS-T/1%FBS with anti-BrdU-FITC antibody (1:20; 200µl for $5x10^5$ cells). After incubation for 1 hour at room temperature cell were washed again with PBS-T/1%FBS and resuspended in eBioscience Propidium Iodide Staining Solution supplemented with 0.1 mg/ml of RNase A. After incubation for 30 min at room temperature, samples were measured on flow cytometer.

Kinetics of reactive oxygen species production after 3, 6, 12 and 24 hour treatment of $CD34^+$ P-ECs with inflammatory cytokines was measured by post-treatment CellROX Green Flow Cytometry Assay Kit probe loading (1:2500), protected from light for 30 min at 37°C and 1% O_2 atmosphere. Cells were afterwards pelleted at 250g for 3 min and 4°C and resuspended in ice-cold PBS and immediately measured by flow cytometer.

For analysis of CD34, CD41 and CD43 surface markers, single cell suspension from $CD34^+$ P-ECs was stained in PBS with 1% bovine serum albumin (BSA) by FITC tagged anti-CD34 antibody (1:20), APC conjugated anti-CD43 (1:20) and anti-CD41a-PerCP-5.5 antibody (1:5).

All the antibodies used in flow cytometry are enlisted in Table S1 (section section 7. Supplements).

Flow cytometry analysis was done by Cytomics FC 500 and data processing CXP software.

4.14 Enzyme assay

The activity of enzymes involved in antioxidative defense system was determined by my colleague Pavla Kořalková, Ph.D. (Department of Biology, Faculty of Medicine and Dentistry, Palacky University Olomouc) according to the methods recommended by the International Committee for Standardization in Haematology as previously described (Beutler et al., 1977; Horvathova et al., 2012). The measurements were adopted for protein lysates of $CD34^+$ P-ECs in RIPA buffer. Briefly, the enzyme reaction was pre-incubated for 10 min at 37°C, thereafter substrate and cell lysate were added. Absorbance was measured at 340 nm in 1 min intervals for 20 min at 37°C (spectrophotometer Infinite 200 Nanoquant) and specific enzyme activity was calculated using the Lambert-Beer law.

4.15 Immunocytochemistry on EBs in agarose gel matrix saturated with paraffin

EBs from $CD34^+$ P-ECs were centrifuged at 250g for 5 min, resuspended in 1ml of 4% neutral-buffered formaldehyde and let incubated at 4°C overnight. Fixed EBs were centrifuged next day at 250g for 5 min and resuspended in 200μl of 5% low-melting seaplaque agarose matrix, pre-warmed to 65°C. This suspension was then loaded into individual wells of 96 well plate (TPP, Schaffhausen, Switzerland) and let cooled to 4°C. Samples were then embedded into paraffin and 3-5 μm thick slides were cut on a microtome. After deparaffinization in xylene and hydration in graded alcohols, antigen unmasking was done in the microwave histoprocessor by 10mM citrate buffer, pH 6.0, 120°C, using high pressure, for 15 minutes with gradual cooling. Samples were afterwards washed two times in PBS for 3 min and blocked in 0,2% BSA in PBS-T for 1 hour at room temperature, followed by sequential primary antibodies (listed in Table S1) incubation at room temperature for 1 hour, with short PBS-T washes between each incubation. After five short washes by PBS-T, goat anti-rabbit Alexa Fluor 488 antibody and goat anti-mouse Alexa Fluor 568 conjugated secondary (listed in Table S1) was sequentially incubated at 1:1000 dilution at RT for 90 min with short PBS-T washes between each incubation. Samples were washed afterwards five times in PBS-T, one time in PBS for 3 min and incubated for 10 min at room temperature with DAPI (50ug/mL) at 1:100 dilution. After two brief washes in PBS and one time in distilled water, slides

were cover-slipped in MOWIOL 4-88 solution. Images were acquired using an Olympus BX51 inverted microscope equipped with ColorViewIII digital CCD camera.

4.16 Immunocytochemistry of CD34$^+$ P-ECs

EBs were pelleted by 250g for 5 min and dissociated into single cell suspension by TrypLE Express for 10 min at 37°C, followed by 2 min of extensive pipetting with 1ml pipette tip. Single cell suspension was washed afterwards with ice-cold 1% BSA in PBS and strained through 40 µm cell strainer. Cells were then cytospined on SuperFrost Plus adhesion microscope slides (Thermo Fischer Scientific) and fixed by 3% paraformaldehyde in PBS at room temperature for 15 min. After fixation were samples washed two times by PBS for 3 min and finally permeabilized in methanol at –20°C for 10 min and let fully air-dried.

For γH2AX/RAD51 dual staining, slides with cells were washed three times in PBS-T for 3 min and blocked in 1% BSA, 10% goat serum, 0.1% Tween20 and 0.3M Glycine in PBS for 1 hour at room temperature, followed by sequential primary antibodies (listed in Table S1) incubation diluted in 5%BSA in PBS at room temperature for 1 hour with 3 short PBS-T washes between incubations. Samples were then washed 3 times in PBS-T, once with PBS and then incubated sequentially with secondary goat anti-rabbit Alexa Fluor 488 antibody and goat anti-mouse Alexa Fluor 568 conjugated secondary antibody (both diluted in 5 % BSA in PBS at 1:1000) for 60 min at RT, with short PBS-T washes between each incubation. Samples were then mounted onto slides using the DAPI containing Vectashield mounting reagent. Slides were visualized by the Axio Observer.Z1/Cell Observer Spinning Disc microscopic system equipped with an Evolve 512 EMCCD camera. For quantitative image analysis, a series of random fields were recorded using ScanR imaging workstation. Intensity and numbers of nuclear foci were quantified using the ScanR image analysis software.

4.17 Inhibition of dual-specificity phosphatases (DUSPs)

To test effects of DUSP 1/6 Inhibitor (BCI - CAS 15982-84-0) *JAK2* wt and V617F$^+$ HEL cells were incubated with 10µM BCI in defined timepoints (0.5, 1, 2, 4 and 6h). Cells which were also treated with inflammatory cytokines (IFNγ, TNFα and TGFβ1 / 24 hours) were incubated with 10µM BCI in defined timepoints prior the end of 24-hour cytokine

treatment. Relative expression of total and phosphorylated forms of p38 MAPK, ERK1/2 and SAPK/JNK was afterwards analyzed by western blotting.

4.18 Western blotting

Cell were harvested by centrifugation at 250g for 5 min, washed by PBS and lysed in IP buffer with 1x phosphatase inhibitor cocktail.
40 μg of proteins heated up to 90°C for 10 minutes with 1x loading buffer was loaded and run in 10% precast SDS-PAGE gel (100V, 1 hour) and subsequently transferred to a PVDF membrane. Proteins of interest were detected using primary antibodies (1:500, listed in Table S1) diluted in PBS with 5% BSA and 0.1% Tween20. HRP-conjugated anti-rabbit or mouse secondary antibodies (1:1000) diluted in 5% non-fat dry milk, were used together with SuperSignal HRP Chemiluminescent Substrates to visualize proteins of interest with Odyssey Imaging System.

4.19 Immunohistochemistry of patient samples

Tissue processing and immunohistochemistry staining was done by my colleague Pavla Vyhlídalová, Ph.D. (Department of Biology, Faculty of Medicine and Dentistry, Palacky University Olomouc) and my wife Bc. Ivana Štetková (Department of Histology and Embryology, Faculty of Medicine and Dentistry, Palacky University Olomouc). Briefly, all tissue samples were fixed in neutral buffered 4% formalin for 24 hours and finally embedded into paraffin according to the standard protocol used for biopsy samples processing. In the cases of BM trephine biopsies, the necessary process of demineralization was performed by 10% chelatone 3 (pH8) directly after fixation. Further, 3-5 μm thick slides were cut on a microtome and a routine HE (hematoxylin-eosin) staining was performed. The skilled pathologist evaluated the diagnosis. To assess the grading of fibrosis in PV, Gomori's silver impregnation for reticulin was performed on BM trephine biopsies.
For visualization of desired antigens two step immunohistochemical staining was performed. The primary antibodies used are specified in Table S1. Antigen unmasking was done in the microwave histoprocessor by 10mM citrate buffer, pH6.0, 120°C, using high pressure, for 15 minutes with gradual cooling. The following detection system was used: Dako EnVision + Dual Link System-HRP (polymer labeled by HRP) and conjugated with secondary antibodies (DAKO, Glostrup, Denmark). Liquid DAB +

Substrate Chromogen System (DAKO, Glostrup, Denmark) was used for visualization of reaction. All the washing steps were made twice in 0.5M Tris-HCl pH7.6 (5 minutes each) and once in 0.5M Tris-HCl pH7.6 with 0.5% Tween 20 (5 minutes). Finally, cell nuclei were counterstained by hematoxylin and the slide was coverslipped.

For the staining evaluation, the scoring system access according to the paper (van Dekken et al., 2008) was chosen. This scoring is based on 4 score values (0, 1, 2, 3) which are assigned to the % of positive cells stained. 0 represents negative staining, 1 responds to 25 % of positivity, 2 to 25 - 50% positivity in the specimen and positivity over 50 % is characterized by score 3. Cell positivity counts were done under the magn.x100 and 3 fields of view/sample were observed. In the case of γH2AX staining, the scoring system was modified. The overall γH2AX positivity was weak, so following score was used (value 0 = 0 of positive cells/field of view; value 1 = 1-2 of positive cells/field of view and 2 = 3 and more pos. cells/field of view; totally 10 fields of view per sample were evaluated). Images were acquired using an Olympus BX51 inverted microscope equipped with ColorViewIII digital CCD camera.

4.20 Iron deficient diet and iron injections

To induce dietary iron deficiency, mice were placed on iron-deficient diet (iron content < 5 mg iron/kg, SAFE, Augy, France), or on identical control diet supplemented with 200 mg/kg carbonyl-iron (SAFE, Augy, France). In a subgroup of mice on iron-deficient diet, additional tail bleedings (max. 200μL) were performed every 4 weeks to accentuate iron deficiency. For parenteral iron injections Iron-Dextran (D8517, Sigma Aldrich) was injected intraperitoneally (250 mg/kg per mouse).

4.21 Liver iron content

To measure iron content in liver tissue, livers were fixed in 4% phosphate-buffered formalin and weighted amount were digested by concentrated HNO_3 (69%, ROTIPURAN Supra, Roth) inside a microwave oven (synthWave, MWS Mikrowelle GmbH) for 10 min at 170°C and 25 min at 200°C. After digestion iron content was analyzed by inductively coupled plasma mass spectrometry (ICP-MS) using KED mode (He value 4.5) on NexIon 350 D ICP-MS instrument (PerkinElmer). Y was used as an internal standard and iron quantitation was performed using external calibration curve with standards in 0.05-50 ppb range. All measurements were performed in triplicates.

4.22 Iron parameters and regulatory cytokines

Transferrin saturation was calculated as the ratio between serum iron and total iron binding capacity, estimated with Flex reagent cartridge (DF84, DF85) of Dimension clinical chemistry system (Siemens), according to the manufacturer's instructions. Hepcidin Murine-Compete and Intrinsic Mouse Erythroferrone ELISA kits (Intrinsic Lifesciences) were used to analyze serum levels of hepcidin and erythroferrone. Serum and bone marrow lavage thrombopoietin (Tpo) levels were measured using mouse Tpo quantikine set (R&D System). Erythropoietin (Epo) levels in serum were analyzed by Legendplex Mouse HSC Erythroid Panel (Biolegend).

4.23 Statistical analysis

Mean values +/- SD for human samples or SEM for mouse samples are shown. Student t test, Wilcoxon signed-rank test, two-way and one-way ANOVA was used for obtaining statistical significance values with multiple comparison posttests (using Graph-Pad Prism software).

5. Summary

The myeloproliferative neoplasms (MPN) - polycythemia vera (PV), essential thrombocythemia (ET) and primary myelofibrosis (PMF) - are hematopoietic stem-cell disorders, which share mutations that constitutively activate the cytokine receptor/JAK-STAT pathway (Campbell and Green, 2006). The most frequent driver mutation in MPN is *JAK2* V617F (Baxter et al., 2005; James et al., 2005; Kralovics et al., 2005; Levine et al., 2005), with predominant frequency of approximately 95% of patients in PV, it is also detectable in about 50% of patients with ET and PMF (Tefferi, 2016). Virtually all clinical entities of MPN are also characterized by systemic inflammatory signaling. Recent studies suggest that inflammation may be not only a consequence of malignant propagation of a clone but also important driving force of clonal evolution and disease progression (Hasselbalch et al., 2015). Various questions of MPN disease biology, however, remain open, including how MPN progenitors are able to cope and proliferate in inflammatory microenvironment and maintain the previously described genome-wide stability. Furthermore, how the identical *JAK2* V617F mutation can cause distinct clinical entities and how is the pegylated interferon alpha, the only therapy which is able to deliver complete molecular remission, able to selectively target the *JAK2* V617F disease initiating stem cell pool. We have, therefore, sought to contribute with here presented dataset to each of these questions.

First, we used PV patient-specific iPSCs along with genetically modified *JAK2* V617F-positive or *JAK2* wildtype HEL cells as well as immunohistochemistry staining of PV patients' bone marrow to investigate the hierarchy and consequences of inflammatory signature activation in PV. We have successfully described intrinsic inflammatory profile of $CD34^+$ patient-specific iPSCs-derived hematopoietic stem cells, which show to upregulate IFN-gamma and NF-κB-associated inflammatory program. As a consequence, these PV progenitors upregulate reactive oxygen species (ROS) antioxidant system and expression of dual specificity phosphatase (DUSP) 1. DUSP1 then suppress JNK and p38MAPK activities, including inflammation-evoked DNA damage, cell cycle arrest and apoptosis of *JAK2* V617F-positive cells. Therefore, we provide evidence that hyperactivated ROS buffering system and overexpression of DUSP1 in *JAK2* V617F-positive cells is a candidate mechanism keeping fast-cycling PV progenitors in proliferative phase despite the presence of DNA damaging inflammatory microenvironment. Our data also suggest that these mechanisms then delay stress-

induced regulatory circuits in hematopoiesis associated with myelofibrosis and decreasing DNA damage accumulation associated with rapid malignant transformation.

Second, under supervision of prof. Radek C. Skoda and with my colleague Dr. Rao N. Tata (Basel) we studied the phenomena of megakaryocyte-biased CD41^{hi} hematopoietic stem cells induced by mutant *JAK2* with lower long-term engraftment potential in MPN mouse models. We showed that long-term treatment with pegylated interferon alpha further increased the proportion of CD41^{hi} HSCs and depletes *JAK2* mutant HSCs in mice and MPN patients. Consequently, expression of CD41 not only provides insight into mechanism by which interferon exhausts pool of long-term hematopoietic stem cells, but also an easily accessible surface marker of interferon therapy effectiveness.

Third, we hypothesized that iron availability is one of the key factors influencing MPN phenotype manifestation, especially in regards to erythroid expansion in PV and platelet production in ET. By reciprocal approaches of inducing iron deficiency or iron overload in PV and ET mouse models, we were able to uncover iron-dependency in these models at early stages of hematopoietic differentiation that drives iron-dependent switch between thrombocytosis and erythrocytosis.

Overall, we present a comprehensive dataset aimed at better understanding of underlying mechanisms of MPN disease biology that could provide possible targets for innovative therapies and markers of disease remission.

6. References

Aggarwal, V., Tuli, H.S., Varol, A., Thakral, F., Yerer, M.B., Sak, K., Varol, M., Jain, A., Khan, Md.A., Sethi, G., 2019. Role of Reactive Oxygen Species in Cancer Progression: Molecular Mechanisms and Recent Advancements. Biomolecules 9. https://doi.org/10.3390/biom9110735

Ahn, J.S., Li, J., Chen, E., Kent, D.G., Park, H.J., Green, A.R., 2016. JAK2V617F mediates resistance to DNA damage-induced apoptosis by modulating FOXO3A localization and Bcl-xL deamidation. Oncogene 35, 2235–2246. https://doi.org/10.1038/onc.2015.285

Alexander, A., Walker, C.L., 2010. Differential localization of ATM is correlated with activation of distinct downstream signaling pathways. Cell Cycle 9, 3685–3686. https://doi.org/10.4161/cc.9.18.13253

Allan, J.M., Smith, A.G., Wheatley, K., Hills, R.K., Travis, L.B., Hill, D.A., Swirsky, D.M., Morgan, G.J., Wild, C.P., 2004. Genetic variation in XPD predicts treatment outcome and risk of acute myeloid leukemia following chemotherapy. Blood 104, 3872–3877. https://doi.org/10.1182/blood-2004-06-2161

Arber, D.A., Orazi, A., Hasserjian, R., Thiele, J., Borowitz, M.J., Le Beau, M.M., Bloomfield, C.D., Cazzola, M., Vardiman, J.W., 2016. The 2016 revision to the World Health Organization classification of myeloid neoplasms and acute leukemia. Blood 127, 2391–2405. https://doi.org/10.1182/blood-2016-03-643544

Arranz, L., Sánchez-Aguilera, A., Martín-Pérez, D., Isern, J., Langa, X., Tzankov, A., Lundberg, P., Muntión, S., Tzeng, Y.-S., Lai, D.-M., Schwaller, J., Skoda, R.C., Méndez-Ferrer, S., 2014. Neuropathy of haematopoietic stem cell niche is essential for myeloproliferative neoplasms. Nature 512, 78–81. https://doi.org/10.1038/nature13383

Arthur, J.S.C., Ley, S.C., 2013. Mitogen-activated protein kinases in innate immunity. Nat. Rev. Immunol. 13, 679–692. https://doi.org/10.1038/nri3495

Auerbach, A.D., 1992. Fanconi anemia and leukemia: tracking the genes. Leukemia 6 Suppl 1, 1–4.

Baba, T., Tanabe, Y., Yoshikawa, S., Yamanishi, Y., Morishita, S., Komatsu, N., Karasuyama, H., Hirao, A., Mukaida, N., 2016. MIP-1α/CCL3-expressing basophil-lineage cells drive the leukemic hematopoiesis of chronic myeloid leukemia in mice. Blood 127, 2607–2617. https://doi.org/10.1182/blood-2015-10-673087

Babicki, S., Arndt, D., Marcu, A., Liang, Y., Grant, J.R., Maciejewski, A., Wishart, D.S., 2016. Heatmapper: web-enabled heat mapping for all. Nucleic Acids Res 44, W147–W153. https://doi.org/10.1093/nar/gkw419

Balazs, A.B., Fabian, A.J., Esmon, C.T., Mulligan, R.C., 2006. Endothelial protein C receptor (CD201) explicitly identifies hematopoietic stem cells in murine bone marrow. Blood 107, 2317–2321. https://doi.org/10.1182/blood-2005-06-2249

Baldridge, M.T., King, K.Y., Boles, N.C., Weksberg, D.C., Goodell, M.A., 2010. Quiescent hematopoietic stem cells are activated by IFNγ in response to chronic infection. Nature 465, 793–797. https://doi.org/10.1038/nature09135

Bănescu, C., Duicu, C., Trifa, A.P., Dobreanu, M., 2014. XRCC1 Arg194Trp and

Arg399Gln polymorphisms are significantly associated with shorter survival in acute myeloid leukemia. Leuk. Lymphoma 55, 365–370. https://doi.org/10.3109/10428194.2013.802781

Bartek, J., Hodny, Z., Lukas, J., 2008. Cytokine loops driving senescence. Nat. Cell Biol. 10, 887–889. https://doi.org/10.1038/ncb0808-887

Bartkova, J., Horejsí, Z., Koed, K., Krämer, A., Tort, F., Zieger, K., Guldberg, P., Sehested, M., Nesland, J.M., Lukas, C., Ørntoft, T., Lukas, J., Bartek, J., 2005. DNA damage response as a candidate anti-cancer barrier in early human tumorigenesis. Nature 434, 864–870. https://doi.org/10.1038/nature03482

Baxter, E.J., Scott, L.M., Campbell, P.J., East, C., Fourouclas, N., Swanton, S., Vassiliou, G.S., Bench, A.J., Boyd, E.M., Curtin, N., Scott, M.A., Erber, W.N., Green, A.R., Cancer Genome Project, 2005. Acquired mutation of the tyrosine kinase JAK2 in human myeloproliferative disorders. Lancet 365, 1054–1061. https://doi.org/10.1016/S0140-6736(05)71142-9

Bennett, B.T., Bewersdorf, J., Knight, K.L., 2009. Immunofluorescence imaging of DNA damage response proteins: optimizing protocols for super-resolution microscopy. Methods 48, 63–71. https://doi.org/10.1016/j.ymeth.2009.02.009

Ben-Yehuda, D., Krichevsky, S., Caspi, O., Rund, D., Polliack, A., Abeliovich, D., Zelig, O., Yahalom, V., Paltiel, O., Or, R., Peretz, T., Ben-Neriah, S., Yehuda, O., Rachmilewitz, E.A., 1996. Microsatellite instability and p53 mutations in therapy-related leukemia suggest mutator phenotype. Blood 88, 4296–4303.

Beutler, E., Blume, K.G., Kaplan, J.C., Löhr, G.W., Ramot, B., Valentine, W.N., 1977. International Committee for Standardization in Haematology: Recommended Methods for Red-Cell Enzyme Analysis*. British Journal of Haematology 35, 331–340. https://doi.org/10.1111/j.1365-2141.1977.tb00589.x

Blaser, H., Dostert, C., Mak, T.W., Brenner, D., 2016. TNF and ROS Crosstalk in Inflammation. Trends Cell Biol. 26, 249–261. https://doi.org/10.1016/j.tcb.2015.12.002

Block, M., Jacobson, L.O., Bethard, W.F., 1953. Preleukemic acute human leukemia. J Am Med Assoc 152, 1018–1028. https://doi.org/10.1001/jama.1953.03690110032010

Bock, O., Loch, G., Schade, U., von Wasielewski, R., Schlué, J., Kreipe, H., 2005. Aberrant expression of transforming growth factor beta-1 (TGF beta-1) per se does not discriminate fibrotic from non-fibrotic chronic myeloproliferative disorders. J. Pathol. 205, 548–557. https://doi.org/10.1002/path.1744

Bohr, V.A., 2008. Rising from the RecQ-age: the role of human RecQ helicases in genome maintenance. Trends Biochem. Sci. 33, 609–620. https://doi.org/10.1016/j.tibs.2008.09.003

Borthakur, G., Estey, A.E.E., 2007. Therapy-related acute myelogenous leukemia and myelodysplastic syndrome. Curr Oncol Rep 9, 373–377. https://doi.org/10.1007/s11912-007-0050-z

Bowman, R.L., Busque, L., Levine, R.L., 2018. Clonal Hematopoiesis and Evolution to Hematopoietic Malignancies. Cell Stem Cell 22, 157–170. https://doi.org/10.1016/j.stem.2018.01.011

Bryder, D., Ramsfjell, V., Dybedal, I., Theilgaard-Mönch, K., Högerkorp, C.-M.,

Adolfsson, J., Borge, O.J., Jacobsen, S.E.W., 2001. Self-Renewal of Multipotent Long-Term Repopulating Hematopoietic Stem Cells Is Negatively Regulated by FAS and Tumor Necrosis Factor Receptor Activation. J Exp Med 194, 941–952. https://doi.org/10.1084/jem.194.7.941

Busque, L., Buscarlet, M., Mollica, L., Levine, R.L., 2018. Concise Review: Age-Related Clonal Hematopoiesis: Stem Cells Tempting the Devil. Stem Cells 36, 1287–1294. https://doi.org/10.1002/stem.2845

Camaschella, C., Pagani, A., 2018. Advances in understanding iron metabolism and its crosstalk with erythropoiesis. British Journal of Haematology 182, 481–494. https://doi.org/10.1111/bjh.15403

Campbell, P.J., Green, A.R., 2006. The myeloproliferative disorders. N. Engl. J. Med. 355, 2452–2466. https://doi.org/10.1056/NEJMra063728

Carrelha, J., Meng, Y., Kettyle, L.M., Luis, T.C., Norfo, R., Alcolea, V., Boukarabila, H., Grasso, F., Gambardella, A., Grover, A., Högstrand, K., Lord, A.M., Sanjuan-Pla, A., Woll, P.S., Nerlov, C., Jacobsen, S.E.W., 2018. Hierarchically related lineage-restricted fates of multipotent haematopoietic stem cells. Nature 554, 106–111. https://doi.org/10.1038/nature25455

Carvalho, B.S., Irizarry, R.A., 2010. A framework for oligonucleotide microarray preprocessing. Bioinformatics 26, 2363–2367. https://doi.org/10.1093/bioinformatics/btq431

Casorelli, I., Offman, J., Mele, L., Pagano, L., Sica, S., D'Errico, M., Giannini, G., Leone, G., Bignami, M., Karran, P., 2003. Drug treatment in the development of mismatch repair defective acute leukemia and myelodysplastic syndrome. DNA Repair (Amst.) 2, 547–559.

Cazzola, M., Della Porta, M.G., Travaglino, E., Malcovati, L., 2011. Classification and prognostic evaluation of myelodysplastic syndromes. Semin. Oncol. 38, 627–634. https://doi.org/10.1053/j.seminoncol.2011.04.007

Chagraoui, H., Komura, E., Tulliez, M., Giraudier, S., Vainchenker, W., Wendling, F., 2002. Prominent role of TGF-beta 1 in thrombopoietin-induced myelofibrosis in mice. Blood 100, 3495–3503. https://doi.org/10.1182/blood-2002-04-1133

Chen, E., Ahn, J.S., Massie, C.E., Clynes, D., Godfrey, A.L., Li, J., Park, H.J., Nangalia, J., Silber, Y., Mullally, A., Gibbons, R.J., Green, A.R., 2014. JAK2V617F promotes replication fork stalling with disease-restricted impairment of the intra-S checkpoint response. PNAS 111, 15190–15195. https://doi.org/10.1073/pnas.1401873111

Chen, E., Ahn, J.S., Sykes, D.B., Breyfogle, L.J., Godfrey, A.L., Nangalia, J., Ko, A., DeAngelo, D.J., Green, A.R., Mullally, A., 2015. RECQL5 Suppresses Oncogenic JAK2-Induced Replication Stress and Genomic Instability. Cell Reports 13, 2345–2352. https://doi.org/10.1016/j.celrep.2015.11.037

Chen, E., Beer, P.A., Godfrey, A.L., Ortmann, C.A., Li, J., Costa-Pereira, A.P., Ingle, C.E., Dermitzakis, E.T., Campbell, P.J., Green, A.R., 2010. Distinct clinical phenotypes associated with JAK2V617F reflect differential STAT1 signaling. Cancer Cell 18, 524–535. https://doi.org/10.1016/j.ccr.2010.10.013

Chu, W.K., Hickson, I.D., 2009. RecQ helicases: multifunctional genome caretakers. Nat. Rev. Cancer 9, 644–654. https://doi.org/10.1038/nrc2682

Coombs, C.C., Zehir, A., Devlin, S.M., Kishtagari, A., Syed, A., Jonsson, P., Hyman,

D.M., Solit, D.B., Robson, M.E., Baselga, J., Arcila, M.E., Ladanyi, M., Tallman, M.S., Levine, R.L., Berger, M.F., 2017. Therapy-Related Clonal Hematopoiesis in Patients with Non-hematologic Cancers Is Common and Associated with Adverse Clinical Outcomes. Cell Stem Cell 21, 374-382.e4. https://doi.org/10.1016/j.stem.2017.07.010

Corces-Zimmerman, M.R., Hong, W.-J., Weissman, I.L., Medeiros, B.C., Majeti, R., 2014. Preleukemic mutations in human acute myeloid leukemia affect epigenetic regulators and persist in remission. PNAS 111, 2548–2553. https://doi.org/10.1073/pnas.1324297111

Craver, B.M., Ramanathan, G., Hoang, S., Chang, X., Mendez Luque, L.F., Brooks, S., Lai, H.Y., Fleischman, A.G., 2020. N-acetylcysteine inhibits thrombosis in a murine model of myeloproliferative neoplasm. Blood Adv 4, 312–321. https://doi.org/10.1182/bloodadvances.2019000967

de Boer, J., Williams, A., Skavdis, G., Harker, N., Coles, M., Tolaini, M., Norton, T., Williams, K., Roderick, K., Potocnik, A.J., Kioussis, D., 2003. Transgenic mice with hematopoietic and lymphoid specific expression of Cre. Eur J Immunol 33, 314–325. https://doi.org/10.1002/immu.200310005

Dela Cruz, C.S., Kang, M.-J., 2018. Mitochondrial Dysfunction and Damage Associated Molecular Patterns (DAMPs) in Chronic Inflammatory Diseases. Mitochondrion 41, 37–44. https://doi.org/10.1016/j.mito.2017.12.001

Desai, P., Mencia-Trinchant, N., Savenkov, O., Simon, M.S., Cheang, G., Lee, S., Samuel, M., Ritchie, E.K., Guzman, M.L., Ballman, K.V., Roboz, G.J., Hassane, D.C., 2018. Somatic mutations precede acute myeloid leukemia years before diagnosis. Nat. Med. 24, 1015–1023. https://doi.org/10.1038/s41591-018-0081-z

Desterke, C., Bilhou-Nabéra, C., Guerton, B., Martinaud, C., Tonetti, C., Clay, D., Guglielmelli, P., Vannucchi, A., Bordessoule, D., Hasselbalch, H., Dupriez, B., Benzoubir, N., Bourgeade, M.-F., Pierre-Louis, O., Lazar, V., Vainchenker, W., Bennaceur-Griscelli, A., Gisslinger, H., Giraudier, S., Le Bousse-Kerdilès, M.-C., French Intergroup of Myeloproliferative Disorders, French INSERM, European EUMNET Networks on Myelofibrosis, 2011. FLT3-mediated p38-MAPK activation participates in the control of megakaryopoiesis in primary myelofibrosis. Cancer Res. 71, 2901–2915. https://doi.org/10.1158/0008-5472.CAN-10-1731

Di Micco, R., Fumagalli, M., Cicalese, A., Piccinin, S., Gasparini, P., Luise, C., Schurra, C., Garre', M., Nuciforo, P.G., Bensimon, A., Maestro, R., Pelicci, P.G., d'Adda di Fagagna, F., 2006. Oncogene-induced senescence is a DNA damage response triggered by DNA hyper-replication. Nature 444, 638–642. https://doi.org/10.1038/nature05327

Duek, A., Lundberg, P., Shimizu, T., Grisouard, J., Karow, A., Kubovcakova, L., Hao-Shen, H., Dirnhofer, S., Skoda, R.C., 2014. Loss of Stat1 decreases megakaryopoiesis and favors erythropoiesis in a JAK2-V617F–driven mouse model of MPNs. Blood 123, 3943–3950. https://doi.org/10.1182/blood-2013-07-514208

Dumont, F.J., Palfree, R.G., Coker, L.Z., 1986. Phenotypic changes induced by interferon in resting T cells: major enhancement of Ly-6 antigen expression. J. Immunol. 137, 201–210.

Dybedal, I., Bryder, D., Fossum, A., Rusten, L.S., Jacobsen, S.E.W., 2001. Tumor necrosis factor (TNF)–mediated activation of the p55 TNF receptor negatively regulates maintenance of cycling reconstituting human hematopoietic stem cells.

Blood 98, 1782–1791. https://doi.org/10.1182/blood.V98.6.1782

Essers, M.A.G., Offner, S., Blanco-Bose, W.E., Waibler, Z., Kalinke, U., Duchosal, M.A., Trumpp, A., 2009. IFNalpha activates dormant haematopoietic stem cells in vivo. Nature 458, 904–908. https://doi.org/10.1038/nature07815

Flach, J., Bakker, S.T., Mohrin, M., Conroy, P.C., Pietras, E.M., Reynaud, D., Alvarez, S., Diolaiti, M.E., Ugarte, F., Forsberg, E.C., Le Beau, M.M., Stohr, B.A., Méndez, J., Morrison, C.G., Passegué, E., 2014. Replication stress is a potent driver of functional decline in ageing haematopoietic stem cells. Nature 512, 198–202. https://doi.org/10.1038/nature13619

Fleischman, A.G., Aichberger, K.J., Luty, S.B., Bumm, T.G., Petersen, C.L., Doratotaj, S., Vasudevan, K.B., LaTocha, D.H., Yang, F., Press, R.D., Loriaux, M.M., Pahl, H.L., Silver, R.T., Agarwal, A., O'Hare, T., Druker, B.J., Bagby, G.C., Deininger, M.W., 2011. TNFα facilitates clonal expansion of JAK2V617F positive cells in myeloproliferative neoplasms. Blood 118, 6392–6398. https://doi.org/10.1182/blood-2011-04-348144

Fuster, J.J., MacLauchlan, S., Zuriaga, M.A., Polackal, M.N., Ostriker, A.C., Chakraborty, R., Wu, C.-L., Sano, S., Muralidharan, S., Rius, C., Vuong, J., Jacob, S., Muralidhar, V., Robertson, A.A.B., Cooper, M.A., Andrés, V., Hirschi, K.K., Martin, K.A., Walsh, K., 2017. Clonal hematopoiesis associated with TET2 deficiency accelerates atherosclerosis development in mice. Science 355, 842–847. https://doi.org/10.1126/science.aag1381

Galadari, S., Rahman, A., Pallichankandy, S., Thayyullathil, F., 2017. Reactive oxygen species and cancer paradox: To promote or to suppress? Free Radic. Biol. Med. 104, 144–164. https://doi.org/10.1016/j.freeradbiomed.2017.01.004

Gañán-Gómez, I., Wei, Y., Starczynowski, D., Colla, S., Yang, H., Cabrero-Calvo, M., Bohannan, Z., Verma, A., Steidl, U., Garcia-Manero, G., 2015. Deregulation of innate immune and inflammatory signaling in myelodysplastic syndromes. Leukemia 29, 1458–1469. https://doi.org/10.1038/leu.2015.69

Gekas, C., Graf, T., 2013. CD41 expression marks myeloid-biased adult hematopoietic stem cells and increases with age. Blood 121, 4463–4472. https://doi.org/10.1182/blood-2012-09-457929

Genovese, G., Kähler, A.K., Handsaker, R.E., Lindberg, J., Rose, S.A., Bakhoum, S.F., Chambert, K., Mick, E., Neale, B.M., Fromer, M., Purcell, S.M., Svantesson, O., Landén, M., Höglund, M., Lehmann, S., Gabriel, S.B., Moran, J.L., Lander, E.S., Sullivan, P.F., Sklar, P., Grönberg, H., Hultman, C.M., McCarroll, S.A., 2014. Clonal hematopoiesis and blood-cancer risk inferred from blood DNA sequence. N. Engl. J. Med. 371, 2477–2487. https://doi.org/10.1056/NEJMoa1409405

Gentleman, R.C., Carey, V.J., Bates, D.M., Bolstad, B., Dettling, M., Dudoit, S., Ellis, B., Gautier, L., Ge, Y., Gentry, J., Hornik, K., Hothorn, T., Huber, W., Iacus, S., Irizarry, R., Leisch, F., Li, C., Maechler, M., Rossini, A.J., Sawitzki, G., Smith, C., Smyth, G., Tierney, L., Yang, J.Y.H., Zhang, J., 2004. Bioconductor: open software development for computational biology and bioinformatics. Genome Biol. 5, R80. https://doi.org/10.1186/gb-2004-5-10-r80

Ginzburg, Y.Z., Feola, M., Zimran, E., Varkonyi, J., Ganz, T., Hoffman, R., 2018. Dysregulated iron metabolism in polycythemia vera: etiology and consequences. Leukemia 32, 2105–2116. https://doi.org/10.1038/s41375-018-0207-9

Godley, L.A., Larson, R.A., 2008. Therapy-related Myeloid Leukemia. Semin Oncol 35,

418–429. https://doi.org/10.1053/j.seminoncol.2008.04.012

Gonçalves, A.C., Cortesão, E., Oliveiros, B., Alves, V., Espadana, A.I., Rito, L., Magalhães, E., Lobão, M.J., Pereira, A., Costa, J.M.N., Mota-Vieira, L., Sarmento-Ribeiro, A.B., 2015. Oxidative stress and mitochondrial dysfunction play a role in myelodysplastic syndrome development, diagnosis, and prognosis: A pilot study. Free Radical Research 49, 1081–1094. https://doi.org/10.3109/10715762.2015.1035268

Göthert, J.R., Gustin, S.E., Hall, M.A., Green, A.R., Göttgens, B., Izon, D.J., Begley, C.G., 2005. In vivo fate-tracing studies using the Scl stem cell enhancer: embryonic hematopoietic stem cells significantly contribute to adult hematopoiesis. Blood 105, 2724–2732. https://doi.org/10.1182/blood-2004-08-3037

Grisouard, J., Li, S., Kubovcakova, L., Rao, T.N., Meyer, S.C., Lundberg, P., Hao-Shen, H., Romanet, V., Murakami, M., Radimerski, T., Dirnhofer, S., Skoda, R.C., 2016. JAK2 exon 12 mutant mice display isolated erythrocytosis and changes in iron metabolism favoring increased erythropoiesis. Blood 128, 839–851. https://doi.org/10.1182/blood-2015-12-689216

Grover, A., Sanjuan-Pla, A., Thongjuea, S., Carrelha, J., Giustacchini, A., Gambardella, A., Macaulay, I., Mancini, E., Luis, T.C., Mead, A., Jacobsen, S.E.W., Nerlov, C., 2016. Single-cell RNA sequencing reveals molecular and functional platelet bias of aged haematopoietic stem cells. Nat Commun 7, 11075. https://doi.org/10.1038/ncomms11075

Guo, Z., Kozlov, S., Lavin, M.F., Person, M.D., Paull, T.T., 2010. ATM activation by oxidative stress. Science 330, 517–521. https://doi.org/10.1126/science.1192912

Haas, S., Hirche, C., Schnell, A., Sönmezer, C., Langstein, J., Wurzer, S., Thier, M., Blaszkiewicz, S., Pilz, F., Milsom, M.D., Trumpp, A., Lipka, D., Kalinke, U., Essers, M.A.G., 2017. A Stem Cell-Based Epigenetic Memory Mediates Interferon Response-Heterogeneity within the Hematopoietic System. Blood 130 (Suppl1), 634 (abstract 501).

Haas, S., Trumpp, A., Milsom, M.D., 2018. Causes and Consequences of Hematopoietic Stem Cell Heterogeneity. Cell Stem Cell 22, 627–638. https://doi.org/10.1016/j.stem.2018.04.003

Haase, D., Germing, U., Schanz, J., Pfeilstöcker, M., Nösslinger, T., Hildebrandt, B., Kundgen, A., Lübbert, M., Kunzmann, R., Giagounidis, A.A.N., Aul, C., Trümper, L., Krieger, O., Stauder, R., Müller, T.H., Wimazal, F., Valent, P., Fonatsch, C., Steidl, C., 2007. New insights into the prognostic impact of the karyotype in MDS and correlation with subtypes: evidence from a core dataset of 2124 patients. Blood 110, 4385–4395. https://doi.org/10.1182/blood-2007-03-082404

Haferlach, T., Nagata, Y., Grossmann, V., Okuno, Y., Bacher, U., Nagae, G., Schnittger, S., Sanada, M., Kon, A., Alpermann, T., Yoshida, K., Roller, A., Nadarajah, N., Shiraishi, Y., Shiozawa, Y., Chiba, K., Tanaka, H., Koeffler, H.P., Klein, H.-U., Dugas, M., Aburatani, H., Kohlmann, A., Miyano, S., Haferlach, C., Kern, W., Ogawa, S., 2014. Landscape of genetic lesions in 944 patients with myelodysplastic syndromes. Leukemia 28, 241–247. https://doi.org/10.1038/leu.2013.336

Hamdy, M.S., El-Haddad, A.M., Bahaa El-Din, N.M., Makhlouf, M.M., Abdel-Hamid, S.M., 2011. RAD51 and XRCC3 gene polymorphisms and the risk of developing acute myeloid leukemia. J. Investig. Med. 59, 1124–1130. https://doi.org/10.2310/JIM.0b013e3182281da3

Hasan, S., Lacout, C., Marty, C., Cuingnet, M., Solary, E., Vainchenker, W., Villeval, J.-L., 2013. JAK2V617F expression in mice amplifies early hematopoietic cells and gives them a competitive advantage that is hampered by IFNα. Blood 122, 1464–1477. https://doi.org/10.1182/blood-2013-04-498956

Hasselbalch, H.C., 2014. Perspectives on the impact of JAK-inhibitor therapy upon inflammation-mediated comorbidities in myelofibrosis and related neoplasms. Expert Rev Hematol 7, 203–216. https://doi.org/10.1586/17474086.2013.876356

Hasselbalch, H.C., Bjørn, Rn, M.E., 2015. MPNs as Inflammatory Diseases: The Evidence, Consequences, and Perspectives. Mediators of Inflammation 2015, e102476. https://doi.org/10.1155/2015/102476

Horvathova, M., Kapralova, K., Zidova, Z., Dolezal, D., Pospisilova, D., Divoky, V., 2012. Erythropoietin-driven signaling ameliorates the survival defect of DMT1-mutant erythroid progenitors and erythroblasts. Haematologica 97, 1480–1488. https://doi.org/10.3324/haematol.2011.059550

Hubackova, S., Krejcikova, K., Bartek, J., Hodny, Z., 2012. IL1- and TGFβ-Nox4 signaling, oxidative stress and DNA damage response are shared features of replicative, oncogene-induced, and drug-induced paracrine “bystander senescence.” Aging (Albany NY) 4, 932–951. https://doi.org/10.18632/aging.100520

Hubackova, S., Kucerova, A., Michlits, G., Kyjacova, L., Reinis, M., Korolov, O., Bartek, J., Hodny, Z., 2016. IFNγ induces oxidative stress, DNA damage and tumor cell senescence via TGFβ/SMAD signaling-dependent induction of Nox4 and suppression of ANT2. Oncogene 35, 1236–1249. https://doi.org/10.1038/onc.2015.162

Hurtado-Nedelec, M., Csillag-Grange, M.-J., Boussetta, T., Belambri, S.A., Fay, M., Cassinat, B., Gougerot-Pocidalo, M.-A., Dang, P.M.-C., El-Benna, J., 2013. Increased reactive oxygen species production and p47phox phosphorylation in neutrophils from myeloproliferative disorders patients with JAK2 (V617F) mutation. Haematologica 98, 1517–1524. https://doi.org/10.3324/haematol.2012.082560

Inoue, S., Li, W.Y., Tseng, A., Beerman, I., Elia, A.J., Bendall, S.C., Lemonnier, F., Kron, K.J., Cescon, D.W., Hao, Z., Lind, E.F., Takayama, N., Planello, A.C., Shen, S.Y., Shih, A.H., Larsen, D.M., Li, Q., Snow, B.E., Wakeham, A., Haight, J., Gorrini, C., Bassi, C., Thu, K.L., Murakami, K., Elford, A.R., Ueda, T., Straley, K., Yen, K.E., Melino, G., Cimmino, L., Aifantis, I., Levine, R.L., De Carvalho, D.D., Lupien, M., Rossi, D.J., Nolan, G.P., Cairns, R.A., Mak, T.W., 2016. Mutant IDH1 Downregulates ATM and Alters DNA Repair and Sensitivity to DNA Damage Independent of TET2. Cancer Cell 30, 337–348. https://doi.org/10.1016/j.ccell.2016.05.018

Iwasa, H., Han, J., Ishikawa, F., 2003. Mitogen-activated protein kinase p38 defines the common senescence-signalling pathway. Genes Cells 8, 131–144.

Iwasaki, H., Arai, F., Kubota, Y., Dahl, M., Suda, T., 2010. Endothelial protein C receptor-expressing hematopoietic stem cells reside in the perisinusoidal niche in fetal liver. Blood 116, 544–553. https://doi.org/10.1182/blood-2009-08-240903

Jaiswal, S., Ebert, B.L., 2019. Clonal hematopoiesis in human aging and disease. Science 366. https://doi.org/10.1126/science.aan4673

Jaiswal, S., Fontanillas, P., Flannick, J., Manning, A., Grauman, P.V., Mar, B.G., Lindsley, R.C., Mermel, C.H., Burtt, N., Chavez, A., Higgins, J.M., Moltchanov, V.,

Kuo, F.C., Kluk, M.J., Henderson, B., Kinnunen, L., Koistinen, H.A., Ladenvall, C., Getz, G., Correa, A., Banahan, B.F., Gabriel, S., Kathiresan, S., Stringham, H.M., McCarthy, M.I., Boehnke, M., Tuomilehto, J., Haiman, C., Groop, L., Atzmon, G., Wilson, J.G., Neuberg, D., Altshuler, D., Ebert, B.L., 2014. Age-related clonal hematopoiesis associated with adverse outcomes. N. Engl. J. Med. 371, 2488–2498. https://doi.org/10.1056/NEJMoa1408617

Jaiswal, S., Natarajan, P., Silver, A.J., Gibson, C.J., Bick, A.G., Shvartz, E., McConkey, M., Gupta, N., Gabriel, S., Ardissino, D., Baber, U., Mehran, R., Fuster, V., Danesh, J., Frossard, P., Saleheen, D., Melander, O., Sukhova, G.K., Neuberg, D., Libby, P., Kathiresan, S., Ebert, B.L., 2017. Clonal Hematopoiesis and Risk of Atherosclerotic Cardiovascular Disease. N. Engl. J. Med. 377, 111–121. https://doi.org/10.1056/NEJMoa1701719

James, C., Ugo, V., Le Couédic, J.-P., Staerk, J., Delhommeau, F., Lacout, C., Garçon, L., Raslova, H., Berger, R., Bennaceur-Griscelli, A., Villeval, J.L., Constantinescu, S.N., Casadevall, N., Vainchenker, W., 2005. A unique clonal JAK2 mutation leading to constitutive signalling causes polycythaemia vera. Nature 434, 1144–1148. https://doi.org/10.1038/nature03546

Jankowska, A.M., Gondek, L.P., Szpurka, H., Nearman, Z.P., Tiu, R.V., Maciejewski, J.P., 2008. Base excision repair dysfunction in a subgroup of patients with myelodysplastic syndrome. Leukemia 22, 551–558. https://doi.org/10.1038/sj.leu.2405055

Jawad, M., Seedhouse, C.H., Russell, N., Plumb, M., 2006. Polymorphisms in human homeobox HLX1 and DNA repair RAD51 genes increase the risk of therapy-related acute myeloid leukemia. Blood 108, 3916–3918. https://doi.org/10.1182/blood-2006-05-022921

Karigane, D., Kobayashi, H., Morikawa, T., Ootomo, Y., Sakai, M., Nagamatsu, G., Kubota, Y., Goda, N., Matsumoto, M., Nishimura, E.K., Soga, T., Otsu, K., Suematsu, M., Okamoto, S., Suda, T., Takubo, K., 2016. p38α Activates Purine Metabolism to Initiate Hematopoietic Stem/Progenitor Cell Cycling in Response to Stress. Cell Stem Cell 19, 192–204. https://doi.org/10.1016/j.stem.2016.05.013

Kautz, L., Jung, G., Valore, E.V., Rivella, S., Nemeth, E., Ganz, T., 2014. Identification of erythroferrone as an erythroid regulator of iron metabolism. Nat Genet 46, 678–684. https://doi.org/10.1038/ng.2996

Kay, J., Thadhani, E., Samson, L., Engelward, B., 2019. Inflammation-induced DNA damage, mutations and cancer. DNA Repair 83, 102673. https://doi.org/10.1016/j.dnarep.2019.102673

Kennedy, M., Awong, G., Sturgeon, C.M., Ditadi, A., LaMotte-Mohs, R., Zúñiga-Pflücker, J.C., Keller, G., 2012. T lymphocyte potential marks the emergence of definitive hematopoietic progenitors in human pluripotent stem cell differentiation cultures. Cell Rep 2, 1722–1735. https://doi.org/10.1016/j.celrep.2012.11.003

Kesarwani, M., Kincaid, Z., Gomaa, A., Huber, E., Rohrabaugh, S., Siddiqui, Z., Bouso, M.F., Latif, T., Xu, M., Komurov, K., Mulloy, J.C., Cancelas, J.A., Grimes, H.L., Azam, M., 2017. Targeting c-FOS and DUSP1 abrogates intrinsic resistance to tyrosine-kinase inhibitor therapy in BCR-ABL-induced leukemia. Nat. Med. 23, 472–482. https://doi.org/10.1038/nm.4310

Kesarwani, M., Kincaid, Z., Latif, T., Azam, M., 2018. Loss of DUSP1 Is Synthetic Lethal to JAK2V617F. Blood 132, 51–51. https://doi.org/10.1182/blood-2018-99-115503

Kidger, A.M., Keyse, S.M., 2016. The regulation of oncogenic Ras/ERK signalling by dual-specificity mitogen activated protein kinase phosphatases (MKPs). Semin. Cell Dev. Biol. 50, 125–132. https://doi.org/10.1016/j.semcdb.2016.01.009

Klampfl, T., Harutyunyan, A., Berg, T., Gisslinger, B., Schalling, M., Bagienski, K., Olcaydu, D., Passamonti, F., Rumi, E., Pietra, D., Jäger, R., Pieri, L., Guglielmelli, P., Iacobucci, I., Martinelli, G., Cazzola, M., Vannucchi, A.M., Gisslinger, H., Kralovics, R., 2011. Genome integrity of myeloproliferative neoplasms in chronic phase and during disease progression. Blood 118, 167–176. https://doi.org/10.1182/blood-2011-01-331678

Knijnenburg, T.A., Wang, L., Zimmermann, M.T., Chambwe, N., Gao, G.F., Cherniack, A.D., Fan, H., Shen, H., Way, G.P., Greene, C.S., Liu, Y., Akbani, R., Feng, B., Donehower, L.A., Miller, C., Shen, Y., Karimi, M., Chen, H., Kim, P., Jia, P., Shinbrot, E., Zhang, S., Liu, J., Hu, H., Bailey, M.H., Yau, C., Wolf, D., Zhao, Z., Weinstein, J.N., Li, L., Ding, L., Mills, G.B., Laird, P.W., Wheeler, D.A., Shmulevich, I., Cancer Genome Atlas Research Network, Monnat, R.J., Xiao, Y., Wang, C., 2018. Genomic and Molecular Landscape of DNA Damage Repair Deficiency across The Cancer Genome Atlas. Cell Rep 23, 239-254.e6. https://doi.org/10.1016/j.celrep.2018.03.076

Kohlscheen, S., Schenk, F., Rommel, M.G.E., Cullmann, K., Modlich, U., 2019. Endothelial protein C receptor supports hematopoietic stem cell engraftment and expansion in Mpl-deficient mice. Blood 133, 1465–1478. https://doi.org/10.1182/blood-2018-03-837344

Kohno, T., Shinmura, K., Tosaka, M., Tani, M., Kim, S.R., Sugimura, H., Nohmi, T., Kasai, H., Yokota, J., 1998. Genetic polymorphisms and alternative splicing of the hOGG1 gene, that is involved in the repair of 8-hydroxyguanine in damaged DNA. Oncogene 16, 3219–3225. https://doi.org/10.1038/sj.onc.1201872

Kozlov, S.V., Waardenberg, A.J., Engholm-Keller, K., Arthur, J.W., Graham, M.E., Lavin, M., 2016. Reactive Oxygen Species (ROS)-Activated ATM-Dependent Phosphorylation of Cytoplasmic Substrates Identified by Large-Scale Phosphoproteomics Screen. Mol. Cell Proteomics 15, 1032–1047. https://doi.org/10.1074/mcp.M115.055723

Kralovics, R., Passamonti, F., Buser, A.S., Teo, S.-S., Tiedt, R., Passweg, J.R., Tichelli, A., Cazzola, M., Skoda, R.C., 2005. A gain-of-function mutation of JAK2 in myeloproliferative disorders. N. Engl. J. Med. 352, 1779–1790. https://doi.org/10.1056/NEJMoa051113

Kreipe, H., Büsche, G., Bock, O., Hussein, K., 2012. Myelofibrosis: molecular and cell biological aspects. Fibrogenesis & Tissue Repair 5, S21. https://doi.org/10.1186/1755-1536-5-S1-S21

Kumari, S., Badana, A.K., G, M.M., G, S., Malla, R., 2018. Reactive Oxygen Species: A Key Constituent in Cancer Survival. Biomark Insights 13. https://doi.org/10.1177/1177271918755391

Kuramoto, K., Ban, S., Oda, K., Tanaka, H., Kimura, A., Suzuki, G., 2002. Chromosomal instability and radiosensitivity in myelodysplastic syndrome cells. Leukemia 16, 2253–2258. https://doi.org/10.1038/sj.leu.2402703

Kuranda, K., Vargaftig, J., de la Rochere, P., Dosquet, C., Charron, D., Bardin, F., Tonnelle, C., Bonnet, D., Goodhardt, M., 2011. Age-related changes in human hematopoietic stem/progenitor cells. Aging Cell 10, 542–546.

https://doi.org/10.1111/j.1474-9726.2011.00675.x

Kwon, J., Lee, S.-R., Yang, K.-S., Ahn, Y., Kim, Y.J., Stadtman, E.R., Rhee, S.G., 2004. Reversible oxidation and inactivation of the tumor suppressor PTEN in cells stimulated with peptide growth factors. Proc Natl Acad Sci U S A 101, 16419–16424. https://doi.org/10.1073/pnas.0407396101

Landolfi, R., Di Gennaro, L., Barbui, T., De Stefano, V., Finazzi, G., Marfisi, R., Tognoni, G., Marchioli, R., 2007. Leukocytosis as a major thrombotic risk factor in patients with polycythemia vera. Blood 109, 2446–2452. https://doi.org/10.1182/blood-2006-08-042515

Lee, J., Liu, L., Levin, D.E., 2018. Stressing out or stressing in: intracellular pathways for SAPK activation. Curr. Genet. https://doi.org/10.1007/s00294-018-0898-5

Levine, R.L., Gilliland, D.G., 2008. Myeloproliferative disorders. Blood 112, 2190–2198. https://doi.org/10.1182/blood-2008-03-077966

Levine, R.L., Wadleigh, M., Cools, J., Ebert, B.L., Wernig, G., Huntly, B.J.P., Boggon, T.J., Wlodarska, I., Clark, J.J., Moore, S., Adelsperger, J., Koo, S., Lee, J.C., Gabriel, S., Mercher, T., D'Andrea, A., Fröhling, S., Döhner, K., Marynen, P., Vandenberghe, P., Mesa, R.A., Tefferi, A., Griffin, J.D., Eck, M.J., Sellers, W.R., Meyerson, M., Golub, T.R., Lee, S.J., Gilliland, D.G., 2005. Activating mutation in the tyrosine kinase JAK2 in polycythemia vera, essential thrombocythemia, and myeloid metaplasia with myelofibrosis. Cancer Cell 7, 387–397. https://doi.org/10.1016/j.ccr.2005.03.023

Li, G.-M., 2008. Mechanisms and functions of DNA mismatch repair. Cell Research 18, 85–98. https://doi.org/10.1038/cr.2007.115

Li, J., Spensberger, D., Ahn, J.S., Anand, S., Beer, P.A., Ghevaert, C., Chen, E., Forrai, A., Scott, L.M., Ferreira, R., Campbell, P.J., Watson, S.P., Liu, P., Erber, W.N., Huntly, B.J.P., Ottersbach, K., Green, A.R., 2010. JAK2 V617F impairs hematopoietic stem cell function in a conditional knock-in mouse model of JAK2 V617F-positive essential thrombocythemia. Blood 116, 1528–1538. https://doi.org/10.1182/blood-2009-12-259747

Lim, P.J., Duarte, T.L., Arezes, J., Garcia-Santos, D., Hamdi, A., Pasricha, S.-R., Armitage, A.E., Mehta, H., Wideman, S., Santos, A.G., Santos-Gonçalves, A., Morovat, A., Hughes, J.R., Soilleux, E., Wang, C.-Y., Bayer, A.L., Klenerman, P., Willberg, C.B., Hartley, R.C., Murphy, M.P., Babitt, J.L., Ponka, P., Porto, G., Drakesmith, H., 2019. Nrf2 controls iron homeostasis in haemochromatosis and thalassaemia via Bmp6 and hepcidin. Nat Metab 1, 519–531. https://doi.org/10.1038/s42255-019-0063-6

Lin, Y.-W., Slape, C., Zhang, Z., Aplan, P.D., 2005. NUP98-HOXD13 transgenic mice develop a highly penetrant, severe myelodysplastic syndrome that progresses to acute leukemia. Blood 106, 287–295. https://doi.org/10.1182/blood-2004-12-4794

Lisa Ooi, A.G., Karsunky, H., Majeti, R., Butz, S., Vestweber, D., Ishida, T., Quertermous, T., Weissman, I.L., Forsberg, E.C., 2009. The adhesion molecule ESAM1 is a novel hematopoietic stem cell marker. Stem Cells 27, 653–661. https://doi.org/10.1634/stemcells.2008-0824

London, R.E., 2015. The structural basis of XRCC1-mediated DNA repair. DNA Repair (Amst) 30, 90–103. https://doi.org/10.1016/j.dnarep.2015.02.005

Lu, M., Zhang, W., Li, Y., Berenzon, D., Wang, X., Wang, J., Mascarenhas, J., Xu, M.,

Hoffman, R., 2010. Interferon-alpha targets JAK2V617F-positive hematopoietic progenitor cells and acts through the p38 MAPK pathway. Exp. Hematol. 38, 472–480. https://doi.org/10.1016/j.exphem.2010.03.005

Lundberg, P., Takizawa, H., Kubovcakova, L., Guo, G., Hao-Shen, H., Dirnhofer, S., Orkin, S.H., Manz, M.G., Skoda, R.C., 2014. Myeloproliferative neoplasms can be initiated from a single hematopoietic stem cell expressing JAK2-V617F. Journal of Experimental Medicine 211, 2213–2230. https://doi.org/10.1084/jem.20131371

Lussana, F., Rambaldi, A., 2017. Inflammation and myeloproliferative neoplasms. J. Autoimmun. 85, 58–63. https://doi.org/10.1016/j.jaut.2017.06.010

Lutzmann, M., Bernex, F., da Costa de Jesus, C., Hodroj, D., Marty, C., Plo, I., Vainchenker, W., Tosolini, M., Forichon, L., Bret, C., Queille, S., Marchive, C., Hoffmann, J.-S., Méchali, M., 2019. MCM8- and MCM9 Deficiencies Cause Lifelong Increased Hematopoietic DNA Damage Driving p53-Dependent Myeloid Tumors. Cell Rep 28, 2851-2865.e4. https://doi.org/10.1016/j.celrep.2019.07.095

Manshouri, T., Estrov, Z., Quintás-Cardama, A., Burger, J., Zhang, Y., Livun, A., Knez, L., Harris, D., Creighton, C.J., Kantarjian, H.M., Verstovsek, S., 2011. Bone marrow stroma-secreted cytokines protect JAK2(V617F)-mutated cells from the effects of a JAK2 inhibitor. Cancer Res. 71, 3831–3840. https://doi.org/10.1158/0008-5472.CAN-10-4002

Mao, G., Pan, X., Gu, L., 2008. Evidence that a mutation in the MLH1 3'-untranslated region confers a mutator phenotype and mismatch repair deficiency in patients with relapsed leukemia. J. Biol. Chem. 283, 3211–3216. https://doi.org/10.1074/jbc.M709276200

Marty, C., Lacout, C., Droin, N., Le Couédic, J.-P., Ribrag, V., Solary, E., Vainchenker, W., Villeval, J.-L., Plo, I., 2013. A role for reactive oxygen species in JAK2 V617F myeloproliferative neoplasm progression. Leukemia 27, 2187–2195. https://doi.org/10.1038/leu.2013.102

Molina, G., Vogt, A., Bakan, A., Dai, W., Queiroz de Oliveira, P., Znosko, W., Smithgall, T.E., Bahar, I., Lazo, J.S., Day, B.W., Tsang, M., 2009. Zebrafish chemical screening reveals an inhibitor of Dusp6 that expands cardiac cell lineages. Nat. Chem. Biol. 5, 680–687. https://doi.org/10.1038/nchembio.190

Nangalia, J., Massie, C.E., Baxter, E.J., Nice, F.L., Gundem, G., Wedge, D.C., Avezov, E., Li, J., Kollmann, K., Kent, D.G., Aziz, A., Godfrey, A.L., Hinton, J., Martincorena, I., Van Loo, P., Jones, A.V., Guglielmelli, P., Tarpey, P., Harding, H.P., Fitzpatrick, J.D., Goudie, C.T., Ortmann, C.A., Loughran, S.J., Raine, K., Jones, D.R., Butler, A.P., Teague, J.W., O'Meara, S., McLaren, S., Bianchi, M., Silber, Y., Dimitropoulou, D., Bloxham, D., Mudie, L., Maddison, M., Robinson, B., Keohane, C., Maclean, C., Hill, K., Orchard, K., Tauro, S., Du, M.-Q., Greaves, M., Bowen, D., Huntly, B.J.P., Harrison, C.N., Cross, N.C.P., Ron, D., Vannucchi, A.M., Papaemmanuil, E., Campbell, P.J., Green, A.R., 2013. Somatic CALR Mutations in Myeloproliferative Neoplasms with Nonmutated JAK2. N Engl J Med 369, 2391–2405. https://doi.org/10.1056/NEJMoa1312542

Nemeth, E., Tuttle, M.S., Powelson, J., Vaughn, M.B., Donovan, A., Ward, D.M., Ganz, T., Kaplan, J., 2004. Hepcidin Regulates Cellular Iron Efflux by Binding to Ferroportin and Inducing Its Internalization. Science 306, 2090–2093. https://doi.org/10.1126/science.1104742

Novotna, B., Bagryantseva, Y., Siskova, M., Neuwirtova, R., 2009. Oxidative DNA

damage in bone marrow cells of patients with low-risk myelodysplastic syndrome. Leuk. Res. 33, 340–343. https://doi.org/10.1016/j.leukres.2008.07.005

O'Kane, G.M., Connor, A.A., Gallinger, S., 2017. Characterization, Detection, and Treatment Approaches for Homologous Recombination Deficiency in Cancer. Trends Mol Med 23, 1121–1137. https://doi.org/10.1016/j.molmed.2017.10.007

Olipitz, W., Hopfinger, G., Aguiar, R.C.T., Gunsilius, E., Girschikofsky, M., Bodner, C., Hiden, K., Linkesch, W., Hoefler, G., Sill, H., 2002. Defective DNA-mismatch repair: a potential mediator of leukemogenic susceptibility in therapy-related myelodysplasia and leukemia. Genes Chromosomes Cancer 34, 243–248. https://doi.org/10.1002/gcc.10059

Omidvar, N., Kogan, S., Beurlet, S., le Pogam, C., Janin, A., West, R., Noguera, M.-E., Reboul, M., Soulie, A., Leboeuf, C., Setterblad, N., Felsher, D., Lagasse, E., Mohamedali, A., Thomas, N.S.B., Fenaux, P., Fontenay, M., Pla, M., Mufti, G.J., Weissman, I., Chomienne, C., Padua, R.A., 2007. BCL-2 and mutant NRAS interact physically and functionally in a mouse model of progressive myelodysplasia. Cancer Res. 67, 11657–11667. https://doi.org/10.1158/0008-5472.CAN-07-0196

Pandolfi, A., Barreyro, L., Steidl, U., 2013. Concise Review: Preleukemic Stem Cells: Molecular Biology and Clinical Implications of the Precursors to Leukemia Stem Cells. Stem Cells Transl Med 2, 143–150. https://doi.org/10.5966/sctm.2012-0109

Pang, W.W., Price, E.A., Sahoo, D., Beerman, I., Maloney, W.J., Rossi, D.J., Schrier, S.L., Weissman, I.L., 2011. Human bone marrow hematopoietic stem cells are increased in frequency and myeloid-biased with age. Proc. Natl. Acad. Sci. U.S.A. 108, 20012–20017. https://doi.org/10.1073/pnas.1116110108

Passamonti, F., Elena, C., Schnittger, S., Skoda, R.C., Green, A.R., Girodon, F., Kiladjian, J.-J., McMullin, M.F., Ruggeri, M., Besses, C., Vannucchi, A.M., Lippert, E., Gisslinger, H., Rumi, E., Lehmann, T., Ortmann, C.A., Pietra, D., Pascutto, C., Haferlach, T., Cazzola, M., 2011. Molecular and clinical features of the myeloproliferative neoplasm associated with JAK2 exon 12 mutations. Blood 117, 2813–2816. https://doi.org/10.1182/blood-2010-11-316810

Pearl, L.H., Schierz, A.C., Ward, S.E., Al-Lazikani, B., Pearl, F.M.G., 2015. Therapeutic opportunities within the DNA damage response. Nature Reviews Cancer 15, nrc3891. https://doi.org/10.1038/nrc3891

Peddie, C.M., Wolf, C.R., McLellan, L.I., Collins, A.R., Bowen, D.T., 1997. Oxidative DNA damage in CD34+ myelodysplastic cells is associated with intracellular redox changes and elevated plasma tumour necrosis factor-alpha concentration. Br. J. Haematol. 99, 625–631.

Perner, F., Perner, C., Ernst, T., Heidel, F.H., 2019. Roles of JAK2 in Aging, Inflammation, Hematopoiesis and Malignant Transformation. Cells 8. https://doi.org/10.3390/cells8080854

Pietras, E.M., Lakshminarasimhan, R., Techner, J.-M., Fong, S., Flach, J., Binnewies, M., Passegué, E., 2014. Re-entry into quiescence protects hematopoietic stem cells from the killing effect of chronic exposure to type I interferons. J Exp Med 211, 245–262. https://doi.org/10.1084/jem.20131043

Plo, I., Nakatake, M., Malivert, L., Villartay, J.-P. de, Giraudier, S., Villeval, J.-L., Wiesmuller, L., Vainchenker, W., 2008. JAK2 stimulates homologous recombination and genetic instability: potential implication in the heterogeneity of myeloproliferative disorders. Blood 112, 1402–1412. https://doi.org/10.1182/blood-2008-01-134114

Pohlers, D., Brenmoehl, J., Löffler, I., Müller, C.K., Leipner, C., Schultze-Mosgau, S., Stallmach, A., Kinne, R.W., Wolf, G., 2009. TGF-beta and fibrosis in different organs - molecular pathway imprints. Biochim. Biophys. Acta 1792, 746–756. https://doi.org/10.1016/j.bbadis.2009.06.004

Popp, H.D., Naumann, N., Brendel, S., Henzler, T., Weiss, C., Hofmann, W.-K., Fabarius, A., 2017. Increase of DNA damage and alteration of the DNA damage response in myelodysplastic syndromes and acute myeloid leukemias. Leukemia Research 57, 112–118. https://doi.org/10.1016/j.leukres.2017.03.011

Poppe, B., Van Limbergen, H., Van Roy, N., Vandecruys, E., De Paepe, A., Benoit, Y., Speleman, F., 2001. Chromosomal aberrations in Bloom syndrome patients with myeloid malignancies. Cancer Genet. Cytogenet. 128, 39–42. https://doi.org/10.1016/s0165-4608(01)00392-2

Popuri, V., Tadokoro, T., Croteau, D.L., Bohr, V.A., 2013. Human RECQL5: Guarding the crossroads of DNA replication and transcription and providing backup capability. Crit Rev Biochem Mol Biol 48, 289–299. https://doi.org/10.3109/10409238.2013.792770

Pourcelot, E., Trocme, C., Mondet, J., Bailly, S., Toussaint, B., Mossuz, P., 2014. Cytokine profiles in polycythemia vera and essential thrombocythemia patients: clinical implications. Exp. Hematol. 42, 360–368. https://doi.org/10.1016/j.exphem.2014.01.006

Puthiyaveetil, A.G., Reilly, C.M., Pardee, T.S., Caudell, D.L., 2013. Non-homologous end joining mediated DNA repair is impaired in the NUP98-HOXD13 mouse model for myelodysplastic syndrome. Leuk. Res. 37, 112–116. https://doi.org/10.1016/j.leukres.2012.10.012

Reilly, J.T., 2008. Pathogenetic insight and prognostic information from standard and molecular cytogenetic studies in the BCR-ABL-negative myeloproliferative neoplasms (MPNs). Leukemia 22, 1818–1827. https://doi.org/10.1038/leu.2008.218

Rossi, D.J., Bryder, D., Zahn, J.M., Ahlenius, H., Sonu, R., Wagers, A.J., Weissman, I.L., 2005. Cell intrinsic alterations underlie hematopoietic stem cell aging. PNAS 102, 9194–9199. https://doi.org/10.1073/pnas.0503280102

Saigo, K., Takenokuchi, M., Hiramatsu, Y., Tada, H., Hishita, T., Takata, M., Misawa, M., Imoto, S., Imashuku, S., 2011. Oxidative stress levels in myelodysplastic syndrome patients: their relationship to serum ferritin and haemoglobin values. J. Int. Med. Res. 39, 1941–1945. https://doi.org/10.1177/147323001103900539

Sallman, D.A., List, A., 2019. The central role of inflammatory signaling in the pathogenesis of myelodysplastic syndromes. Blood 133, 1039–1048. https://doi.org/10.1182/blood-2018-10-844654

Salmeen, A., Andersen, J.N., Myers, M.P., Meng, T.-C., Hinks, J.A., Tonks, N.K., Barford, D., 2003. Redox regulation of protein tyrosine phosphatase 1B involves a sulphenyl-amide intermediate. Nature 423, 769–773. https://doi.org/10.1038/nature01680

Sanjuan-Pla, A., Macaulay, I.C., Jensen, C.T., Woll, P.S., Luis, T.C., Mead, A., Moore, S., Carella, C., Matsuoka, S., Bouriez Jones, T., Chowdhury, O., Stenson, L., Lutteropp, M., Green, J.C.A., Facchini, R., Boukarabila, H., Grover, A., Gambardella, A., Thongjuea, S., Carrelha, J., Tarrant, P., Atkinson, D., Clark, S.-A., Nerlov, C., Jacobsen, S.E.W., 2013. Platelet-biased stem cells reside at the apex of the haematopoietic stem-cell hierarchy. Nature 502, 232–236.

https://doi.org/10.1038/nature12495

Schepers, K., Pietras, E.M., Reynaud, D., Flach, J., Binnewies, M., Garg, T., Wagers, A.J., Hsiao, E.C., Passegué, E., 2013. Myeloproliferative neoplasia remodels the endosteal bone marrow niche into a self-reinforcing leukemic niche. Cell Stem Cell 13, 285–299. https://doi.org/10.1016/j.stem.2013.06.009

Schnöder, T.M., Eberhardt, J., Koehler, M., Bierhoff, H.B., Weinert, S., Pandey, A.D., Nimmagadda, S.C., Wolleschak, D., Jöhrens, K., Fischer, T., Heidel, F.H., 2017. Cell autonomous expression of CXCL-10 in JAK2V617F-mutated MPN. J. Cancer Res. Clin. Oncol. 143, 807–820. https://doi.org/10.1007/s00432-017-2354-1

Scott, L.M., Tong, W., Levine, R.L., Scott, M.A., Beer, P.A., Stratton, M.R., Futreal, P.A., Erber, W.N., McMullin, M.F., Harrison, C.N., Warren, A.J., Gilliland, D.G., Lodish, H.F., Green, A.R., 2007. JAK2 exon 12 mutations in polycythemia vera and idiopathic erythrocytosis. N Engl J Med 356, 459–468. https://doi.org/10.1056/NEJMoa065202

Seedhouse, C., Faulkner, R., Ashraf, N., Das-Gupta, E., Russell, N., 2004. Polymorphisms in genes involved in homologous recombination repair interact to increase the risk of developing acute myeloid leukemia. Clin. Cancer Res. 10, 2675–2680. https://doi.org/10.1158/1078-0432.ccr-03-0372

Seth, D., Rudolph, J., 2006. Redox regulation of MAP kinase phosphatase 3. Biochemistry 45, 8476–8487. https://doi.org/10.1021/bi060157p

Sheikhha, M.H., Tobal, K., Liu Yin, J.A., 2002. High level of microsatellite instability but not hypermethylation of mismatch repair genes in therapy-related and secondary acute myeloid leukaemia and myelodysplastic syndrome. Br. J. Haematol. 117, 359–365. https://doi.org/10.1046/j.1365-2141.2002.03458.x

Smith, C., Abalde-Atristain, L., He, C., Brodsky, B.R., Braunstein, E.M., Chaudhari, P., Jang, Y.-Y., Cheng, L., Ye, Z., 2015. Efficient and Allele-Specific Genome Editing of Disease Loci in Human iPSCs. Mol Ther 23, 570–577. https://doi.org/10.1038/mt.2014.226

Smyth, G.K., 2004. Linear models and empirical bayes methods for assessing differential expression in microarray experiments. Stat Appl Genet Mol Biol 3, Article3. https://doi.org/10.2202/1544-6115.1027

Solé, F., Luño, E., Sanzo, C., Espinet, B., Sanz, G.F., Cervera, J., Calasanz, M.J., Cigudosa, J.C., Millà, F., Ribera, J.M., Bureo, E., Marquez, M.L., Arranz, E., Florensa, L., 2005. Identification of novel cytogenetic markers with prognostic significance in a series of 968 patients with primary myelodysplastic syndromes. Haematologica 90, 1168–1178.

Steensma, D.P., 2018. Clinical consequences of clonal hematopoiesis of indeterminate potential. Blood Adv 2, 3404–3410. https://doi.org/10.1182/bloodadvances.2018020222

Steensma, D.P., Bejar, R., Jaiswal, S., Lindsley, R.C., Sekeres, M.A., Hasserjian, R.P., Ebert, B.L., 2015. Clonal hematopoiesis of indeterminate potential and its distinction from myelodysplastic syndromes. Blood 126, 9–16. https://doi.org/10.1182/blood-2015-03-631747

Stetka, J., Vyhlidalova, P., Lanikova, L., Koralkova, P., Gursky, J., Hlusi, A., Flodr, P., Hubackova, S., Bartek, J., Hodny, Z., Divoky, V., 2019. Addiction to DUSP1 protects JAK2V617F-driven polycythemia vera progenitors against inflammatory stress and

DNA damage, allowing chronic proliferation. Oncogene 38, 5627–5642. https://doi.org/10.1038/s41388-019-0813-7

Storey, J.D., Tibshirani, R., 2003. Statistical significance for genomewide studies. PNAS 100, 9440–9445. https://doi.org/10.1073/pnas.1530509100

Strom, S.S., Estey, E., Outschoorn, U.M., Garcia-Manero, G., 2010. Acute myeloid leukemia outcome: role of nucleotide excision repair polymorphisms in intermediate risk patients. Leuk. Lymphoma 51, 598–605. https://doi.org/10.3109/10428190903582804

Subramanian, A., Tamayo, P., Mootha, V.K., Mukherjee, S., Ebert, B.L., Gillette, M.A., Paulovich, A., Pomeroy, S.L., Golub, T.R., Lander, E.S., Mesirov, J.P., 2005. Gene set enrichment analysis: A knowledge-based approach for interpreting genome-wide expression profiles. PNAS 102, 15545–15550. https://doi.org/10.1073/pnas.0506580102

Sun, D., Luo, M., Jeong, M., Rodriguez, B., Xia, Z., Hannah, R., Wang, H., Le, T., Faull, K.F., Chen, R., Gu, H., Bock, C., Meissner, A., Göttgens, B., Darlington, G.J., Li, W., Goodell, M.A., 2014. Epigenomic Profiling of Young and Aged HSCs Reveals Concerted Changes during Aging that Reinforce Self-Renewal. Cell Stem Cell 14, 673–688. https://doi.org/10.1016/j.stem.2014.03.002

Takacova, S., Slany, R., Bartkova, J., Stranecky, V., Dolezel, P., Luzna, P., Bartek, J., Divoky, V., 2012. DNA damage response and inflammatory signaling limit the MLL-ENL-induced leukemogenesis in vivo. Cancer Cell 21, 517–531. https://doi.org/10.1016/j.ccr.2012.01.021

Tao, L.C., Stecker, E., Gardner, H.A., 1971. Werner's syndrome and acute myeloid leukemia. Can Med Assoc J 105, 951 passim.

Tefferi, A., 2016. Myeloproliferative neoplasms: A decade of discoveries and treatment advances. Am. J. Hematol. 91, 50–58. https://doi.org/10.1002/ajh.24221

Tefferi, A., Guglielmelli, P., Larson, D.R., Finke, C., Wassie, E.A., Pieri, L., Gangat, N., Fjerza, R., Belachew, A.A., Lasho, T.L., Ketterling, R.P., Hanson, C.A., Rambaldi, A., Finazzi, G., Thiele, J., Barbui, T., Pardanani, A., Vannucchi, A.M., 2014. Long-term survival and blast transformation in molecularly annotated essential thrombocythemia, polycythemia vera, and myelofibrosis. Blood 124, 2507–2513. https://doi.org/10.1182/blood-2014-05-579136

Tefferi, A., Vaidya, R., Caramazza, D., Finke, C., Lasho, T., Pardanani, A., 2011. Circulating interleukin (IL)-8, IL-2R, IL-12, and IL-15 levels are independently prognostic in primary myelofibrosis: a comprehensive cytokine profiling study. J. Clin. Oncol. 29, 1356–1363. https://doi.org/10.1200/JCO.2010.32.9490

Tiedt, R., Hao-Shen, H., Sobas, M.A., Looser, R., Dirnhofer, S., Schwaller, J., Skoda, R.C., 2008. Ratio of mutant JAK2-V617F to wild-type Jak2 determines the MPD phenotypes in transgenic mice. Blood 111, 3931–3940. https://doi.org/10.1182/blood-2007-08-107748

Toyama, K., Ohyashiki, K., Yoshida, Y., Abe, T., Asano, S., Hirai, H., Hirashima, K., Hotta, T., Kuramoto, A., Kuriya, S., 1993. Clinical implications of chromosomal abnormalities in 401 patients with myelodysplastic syndromes: a multicentric study in Japan. Leukemia 7, 499–508.

Vaidya, R., Gangat, N., Jimma, T., Finke, C.M., Lasho, T.L., Pardanani, A., Tefferi, A., 2012. Plasma cytokines in polycythemia vera: phenotypic correlates, prognostic

relevance, and comparison with myelofibrosis. Am. J. Hematol. 87, 1003–1005. https://doi.org/10.1002/ajh.23295

Vainchenker, W., Kralovics, R., 2017. Genetic basis and molecular pathophysiology of classical myeloproliferative neoplasms. Blood 129, 667–679. https://doi.org/10.1182/blood-2016-10-695940

Valka, J., Vesela, J., Votavova, H., Dostalova-Merkerova, M., Horakova, Z., Campr, V., Brezinova, J., Zemanova, Z., Jonasova, A., Cermak, J., Belickova, M., 2017. Differential expression of homologous recombination DNA repair genes in the early and advanced stages of myelodysplastic syndrome. European Journal of Haematology 99, 323–331. https://doi.org/10.1111/ejh.12920

van Dekken, H., Hop, W.C.J., Tilanus, H.W., Haringsma, J., van der Valk, H., Wink, J.C., Vissers, K.J., 2008. Immunohistochemical evaluation of a panel of tumor cell markers during malignant progression in Barrett esophagus. Am. J. Clin. Pathol. 130, 745–753. https://doi.org/10.1309/AJCPO31THGVEUIDH

Vener, C., Novembrino, C., Catena, F.B., Fracchiolla, N.S., Gianelli, U., Savi, F., Radaelli, F., Fermo, E., Cortelezzi, A., Lonati, S., Menegatti, M., Deliliers, G.L., 2010. Oxidative stress is increased in primary and post-polycythemia vera myelofibrosis. Exp. Hematol. 38, 1058–1065. https://doi.org/10.1016/j.exphem.2010.07.005

Walter, D., Lier, A., Geiselhart, A., Thalheimer, F.B., Huntscha, S., Sobotta, M.C., Moehrle, B., Brocks, D., Bayindir, I., Kaschutnig, P., Muedder, K., Klein, C., Jauch, A., Schroeder, T., Geiger, H., Dick, T.P., Holland-Letz, T., Schmezer, P., Lane, S.W., Rieger, M.A., Essers, M.A.G., Williams, D.A., Trumpp, A., Milsom, M.D., 2015. Exit from dormancy provokes DNA-damage-induced attrition in haematopoietic stem cells. Nature 520, 549–552. https://doi.org/10.1038/nature14131

Wang, Y., Spitz, M.R., Zhu, Y., Dong, Q., Shete, S., Wu, X., 2003. From genotype to phenotype: correlating XRCC1 polymorphisms with mutagen sensitivity. DNA Repair (Amst.) 2, 901–908. https://doi.org/10.1016/s1568-7864(03)00085-5

Wood, C.D., Thornton, T.M., Sabio, G., Davis, R.A., Rincon, M., 2009. Nuclear Localization of p38 MAPK in Response to DNA Damage. Int J Biol Sci 5, 428–437.

Wu, X., Dao Thi, V.L., Huang, Y., Billerbeck, E., Saha, D., Hoffmann, H.-H., Wang, Y., Silva, L.A.V., Sarbanes, S., Sun, T., Andrus, L., Yu, Y., Quirk, C., Li, M., MacDonald, M.R., Schneider, W.M., An, X., Rosenberg, B.R., Rice, C.M., 2018. Intrinsic Immunity Shapes Viral Resistance of Stem Cells. Cell 172, 423-438.e25. https://doi.org/10.1016/j.cell.2017.11.018

Xavier, A.C., Taub, J.W., 2010. Acute leukemia in children with Down syndrome. Haematologica 95, 1043–1045. https://doi.org/10.3324/haematol.2010.024968

Xie, M., Lu, C., Wang, J., McLellan, M.D., Johnson, K.J., Wendl, M.C., McMichael, J.F., Schmidt, H.K., Yellapantula, V., Miller, C.A., Ozenberger, B.A., Welch, J.S., Link, D.C., Walter, M.J., Mardis, E.R., Dipersio, J.F., Chen, F., Wilson, R.K., Ley, T.J., Ding, L., 2014. Age-related mutations associated with clonal hematopoietic expansion and malignancies. Nat. Med. 20, 1472–1478. https://doi.org/10.1038/nm.3733

Xu, D., Zheng, H., Yu, W.-M., Qu, C.-K., 2013. Activating mutations in protein tyrosine phosphatase Ptpn11 (Shp2) enhance reactive oxygen species production that contributes to myeloproliferative disorder. PLoS ONE 8, e63152. https://doi.org/10.1371/journal.pone.0063152

Yahata, T., Takanashi, T., Muguruma, Y., Ibrahim, A.A., Matsuzawa, H., Uno, T., Sheng, Y., Onizuka, M., Ito, M., Kato, S., Ando, K., 2011. Accumulation of oxidative DNA damage restricts the self-renewal capacity of human hematopoietic stem cells. Blood 118, 2941–2950. https://doi.org/10.1182/blood-2011-01-330050

Yalcin, S., Marinkovic, D., Mungamuri, S.K., Zhang, X., Tong, W., Sellers, R., Ghaffari, S., 2010. ROS-mediated amplification of AKT/mTOR signalling pathway leads to myeloproliferative syndrome in Foxo3(-/-) mice. EMBO J. 29, 4118–4131. https://doi.org/10.1038/emboj.2010.292

Ye, Z., Liu, C.F., Lanikova, L., Dowey, S.N., He, C., Huang, X., Brodsky, R.A., Spivak, J.L., Prchal, J.T., Cheng, L., 2014. Differential sensitivity to JAK inhibitory drugs by isogenic human erythroblasts and hematopoietic progenitors generated from patient-specific induced pluripotent stem cells. Stem Cells 32, 269–278. https://doi.org/10.1002/stem.1545

Young, A.L., Challen, G.A., Birmann, B.M., Druley, T.E., 2016. Clonal haematopoiesis harbouring AML-associated mutations is ubiquitous in healthy adults. Nat Commun 7, 12484. https://doi.org/10.1038/ncomms12484

Zambetti, N.A., Ping, Z., Chen, S., Kenswil, K.J.G., Mylona, M.A., Sanders, M.A., Hoogenboezem, R.M., Bindels, E.M.J., Adisty, M.N., Van Strien, P.M.H., van der Leije, C.S., Westers, T.M., Cremers, E.M.P., Milanese, C., Mastroberardino, P.G., van Leeuwen, J.P.T.M., van der Eerden, B.C.J., Touw, I.P., Kuijpers, T.W., Kanaar, R., van de Loosdrecht, A.A., Vogl, T., Raaijmakers, M.H.G.P., 2016. Mesenchymal Inflammation Drives Genotoxic Stress in Hematopoietic Stem Cells and Predicts Disease Evolution in Human Pre-leukemia. Cell Stem Cell 19, 613–627. https://doi.org/10.1016/j.stem.2016.08.021

Zhang, Y., Liu, H., Yan, F., Zhou, J., 2017. Oscillatory dynamics of p38 activity with transcriptional and translational time delays. Scientific Reports 7, 1–11. https://doi.org/10.1038/s41598-017-11149-5

Zhou, A., Scoggin, S., Gaynor, R.B., Williams, N.S., 2003. Identification of NF-kappa B-regulated genes induced by TNFalpha utilizing expression profiling and RNA interference. Oncogene 22, 2054–2064. https://doi.org/10.1038/sj.onc.1206262

Zhou, F., Li, X., Wang, W., Zhu, P., Zhou, J., He, W., Ding, M., Xiong, F., Zheng, X., Li, Z., Ni, Y., Mu, X., Wen, L., Cheng, T., Lan, Y., Yuan, W., Tang, F., Liu, B., 2016. Tracing haematopoietic stem cell formation at single-cell resolution. Nature 533, 487–492. https://doi.org/10.1038/nature17997

Zhou, T., Chen, P., Gu, J., Bishop, A.J.R., Scott, L.M., Hasty, P., Rebel, V.I., 2015. Potential Relationship between Inadequate Response to DNA Damage and Development of Myelodysplastic Syndrome. Int J Mol Sci 16, 966–989. https://doi.org/10.3390/ijms16010966

Zhu, Y.M., Das-Gupta, E.P., Russell, N.H., 1999. Microsatellite instability and p53 mutations are associated with abnormal expression of the MSH2 gene in adult acute leukemia. Blood 94, 733–740.

Zuna, J., Burjanivova, T., Mejstrikova, E., Zemanova, Z., Muzikova, K., Meyer, C., Horsley, S.W., Kearney, L., Colman, S., Ptoszkova, H., Marschalek, R., Hrusak, O., Stary, J., Greaves, M., Trka, J., 2009. Covert preleukemia driven by MLL gene fusion. Genes Chromosomes Cancer 48, 98–107. https://doi.org/10.1002/gcc.20622

7. Supplements

Table S1: Antibodies used in the study

ANTIGEN	HOST	DILUTION	PRODUCT N.	COMPANY
8-oxoG	Mouse	1:400	ab64548	Abcam
actin	Rabbit	1:1000	A-2668	Sigma-Aldrich
Biotinylated CD4	Rat	1:200	100404	Biolegend
Biotinylated CD8	Rat	1:200	100704	Biolegend
Biotinylated B220	Rat	1:200	103204	Biolegend
Biotinylated CD11b	Rat	1:800	101204	Biolegend
Biotinylated Gr1	Rat	1:400	108404	Biolegend
Biotinylated Ter119	Rat	1:100	116204	Biolegend
BrdU, FITC	Mouse	1:20	11202693001	Roche
CCL3	Rabbit	1:100	ab32609	Abcam
CD150, PE	Rat	1:100	115904	Biolegend
CD16, APC	Rat	1:200	158005	Biolegend
CD34	Mouse	1:500	ab762	Abcam
CD34, FITC	Mouse	1:20	CD34-581-01	Thermo Fisher
CD41a, PerCP-Cy5.5	Mouse	1:5	333148	BD Biosciences
CD41, BV 605	Rat	1:100	133921	Biolegend
CD43, APC	Mouse	1:20	MHCD4305	Thermo Fisher
CD48, FITC	Rat	1:100	11-0481-81	eBiosciences
c-Kit, BV711	Rat	1:100	105835	Biolegend
CXCL10	Rabbit	1:100	ab9807	Abcam
CXCL9	Rabbit	1:1000	ab9720	Abcam
DUSP1	Rabbit	1:50	ab61201	Abcam
DUSP1	Mouse	1:200	sc-373841	SANTA CRUZ BIOTECHNOLOGY
DUSP6	Rabbit	1:50	ab76310	Abcam

Epcr. APC	Rat	1:100	12-2012-82	Thermo Fisher Scientific
Esam, PE	Rat	1:100	136204	Biolegend
H2AX (pS139)/γ-H2AX	Rabbit	1:50	9718	Cell Signaling Technology
H2AX (pS139)/γ-H2AX	Mouse	1:500	05-636	Millipore
Chk1	Mouse	1:1000	C9358	Sigma-Aldrich
Chk1 S317	Rabbit	1:500	2344S	Cell Signaling Technology
Chk2	Mouse	1:1000	C9108	Sigma-Aldrich
Chk2 Thr68	Rabbit	1:500	2661S	Cell Signaling Technology
IFNγ	Rabbit	1:750	ab9657	Abcam
IL-6	Rabbit	1:500	ab154367	Abcam
KAP1	Rabbit	1:10 000	ab109545	Abcam
KAP1 S824	Rabbit	1:500	ab70369	Abcam
Ki-67	Mouse	1:25	GA62661-2	DAKO
p21waf1	Rabbit	1:500	sc-397	SANTA CRUZ BIOTECHNOLOGY
p38	Rabbit	1:1000	9212	Cell Signaling Technology
p38 T180/Y182	Rabbit	1:500	9211	Cell Signaling Technology
p53	Mouse	1:1000	2524	Cell Signaling Technology
p53 S15	Rabbit	1:500	9284S	Cell Signaling Technology
pATMS1981	Mouse	1:500	200-301-500	Rockland Immunochemicals
pATRT1989	Rabbit	1:100	ab227851	Abcam
RAD51	Rabbit	1:250	ab63801	Abcam
SAPK/JNK	Rabbit	1:1000	9252	Cell Signaling Technology
SAPK/JNK T183/Y185	Rabbit	1:500	9251	Cell Signaling Technology
Sca-1, PE/Cy7	Rat	1:100	25-5981-82	eBiosciences
STAT1	Rabbit	1:1000	9172	Cell Signaling Technology
STAT1 Tyr701	Rabbit	1:1000	9167	Cell Signaling Technology
TGFβ1	Rabbit	1:1000	ab92486	Abcam

TNFα	Rabbit	1:100	ab6671	Abcam

8. Acronyms and abbreviations

8-OG	8-oxoguanine
8-oxoG	8-oxoguanine
AML	acute myeloid leukemia
ASXL1	ASXL transcriptional regulator 1
ATM	ATM serine/threonine kinase
ATR	ATR serine/threonine kinase
B2M	beta-2-microglobulin
Ba/F3	cellosaurus cell line Ba/F3
BCI	(E)-2-benzylidene-3-(cyclohexylamino)-2,3-dihydro-1H-inden-1-one
BM	bone marrow
BMP-4	bone morphogenetic protein 4
BrdU	5-Bromo-2′-deoxyuridine (nucleotide analog)
BSA	bovine serum albumin
c-Kit	KIT proto-oncogene receptor tyrosine kinase
Cas9	CRISPR associated protein 9
CBC	complete blood count
CCD	charge-coupled device
CCL3	C-C motif chemokine ligand 3
CD	Cluster of Differentiation
$CD34^+$ P-ECs	CD34+ progenitor-enriched cultures
cDNA	complementary DNA
CFU-E	colony forming unit erythroid
CHEK2	checkpoint kinase 2
Chk1	checkpoint kinase 1
CML	chronic myeloid leukemia
CMP	common myeloid progenitor
Cre	cyclization recombinase
CRISPR	clustered regularly interspaced short palindromic repeats
CXCL10	C-X-C motif chemokine ligand 10
CXCL9	C-X-C motif chemokine ligand 9
DAPI	4′,6-diamidino-2-phenylindole
DDR	DNA damage response
DEGs	differentially expressed genes

DKK-1	dickkopf-related protein 1
DMEM	dulbecco's modified eagle medium
DNA	Deoxyribonucleic acid
DNMT3A	DNA (cytosine-5)-methyltransferase 3A
DSB	double-strand break
dsDNA	double-stranded DNA
DUSP	dual-specificity phosphatase
EB	embryoid body
Epcr	Endothelial protein C receptor
EPO, Epo	erythropoietin
ERCC3	ERCC excision repair 3, TFIIH core complex helicase subunit
ERCC5	ERCC excision repair 5, endonuclease
ERK	extracellular signal–regulated kinase
ERtm	truncated form of mutant estrogen receptor
Esam	endothelial cell adhesion molecule
ET	essential thrombocythemia
EZH2	Enhancer of zeste homolog 2
FACS	Fluorescence-activated cell sorting
FBS	fetal bovine serum
FGF	fibroblast growth factor
FGF-Basic	fibroblast growth factor-basic
FLT3	fms like tyrosine kinase 3
FLT3LG	Fms-related tyrosine kinase 3 ligand
G6PD	glucose-6-phosphate dehydrogenase
GBP1	guanylate binding protein 1
GBP2	guanylate binding protein 2
GFP	green fluorescent protein
GPx	glutathione peroxidase
GR	glutathione reductase
GSEA	gene set enrichment analysis
HCL	hydrochloric acid
HEL	human erythroleukemia cell line
HGD	high-grade dysplasia
HK	hexokinase
HPRT1	hypoxanthine phosphoribosyltransferase 1
HR	homology-dependent recombination
HRP	horseradish peroxidase

HSC	hematopoietic stem cell
IDH1/2	isocitrate dehydrogenase (NADP(+)) 1/2
IFN	interferon
IFNγ	interferon gamma
IGF-1	Insulin-like growth factor 1
IHC	Immunohistochemistry
IL	Interleukin
iPSCs	induced pluripotent stem cells
IRF1	interferon regulatory factor 1
JAK2	Janus kinase 2
JNK	c-Jun N-terminal kinase
Jun	Jun proto-oncogene, AP-1 transcription factor subunit
KAP1	KRAB-associated protein-1
Ki-67	marker of proliferation Ki-67
KIT	KIT proto-oncogene
logFC	log of fold change
LSC	leukemia stem cell
LSK	Linage-negative, Sca-1-positive, c-Kit-positive cells
MAPK	Mitogen-activated protein kinase
MCH	Mean corpuscular hemoglobin
MCV	Mean corpuscular volume
MDS	myelodysplastic syndrome
MEFs	mouse embryonic fibroblasts
MEP	megakaryocyte-erythrocyte progenitor
MF	myelofibrosis
Mk	Megakaryocyte
MkP	megakaryocyte progenitor
MKPs	Dual-specificity MAP kinase phosphatases
MLH1	mutL homolog 1
MLL	mixed-lineage leukemia
MLL-ENL	MLL–eleven nineteen leukemia
MMR	mismatch repair
MOWIOL	Poly(vinyl alcohol)
MPN	myeloproliferative neoplasms
mRNA	messenger RNA
MSH2	mutS homolog 2
NF-κB	nuclear factor kappa B

NGS	next generation sequencing
OGG1	8-oxoguanine DNA glycosylase
p21	cyclin-dependent kinase inhibitor 1
p38 MAPK	p38 mitogen-activated protein kinases
p53	Tumor protein p53
PB	peripheral blood
PBS	phosphate-Buffered Saline
PBS-T	phosphate buffered saline with Tween20
PCR	polymerase chain reaction
pegIFNα	pegylated interferon alpha
PI3K	phosphatidylinositol 3-kinase,
pIpC	Polyinosinic:polycytidylic acid
PKB	Protein kinase B
PMF	primary myelofibrosis
pre-LSC	pre-leukemia stem cell
Pre-MegE	pre-megakaryocyte-erythrocyte
PV	polycythemia vera
PVDF	polyvinylidene fluoride
RAD51	RAD51 recombinase
RAS	Ras GTPase
RECQ	DNA helicase RecQ
RECQL5	RecQ like helicase 5
RIN	RNA integrity number
RNA	ribonucleic acid
RNAseq	RNA sequencing
ROS	reactive oxygen species
RPLP0	ribosomal protein lateral stalk subunit P0
RT	room temperature
SAPK	Stress-activated protein kinases
Sca-1	Stem cells antigen-1
SCF	stem cell factor
scr	scrambled small interfering RNA control
SD	standard deviation
SDS-APGE	sodium dodecyl sulfate–polyacrylamide gel electrophoresis
SEM	standard error of mean
SFM	serum free medium
siRNA	small interfering RNA

SNP	single nucleotide polymorphism
ssDNA	single-stranded DNA
STAT	signal transducer and activator of transcription
t-AML	therapy-related acute myeloid leukemia
TAP1	transporter 1, ATP binding cassette subfamily B member
TET2	Tet methylcytosine dioxygenase 2
Tfr1	Transferrin receptor 1
TGFβ1	transforming growth factor beta 1
TIBC	total iron binding capacity
TNFα	tumor necrosis factor alpha
TP53	tumor protein p53
TPO, Tpo	thrombopoietin
UBC	ubiquitin C
UBD	ubiquitin D
UHOL	University Hospital Olomouc
VCAM1	vascular cell adhesion molecule 1
VEGF	vascular endothelial growth factor
VF	JAK2 V617F
WHO	World Health Organization
WT	wildtype
XPC	XPC complex subunit, DNA damage recognition and repair factor
XPD	Xeroderma pigmentosum D
XRCC1	X-ray repair cross complementing 1
XRCC3	X-ray repair cross complementing 3
YWHAZ	tyrosine 3-monooxygenase/tryptophan 5-monooxygenase activation protein zeta
γH2AX	phosphorylated form of H2A histone family member X

9. List of publications

Articles:

Stetka, J., Vyhlidalova, P., Lanikova, L., Koralkova, P., Gursky, J., Hlusi, A., Flodr, P., Hubackova, S., Bartek, J., Hodny, Z., Divoky, V., 2019. Addiction to DUSP1 protects JAK2V617F-driven polycythemia vera progenitors against inflammatory stress and DNA damage, allowing chronic proliferation. Oncogene 38, 5627–5642. https://doi.org/10.1038/s41388-019-0813-7
Impact factor: 7.971

Stetka, J., Gursky, J., Liñan Velasquez, J., Mojzikova, R., Vyhlidalova, P., Vrablova, L., Bartek, J., Divoky, V., 2020. Role of DNA Damage Response in Suppressing Malignant Progression of Chronic Myeloid Leukemia and Polycythemia Vera: Impact of Different Oncogenes. Cancers (Basel) 12. https://doi.org/10.3390/cancers12040903
Impact factor: 6.126

Rao, T.N., Hansen, N., Stetka, J., Kalmer, M., Hilfiker, J., Endele, M., Kubovcakova, L., Rybarikova, M., Hao-Shen, H., Geier, F., Beisel, Ch., Dirnhofer, S., Schroeder, T., Brümmendorf, T., Wolf, D., Koschmieder, S., Skoda, R.C., 2020. Interferon-α achieves molecular remission in myeloproliferative neoplasms by inducing megakaryocyte-biased stem cells. *Manuscript submitted in Blood – second round of revisions*
Impact factor: 17.543

Abstracts published in WoS Core Collection Journals:

Raskova Kafkova, L., Somikova, Z., Kucerova, J., Calabkova, L., Luzna, P., Stetka, J., Simkova, D., Dolezal, D., Divoky, V., 2015. Iron Chelation Reinforces DNA Damage Response and Leads to G2/M Checkpoint Activation and Autophagy in Myeloid Bone Marrow Cells of Preleukemia Mouse Model. Blood 126, 3351–3351. https://doi.org/10.1182/blood.V126.23.3351.3351

Stetka, J., Luzna, P., Lanikova, L., Koralkova, P., Gursky, J., Hodny, Z., S., Bartek, J., Divoky, V., 2017. JAK2 V617F Progenitors Utilize Adaptations to Cell-Autonomous and Microenvironment-Dependent Inflammatory Stress in Polycythemia Vera, Likely Exhibiting Barrier Against Rapid Transformation to Myelofibrosis. Blood 130, (Supplement 1): 1667

Stetka, J., Hansen, N., Kubovcakova, L., Hao-Shen, H., Dirnhofer, S., Skoda, R.C., 2020. Loss of Dnmt3a Confers Resistance to Pegifnα in JAK2 -V617F Mouse Model. Swiss Medical Weekly 150:w20411, https://doi.org/10.4414/smw.2020.20411
Received Swiss Society of Hematology and Swiss Society of Medical Oncology price for best abstract.

Stetka, J., Hansen, N., Kubovcakova, L., Hao-Shen, H., Dirnhofer, S., Skoda, R.C., 2020. Loss of Dnmt3a Confers Resistance to Pegifnα in *JAK2* -V617F Mouse Model. Blood 136, (Supplement 1): 8–9
Received ASH Abstract Achievement Award.

Other published abstracts:

Stetka, J., Luzna, P., Lanikova, L., Bartek, J., Divoky, V., 2015. Inflammatory response of hematopoietic progenitors differentiated from polycythemia vera patient-specific induced pluripotent stem cells. International Conference on the tumour microenvironment in the haematological malignancies and its therapeutic targeting, 2015, Lisbon, Portugal, abstracts, poster 24

Stetka, J., Luzna, P., Lanikova, L., Bartek, J., Divoky, V., 2015 Inflammatory response of polycythemia vera hematopoietic progenitors differentiated from patient-specific induced pluripotent stem cells. Olomouc Hematological Days, 2015, Olomouc, abstracts, ISBN 978-80-244-4697-4, page 6

Stetka, J., Luzna, P., Lanikova, L., Koralkova, P., Hodny, Z., Prchal, J., Bartek, J., Divoky, V., 2016. JAK2 V617F progenitors exhibit intrinsic inflammatory signaling and protection against inflammation induced DNA damage. ESH 7th International Conference on MYELOPROLIFERATIVE NEOPLASMS, 2016, Estoril, Portugal, abstracts, poster 21

Stetka, J., Luzna, P., Lanikova, L., Koralkova, P., Hodny, Z., Bartek, J., Divoky, V., 2016. JAK2 V617F progenitors exhibit intrinsic inflammatory signaling and protection against inflammation induced DNA damage. Olomouc Hematological Days, 2016, Olomouc, abstracts, ISSN 1213-5763, page 28-29
Received Award for best abstract in its category.

Stetka, J., Luzna, P., Lanikova, L., Koralkova, P., Hodny, Z., Bartek, J., Divoky, V., 2016. JAK2 V617F progenitors exhibit intrinsic inflammatory signaling and protection against

inflammation induced DNA damage. 12th International Congress of Cell Biology in Prague, 2016, Praha, abstracts, page 110